Establishing the Maximum Carbon Number for Reliable Quantitative Gas Chromatographic Analysis of Heavy Ends Hydrocarbons

Diana Margarita HERNANDEZ BAEZ

Thesis submitted for the degree of Doctor of Philosophy

Heriot-Watt University

Institute of Petroleum Engineering

March 2013

ABSTRACT

This Thesis investigates the two main limitations of high temperature gas chromatography (HTGC) in the analysis of heavy n-alkanes: pyrolysis inside the GC column and incomplete elution.

The former is studied by developing and reducing a radical pyrolysis model (7055 reactions) into a molecular pyrolysis model (127 reactions) capable of predicting low conversions of ($nC_{14}H_{30}$-$nC_{80}H_{162}$) at temperatures up to 430°C. Validation of predicted conversion with literature data for $nC_{14}H_{30}$, $nC_{16}H_{34}$ and $nC_{25}H_{52}$ yielded an error lower than 5.4%.

The latter is addressed by developing an analytical model which solves recursively the diffusion and convection phenomena separately. The model is capable of predicting the position and molar distribution of components, using as main input the analytes' distribution factors and yielded an error lower than 4.4% in the prediction of retention times.

This thesis provides an extension of the data set of distribution factors of ($nC_{12}H_{26}$–$nC_{98}H_{198}$) in a SGE HT5 GC capillary column, based on isothermal GC measurements at both constant inlet pressure and flow rate.

Finally, the above two models were coupled, yielding a maximum mass lost of 1.3 % in the case of $nC_{80}H_{162}$ due to pyrolysis and complete elution up to $nC_{70}H_{142}$, in a 12 m HT5 column.

DEDICATION

This thesis is dedicated to God, for whom nothing is impossible, and to each one of the members of my beloved family: my parents: Manuel HERNANDEZ and Margarita BAEZ MEDINA, my brothers and sisters: Nelson, Sandra, Alexander and Marisol HERNANDEZ BAEZ, and my beautiful grandmothers who helped raise me during my childhood: Maria Elpidia MEDINA MELGAREJO, and Josefina HERNANDEZ. They are the reason why I am where I am and who I am.

ACKNOWLEDGEMENTS

I wish to thank Alastair Reid for his invaluable help and untiring technical support (and English corrections), and for all the interesting discussions which introduced me to the GC world.

I wish to thank Antonin Chapoy, who believed on me during these three years, even knowing how difficult the project would be. Thank you for supporting me until the end of my PhD, and for letting me explore beyond the limits.

I wish to thank Roda Bounaceur, for helping me disinterestedly and who introduced me to the Pyrolysis modelling. Thank you for your unwavering kindness and your friendship.

I wish to thank Professor Bahman Tohidi, for giving me a place in the PVT group and for believing on me and all my ideas during my whole PhD.

I want to thank the Sponsors of my project: Marathon Oil Corporation, Schlumberger and Total, especially to Francois MONTEL, for being my most appreciated tutor and for teaching me to enjoy science and to be open to the surprises of Mother Nature.

I wish to thanks my beloved friends; Martha Hajiw (my little French sister), Chucks (Ñelu), Mohamed Regaieg, Luis Pereira, for your company, your smiles, your support, for all the good moments that we shared, I will not forget these three years, and for all your help with the format of my thesis and my English, especially to Marisol Hernandez (Magic, my twin soul sister☺).

I wish to thank my family, for their prayers for always being there for me, and for continually making my life more beautiful.

Finally, I want to thank God, for accompanying me during my life and being my best friend, and to the Holy Mary, for covering me with her mantle and making me feel the love of my family wherever I go.

" Ni la mente es dueña de sus miedos, Ni el corazón de sus deseos.
Ni l'esprit est propriétaire de ses peurs, Ni le coeur de ses désirs.
Neither the mind is owner of its fears, nor the heart of its desires."

DMHB

ACADEMIC REGISTRY

Research Thesis Submission

Name*:*	DIANA MARGARITA HERNANDEZ BAEZ		
School/PGI:	INSTITUTE OF PETROLEUM ENGINEERING		
Version: *(i.e. First, Resubmission, Final)*	FIRST	Degree Sought (Award **and** Subject area)	PhD in Petroleum Engineering

Declaration

In accordance with the appropriate regulations I hereby submit my thesis and I declare that:

1) the thesis embodies the results of my own work and has been composed by myself
2) where appropriate, I have made acknowledgement of the work of others and have made reference to work carried out in collaboration with other persons
3) the thesis is the correct version of the thesis for submission and is the same version as any electronic versions submitted*.
4) my thesis for the award referred to, deposited in the Heriot-Watt University Library, should be made available for loan or photocopying and be available via the Institutional Repository, subject to such conditions as the Librarian may require
5) I understand that as a student of the University I am required to abide by the Regulations of the University and to conform to its discipline.

* *Please note that it is the responsibility of the candidate to ensure that the correct version of the thesis is submitted.*

Signature of Candidate*:*		Date:	

Submission

Submitted By *(name in capitals):*	DIANA MARGARITA HERNANDEZ BAEZ
Signature of Individual Submitting:	
Date Submitted:	

For Completion in the Student Service Centre (SSC)

Received in the SSC by *(name in capitals):*			
Method of Submission *(Handed in to SSC; posted through internal/external mail):*			
E-thesis Submitted (**mandatory for final theses)**			
Signature:		Date:	

TABLE OF CONTENTS

LIST OF SYMBOLS

D_M= Diffusion constant, mobile phase. (unit length^2/ unit time)

D_S= Diffusion constant, stationary phase. (unit length^2/ unit time)

D= Dispersion coefficient. (unit length^2/ unit time)

D_{eff}= Effective average Diffusivity. (unit length^2/ unit time)

H(x,t))= Column plate height, spatial rate of dispersion of a zone. (unit length)

K=Distribution factor of a compound. (moles/volume) in stationary phase/ (moles/volume) in gas phase).

k= retention factor of a compound.(moles in stationary phase/moles in gas phase).

L= Length of the GC column (unit length).

N(x,to) = mole profile for every analytie (particles/unit length).

N_G(x,t) = Mole profile for every analyte in the gas phase. (particles/unit length).

N_S(x,t) = Mole profile for every analyte in the stationary phase. (particles/unit length).

$N_{i,M}$=Moles of component "i" in the mobile phase.

$N_{i,S}$=Moles of component "i" in the stationary phase.

MW_A= Molecular weight of the component "i".

MW_B= Molecular weight of the carrier gas.

P(x)= Pressure at position x. (Pa)

Pin=Pressure at the GC colum inlet.

Pout=Pressure at the GC column outlet. (Pa)

r_o=internal radius of GC column. (unit length)

rampT= ramp of temperature of the temperature programmed.

T(t)= temperature at the time t.

To= Initial temperature of the temperature programmed.

t=time (unit time)

v_{eff}=Effective cross-sectional average velocity.(unit length/ unit time)

v_M= velocity of migration of the carrier gas.(unit length/ unit time)

v_A, v_B =

w=film thicknes. (unit length)

X_i=Fraction of component i in the gas phase relative to the moles in both stationary and gas phase.

$x_{0=}$ centroid of Gaussian distribution of distribution of component inside the GC column. (unit length)

x = position of the component's dispersal around the centroid x_0.(unit length)

Greek letters

σ = standard deviation of the component's distribution.

σ_x = standard deviation of the zone's component's distribution. (unit length)

β=phase ratio.(volume of mobile phase in the column to the volume of stationary phase)

η_m =Viscosity of the carrier gas.(μPa·s)

Δt=time step. (unit time)

TABLE OF TYPICAL GC VALUES

Variable	min	max	Units
D_M	$5.6\cdot10^{-6}$	$3.22\cdot10^{-5}$	m^2/s
$D_§$	$1.1\cdot10^{-10}$	$1.2\cdot10^{-9}$	m^2/s
D	$4.5\cdot10^{-5}$	$1.4\cdot10^{-3}$	m^2/s
D_{eff}	$6.6\cdot10^{-25}$	$6.4\cdot10^{-5}$	m^2/s
H(x,t))	$5.6\cdot10^{-4}$	$4.4\cdot10^{-3}$	m
K	1156	$3.7\cdot10^{+18}$	$(\text{mole i/m}^3)^S/(\text{mole i/m}^3)^G$
k	1.31	$4.2\cdot10^{+21}$	$(\text{mole i})^S/(\text{mole i})^G$
L	12		m
$N_G(x,t)$	$2.1\cdot10^{-33}$	1.1·10-11	moles
$N_§(x,t)$	$3.43\cdot10^{-17}$	4.3·10-11	moles
N(x,to)	$2.1\cdot10^{-33}$	$4.35\cdot10^{-11}$	moles
MW_A	198	1122	g/mol
MW_B	4		g/mol
P(x)	119607	101325	Pa
Pin	119607.1		Pa
Pou	101325		Pa
r_o	0.000265		m
rampT	10, 15, 20		°C/s
T(t)	10	430	°C
To	10		°C
t	0	42	min
v_{eff}	$1.5\cdot10^{-22}$	0.2323	m/s
v_M	0.34	0.76	m/s
w	$1.5\cdot10^{-7}$		m
x_0,x	0	12	m
σ_x	$2.2\cdot10^{-3}$	0.13	m
β	882.6		$(m^3)^G/(m^3)^S$
η_m	$1.97\cdot10^{-5}$	$3.6\cdot10^{-5}$	Pa·s
Δt	1	4	s

LIST OF PUBLICATIONS BY THE CANDIDATE

Hernandez-Baez, D.M., Tohidi, B., Chapoy, A., Bounaceur, R. and Reid, A. *'Establishing the maximum carbon number for reliable quantitative gas chromatographic analysis of heavy ends hydrocarbons. Part 1. Low conversion thermal cracking Modeling.* Energy & Fuels, 26(5), 2600-2610, 2012.

(Oral Presentation) at The 12th International Conference on Petroleum Phase Behavior and Fouling. **Petrophase 2011.** Imperial Collegue, London, UK.
(Oral Presentation) at The World Heavy Oil Congress **WHOC 2012.** Abeerden, Scotland UK.

Hernandez-Baez, D.M., Tohidi, B., Chapoy, A., Bounaceur, R. and Reid, A. *'Establishing the maximum carbon number for reliable quantitative gas chromatographic analysis of heavy ends hydrocarbons. Part 2. Gas Chromatography, Migration/Separation Modeling.* Energy & Fuels, March 9, 2013**.** **DOI:** 10.1021/ef302009n

(Oral Presentation) at The World Heavy Oil Congress **WHOC 2012.** Abeerden, Scotland UK.

Hernandez-Baez, D.M., Tohidi, B., Chapoy, A., Bounaceur, R. and Reid, A. 'Establishing the maximum carbon number for reliable quantitative gas chromatographic analysis of heavy ends hydrocarbons. Part 3. (Coupled Gas Chromatography & Pyrolysis Modelling). (Unpublished paper)

Hernandez-Baez, D.M., Tohidi, B., Chapoy, A., Bounaceur, R. and Reid, A. 'Establishing the maximum carbon number for reliable quantitative gas chromatographic analysis of heavy ends hydrocarbons. Part 4. (Determination of distribution factors (nC12-nC98) in an HT5 GC column). (Unpublished paper)

Alsiyabi, I., **Hernandez-Baez, D.M**., Chapoy, A. Tohidi, B." the effect of common impurities on the ift, swelling factor and mmp of CO_2/n-decane system". (Unpublished paper)

CHAPTER 1 – INTRODUCTION

Gas chromatography (GC) is a separation technique for compounds, which also provides information regarding their concentrations in a mixture. The components are required to be sufficiently volatile and thermally stable in order to perform a reliable Gas Chromatography analysis.

Reservoir fluid characterization by Gas Chromatography has an impressive capability of detection and quantification of a wide range of Single Carbon Number (SCN) groups in oil analyses. However, some researchers prefer to report analyses to C_{20+} only, with estimation of the Cn+ fraction distribution obtained using various correlations. Conversely, other researchers prefer to extend GC analysis to the highest possible SCN group by using High Temperature Gas Chromatography (HTGC), with programming to c.a. 370-430 °C. However, the reliability of extended GC analyses to high carbon number fractions is questioned because of a possible over-estimation of light and intermediate fractions in the original oils caused by thermal decomposition products.

The thermal stability of heavy hydrocarbons at temperatures above 370 °C is a major concern in the practice of Gas Chromatography [1-3] based on the results of Thermal Gravimetric Analysis (TGA) published by Schwartz et al. (1987) [4]. These results indicated a maximum in the curve of mass lost due to thermal cracking at 430 °C, and therefore the practice of Gas Chromatography at oven temperatures up to 450 °C, was questioned.

In spite of the above publication, little or no evidence of cracking has been observed according to the relative publications [5-7] at ≥400 °C. However, sample thermal decomposition is not only a function of temperature, but is also dependent on pressure, sample composition and the residence time at high temperature [8-9].

It is therefore very important to be able to model the thermal cracking of heavy n-alkanes at HTGC conditions, in order to verify these findings requiring as input data: carrier gas pressure, temperature and concentration of every component through the GC column. This aspect is treated in CHAPTER 2 –, analyzing a range of concentrations rather than a specific concentration.

Therefore, computer simulation of gas chromatography becomes necessary to complete the study of HTGC limits by predicting the precise concentration of every component inside the GC column which can then serve as input to the Pyrolysis model.

Gas Chromatography modelling also provides an insight into the migration/separation of the sample at each point of the column, for both isothermal and temperature programmed GC analysis, and thus potentially to optimize the partitioning process.

CHAPTER 3 – is focused on GC modelling. Two GC models have been developed: one for solving the diffusion-convection equation [11] using finite elements solved by COMSOL [12], which enables the concentration profile to be obtained; and another, solving a simplified iterative convection equation[13] using MATLAB, which allows the retention times to be obtained more quickly.

The retention times obtained with the two models have been compared with the experimental results. Due to the superior results of the convection model (which highlighted the superior performance), it has been used for optimizing the calculation time of the convection-diffusion model.

The main input used in the GC modelling is the database of distribution factors (K), derived from isothermal GC analyses. The HT5 capillary column (SGE) is widely used for HTGC analysis of heavy oil hydrocarbons, thus an HT5 GC column has been chosen in this thesis, for all determinations of the HTGC limits.

In the analysis of CHAPTER 3 –, the distributions factors for the n-alkanes ($nC_{12}H_{26}$–$nC_{62}H_{126}$) [14] on an HT5 capillary column have been used as input for the GC model developed.

Based on the developed Gas Chromatography Model, a new approach for determining the non/incomplete elution of every component has been proposed in this thesis by introducing a new approach: *the degree of elution*, defined as the amount of component which has been eluted in relation to the amount injected. Thus, the degree of elution of each of the heavy n-alkanes studied has been calculated for a typical temperature programme in CHAPTER 3 –.

This thesis focuses mainly on the GC analysis of heavy n-alkanes, and therefore the necessity of extending the data set of n-alkane distribution factors (K values) from nC_{12} through nC_{98} in an HT-5 GC column is the main focus of CHAPTER 4 –. Measurement procedures and data treatment are explained in detail.

For this purpose, numerous isothermal gas chromatography experiments have been carried out, in the temperature range from 80°C to 420°C, at 20°C intervals and at 430°C. Two modes of HTGC operation were applied and are proposed in this thesis work:

a.) High-Efficiency Mode: 12m column, constant inlet pressure, elution up to nC_{64}

b.) Low-Efficiency Mode: 5m column, constant flow rate, elution up to nC_{100}.

Knowledge of K values (distribution factors) is of potential use in optimising the partitioning process and elucidating information on non/incomplete elution of heavy n-alkanes.

CHAPTER 5 –, is focused on coupling the two models introduced previously: the pyrolysis model (CHAPTER 2 –) and the GC model (CHAPTER 3 –), in order to determine the pyrolysis risk inside the GC column, along with the non/incomplete elution of heavy n-alkanes, in a common HTGC column (HT5 capillary column) at common temperature programmings.

This final model is capable of determining the mass lost due to pyrolysis and the degree of elution of every n-alkane studied, as well as determining the HTGC limits in the analysis of heavy n-alkanes.

In order to improve the computing performance of the coupled Pyrolysis-GC model, the free-radical pyrolysis model (CHAPTER 2 –) has been reduced to a molecular pyrolysis model, and the GC model (CHAPTER 3 –) solving the diffusion-convection equation has been replaced by an iterative analytical model for predicting the mole distributions throughout the GC column.

Finally, based on the analysis of the results obtained from the studies carried out in this thesis, several conclusions are drawn and summarized in CHAPTER 6 –

1.1. Reference

[1] Dutriez, T., et al., *High-temperature two-dimensional gas chromatography of hydrocarbons up to nC(60) for analysis of vacuum gas oils*, Journal of Chromatography A, **1216**(14), 2905-2912 (2009)

[2] Dulaurent, A., et al., *Extended simulated distillation by capillary supercritical fluid chromatography*, Oil & Gas Science and Technology-Revue De L Institut Francais Du Petrole, **62**(1), 33-42 (2007)

[3] Carbognani, L., et al., *High temperature simulated distillation of athabasca vacuum residue fractions. bimodal distributions and evidence for secondary "on-column" cracking of heavy hydrocarbons*, Energy & Fuels, **21**(5), 2831-2839 (2007)

[4] Schwartz, H.E., et al., *Simulated distillation of high-boiling petroleum fractions by capillary supercritical fluid chromatography and vacuum thermal gravimentric analysis.*, Analytical Chemistry, **59**(10), 1393-1401 (1987)

[5] Lipsky, S.R. and M.L. Duffy, *High-temperature gas-chromatography - the development of new aluminum clad flexible fused-silica glass-capillary columns coated with thermostable nonpolar phases .1*, Journal of High Resolution Chromatography & Chromatography Communications, **9**(7), 376-382 (1986)

[6] *ASTM D7169 - 11. Standard Test Method for Boiling Point Distribution of Samples with Residues Such as Crude Oils and Atmospheric and Vacuum Residues by High Temperature Gas Chromatography*: ASTM International,West Conshohocken, PA, ,(2010)

[7] Villalanti, D.C., J.C. Raia, and J.B. Maynard, *High-temperature simulated distillation applications in petroleum characterization*, Encyclopedia of Analytical Chemistry,R.A. Meyers(Ed). John Wiley & Sonds Ltd, Chichester, 6726-6741 (2000)

[8] Vercier, P. and M. Mouton, *Préparation de distillats à hauts points d'ébullition par distillation a court trajet*, Analusis, **10**(2), 57-70 (1982)

[9] Fisher, *W. , Erdoel Kohle, Erdgas*, W. , Erdoel Kohle, Erdgas, Petrochem, **36**(1), (1983)

[10] Hernandez-Baez, D.M., et al., *Establishing the Maximum Carbon Number for Reliable Quantitative Gas Chromatographic Analysis of Heavy Ends*

Hydrocarbons. Part 1: Low-Conversion Thermal Cracking Modeling, Energy & Fuels (2011)

[11] Golay, M.J.E., *Theory of chromatography in open and coated tubular columns with round and rectangular cross-sections*, 36–53, (1958)

[12] Aldaeus, F., Y. Thewalim, and A. Colmsjo, *Prediction of retention times and peak widths in temperature-programmed gas chromatography using the finite element method*, Journal of Chromatography A, **1216**(1), 134-139 (2009)

[13] Snijders, H., H.G. Janssen, and C. Cramers, *Optimization of temperature-programmed gas chromatographic separations .1. Prediction of retention times and peak widths from retention indices*, Journal of Chromatography A, **718**(2), 339-355 (1995)

[14] Hernandez-Baez, D.M., et al., *Establishing the Maximum Carbon Number for Reliable Quantitative Gas Chromatographic Analysis of Heavy Ends Hydrocarbons. Part 3. (Determination of Distribution Factors (nC12-nC98) in an HT5 GC column)*, in *Unpublished manuscript*,(2013)

CHAPTER 2 – LOW CONVERSION THERMAL CRACKING MODELING

2.1.Introduction

The thermal stability of heavy hydrocarbons at HTGC conditions has been addressed by different authors, based on the results of Thermal Gravimetric Analysis (TGA) published by Schwartz et al.(1987) [1], who highlighted thermal instability of heavy oils from around 370 °C. In this work, a pyrolysis model spanning the n-alkanes:($nC_{14}H_{30}$ - $nC_{80}H_{162}$) at low conversion has been developed and applied to mixtures at GC column pressure and oven temperatures up to 450 °C.

Based on this model, the minimum SCN which could possibly be at risk of thermal cracking at some commonly used HTGC temperature programmes, has been obtained by comparing the retention time of n-alkanes standards mixtures [$nC_{10}H_{22}$-$nC_{75}H_{152}$], and the minimal pyrolysis time at the same SCN range of equimolar, heavy and light mixtures at different dilutions in helium, and some low iso-conversion pyrolysis curves.

The developed model can be used to gain an insight into the limitation in the practice of GC and introduces a new approach for calculating the minimum SCN which does not suffer pyrolysis inside a particular GC column.

2.2.Pyrolysis risk inside a Gas Chromatography column

Capillary gas-liquid chromatography (GC) is a separation technique based on the partitioning of an initial mixture by means of reaching an ideal rapid equilibrium between the mobile (gas) and stationary (liquid) phase while the net motion of the carrier gas induces the migration of sample through the column. Figure 2-1 explains gas chromatographic separation in more detail, based on a time-step numerical approach for temperature-programmed gas chromatography, introduced by Snijders et al. [2], where a mixture was initially injected, comprising three components: solvent, light component, and heavy component.

However, when there are unexpected chemical reactions occurring within the column, unquantifiable and random products will generate a very different eluent mixture from

the originally injected sample, and therefore, the gas chromatographic analysis is no longer reliable.

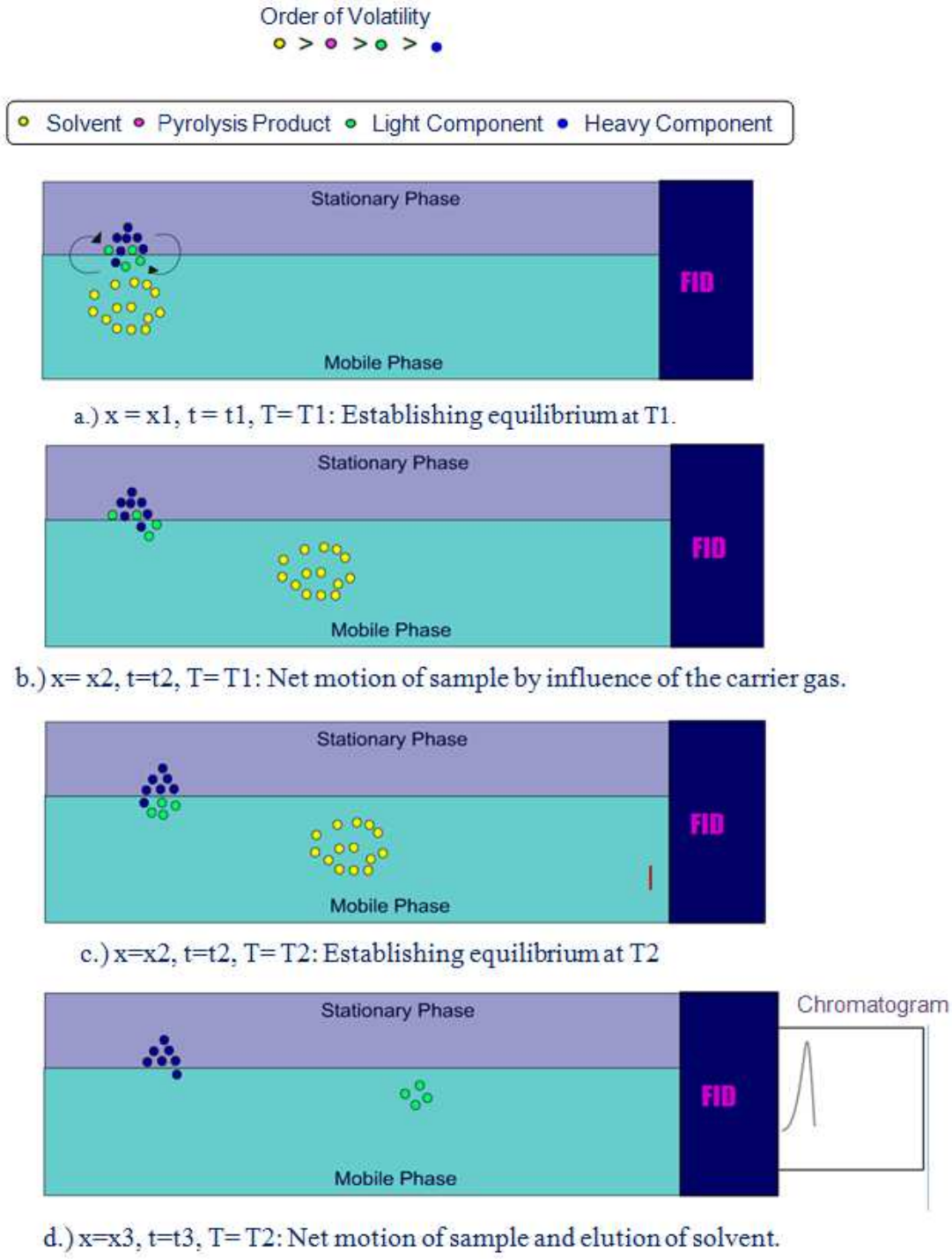

Figure 2-1. Partitioning and migration in a Gas Chromatography Column.

Figure 2-2 shows the continuation of the partitioning detailed in Figure 2-1 where, once the thermal cracking temperature (T3) of the heavy component is reached (Figure 2-2.e), the low boiling, thermal decomposition products appear, as a result of bonds breaking in the heavy component whilst still retained within the column, and after elution of the light component.

The pyrolysis product, being lighter than the light component in Figure 2-2, then partitions between the stationary and mobile phases, eluting ahead of the heavy component, and after the light component, thus producing elution in non-boiling point order(Figure 2-2.h). (Note that whilst co-elution of one or more decomposition products and the 'parent', heavy component is feasible, it is ignored here for simplification).

As a result of the thermal decomposition, the injected oil mixture now indicates four components according to the chromatogram analyzed, whereas the initial mixture injected comprised only three. Hence a gas chromatographic separation under the preceding conditions will complicate the determination of the components, and lead to ambiguous and unreliable results.

In the case of heavy n-alkanes, low conversion thermal cracking mainly produces a whole series of alkenes and alkanes with lower hydrocarbon chain length than the n-alkane reactant undergoing bond breakages, as will be explained in a later section. The resulting complexity of the mixture within the gas chromatographic column, under cracking temperatures therefore leads to confusing chromatographic results, which are no longer representative or consistent with the originally injected mixture.

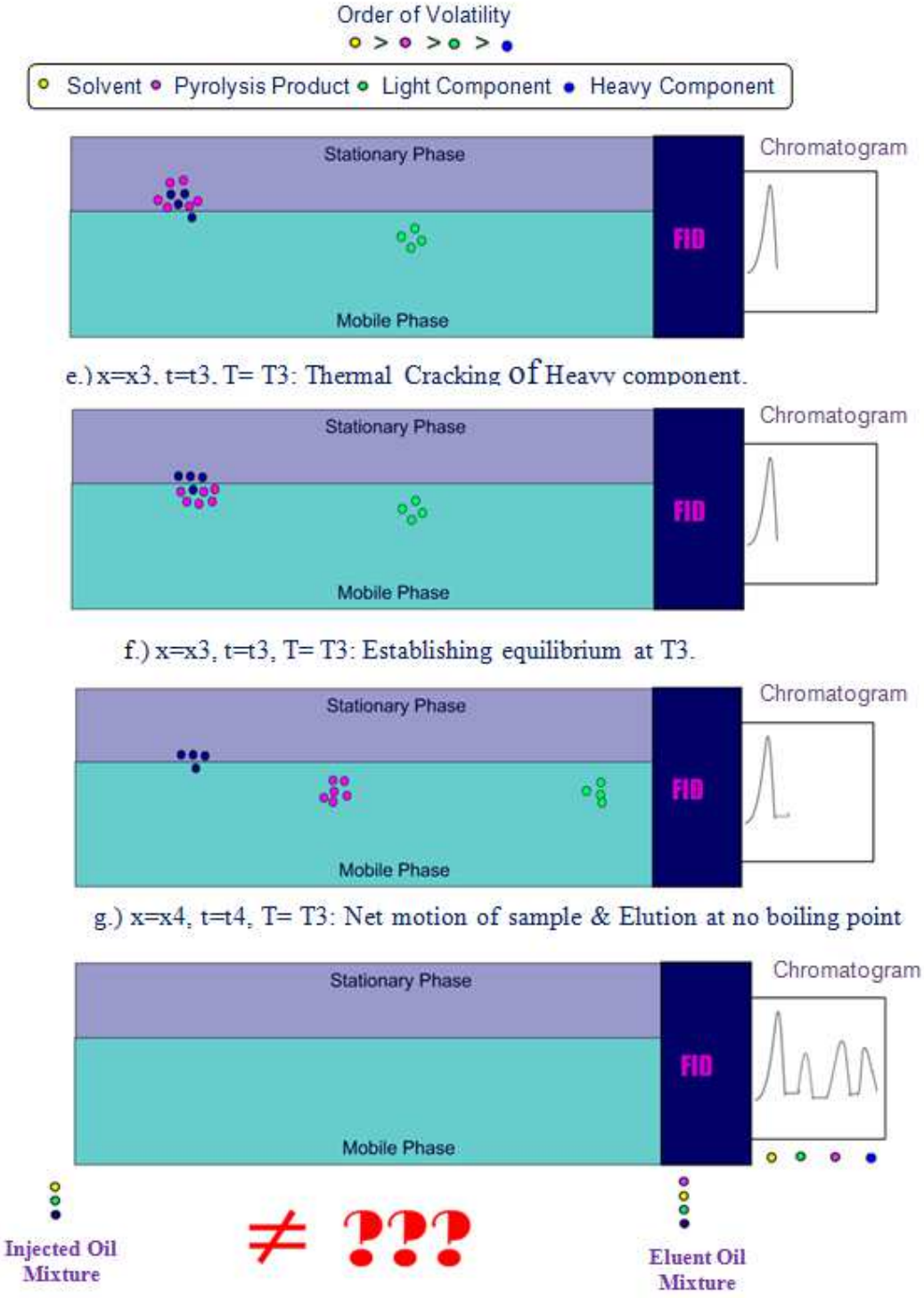

Figure 2-2. Thermal Cracking Risk in a Gas Chromatography Column. (Continuation of Figure 2-1)

2.3.Theory of modelling the thermal cracking of n-alkanes at low conversion

This chapter specifically focuses on low conversion pyrolysis in order to predict the temperature which triggers thermal cracking for each of the n-alkanes studied, comprising $nC_{14}H_{30}$, $nC_{16}H_{34}$, $nC_{20}H_{42}$, $nC_{25}H_{52}$, $nC_{30}H_{62}$, $nC_{35}H_{72}$, $nC_{40}H_{82}$, $nC_{45}H_{92}$, $nC_{50}H_{102}$, $nC_{55}H_{112}$, $nC_{60}H_{122}$, $nC_{65}H_{132}$, $nC_{70}H_{142}$, $nC_{75}H_{152}$, $nC_{80}H_{162}$.

A free-radical primary mechanism has been developed in which only the initial reactant is considered, capable of describing the formation of decomposition products at conversion of around 5-10% molar. However, a secondary mechanism may be developed in future work, covering the validation of pyrolysis products.

The mechanism is based on a Rice-Herzfeld [3] chain scheme (Figure 2-3), comprising:

Initiation Reactions involve a mono-molecular homolysis of hydrocarbons forming β radicals. As the bond dissociation energy of C-H is around 100 Kcal/mol compared with ~85 Kcal/mol for the C-C bond, only C-C homolysis has been considered for temperatures lower than 450 °C.

		Kinetic
Initiation:	$\mu H \rightarrow \beta^{\bullet} + \beta'^{\bullet}$	K_I
H-Transfers:	$\mu H + \beta^{\bullet} \rightarrow \mu^{\bullet} + \beta H$	K_{H-T}
Decomposition:	$\mu^{\bullet} \rightarrow \beta^{\bullet} + \text{alkene}$	K_D
Termination:	$\mu'^{\bullet} + \mu^{\bullet} \rightarrow \text{Products}$	K_T
	$\mu + \beta^{\bullet} \rightarrow \text{Products}$	K_T
	$\beta^{\bullet} + \beta'^{\bullet} \rightarrow \text{Products}$	K_T

Figure 2-3. Reaction mechanism of thermal cracking of alkanes, for low-temperature and low conversion. (Reactant: μH), (radicals: μ•, β•), (alkanes: μH, βH).

H-transfer reactions involve abstraction of a hydrogen (H) atom from the reactant by a radical, forming a new radical and a smaller alkane (lower carbon number) than the reactant.

Decomposition by ß-scission reactions involves a C-C decomposition of µ radicals which yield a β radical and an alkene.

Isomerisation reactions take account of the most important isomerisation involving µ radicals [4], namely 1.5 and 1.4 shift isomerisation of µ radicals.

Termination reactions correspond to all possible combinations of ß and µ radicals.

A completely numerical mechanistic kinetics model [5] has been applied in this thesis, running in a modified version of the source code of SENKIN from the CHEMKIN II package [6], which enables computation of the evolution time of an homogeneous reacting mixture in a batch or tubular reactor, by solving simultaneously the entire set of mass balances for each chemical specie.

The program takes as an input file the mechanism-based kinetic model (for every n-alkane studied) whose development has involved: the manual construction of the reaction mechanism; manual assignment of the kinetic data, for each elementary reaction; and manual assignment of the thermochemical data for each molecule or radical. The thermodynamic data have been sourced from tabulated data [7], and the kinetic data obtained by using the summary of Arrhenius rate parameters [8] (Table 2-1).

The kinetic parameters for initiation and termination reactions are average values corresponding to the decomposition of a normal C-C bond and the recombination of normal primary radicals. The kinetic data calculation of the isomerisation reactions [9] has been obtained with the software KINGAS[10] based on the thermochemical methods of Benson et al.(1976). [7]

The other reactions are considered as reaction families which have the same kinetic constant. Thus, in H-transfer reactions, the reactivity of the type of carbon atom whose hydrogen atom is abstracted by a different kind of radical is considered rather than the chain length of the reactant hydrocarbon. Regarding the decomposition step, the family reactions are classified by the kind of radicals (primary, secondary, or tertiary) formed by β-scission (Table 2-1).

However, the simulation of large reaction mechanisms can result in excessive computational demands/processing time, and consequently it is necessary to reduce the reaction mechanisms to an approximately equivalent, smaller computing model, for which a chemical concepts based reduction method [11-12] was used.

REACTION	KINETIC CONSTANT	Ea ($cal.mol^{-1}$)	A ($cm3.mol^{-1}.s^{-1}$)
Initiation	average value	85000	3.00E+16
H-Transfer	k(CH_3 •,p)	12300	3.98E+11
	k(CH_3•,s)	10400	7.94E+11
	k(CH_3•,t)	10400	7.94E+11
	k(C_2H_5•,p)	12300	3.16E+11
	k(C_2H_5•,s)	10400	1.00E+11
	k(C_2H_5•,t)	10400	1.00E+11
Radical (p: primary, s: secondary, etc.)	k(p,p)	13500	1.00E+11
	k(p,s)	11200	1.00E+11
	k(p,t)	9000	1.00E+11
	k(s,p)	14500	1.00E+11
	k(s,s)	12200	1.00E+11
	k(s,t)	10000	1.00E+11
	k(t,p)	15000	1.00E+11
	k(t,s)	12700	1.00E+11
	k(t,t)	10500	1.00E+11
Decomposition	k(μ→CH_3•)	31000	2.00E+13
	k(μ→p)	28700	2.00E+13
	k(μ→s)	27700	2.00E+13
	k(μ→t)	26700	2.00E+13
Isomerisation	k(5), k(6)	KINGAS[3]	KINGAS[3]
Termination	average value	0	3.00E+12

Table 2-1. Compilation of Kinetic Parameters used in the thermal cracking model of alkanes. [8]

2.4.Detailed free radical kinetic mechanism of the pyrolysis of $nC_{14}H_{30}$

When developing general detailed, mechanism-based kinetics models, it is necessary to account for the Reaction Path Degeneracy (RPD) which represents the number of possible paths by which an elementary step could proceed. Thus, in order to obtain a specific value of rate constant for every single radical reaction, it is necessary to calculate the product of RPD (of the given reaction) and the generic Arrhenius rate

constant, *k*: (Table 2-1), giving as a result a specific frequency factor for each specific reaction: RPD*k.

Figure 2-4 illustrates one reaction of every step of the free-radical kinetic mechanism for $nC_{14}H_{30}$, in order to obtain a better understanding of the developed mechanism.

For *Initiation Reactions*, the C-C bonds which undergo homolytic dissociation to form two free radicals will define the RPD. Therefore, for linear hydrocarbons whose chain consists of C-C pairs, there is only one possible path (RPD = 1) for breaking the C-C bond, located in the centre of the hydrocarbon chain, and in the case of the other C-C bonds, they can be obtained in two possible ways (RPD=2), e.g., obtaining the radicals: rCH_3 and $rC_{13}H_{27}$-1, can be possible by breaking the two equivalents bonds: C_1-C_2 or C_{13}-C_{14}.

Regarding *H-transfer Reactions*, the type of carbon atoms (primary, secondary, or tertiary) which undergoes the hydrogen abstraction to form a radical $\mu^{\bullet}$ will define the RPD. For example, in the formation of a primary radical such as $rC_{14}H_{29}$-1, there are six equivalents ways (RPD=6) to transfer the H atom, as a result of the two primary carbons (three C-H bonds) present in the $C_{14}H_{30}$ molecule, and (RPD = 4) in the case of the secondary carbons (two C-H bonds) in a linear chain.

In the case of *Decomposition (by β-scission) reactions*, the free radical breaks into two carbons from the charged carbon, producing an α-olefin and a primary free-radical, (RPD = 1).

Finally, regarding *Termination Reactions*, these represent essentially a recombination of all radicals formed, e.g., the termination reactions of the radical $rC_{14}H_{29}$-1, with all its isomers: $rC_{14}H_{29}$-1, $rC_{14}H_{29}$-2, $rC_{14}H_{29}$-3, $rC_{14}H_{29}$-4, $rC_{14}H_{29}$-5, $rC_{14}H_{29}$-6, $rC_{14}H_{29}$-7. (Figure 2-5)

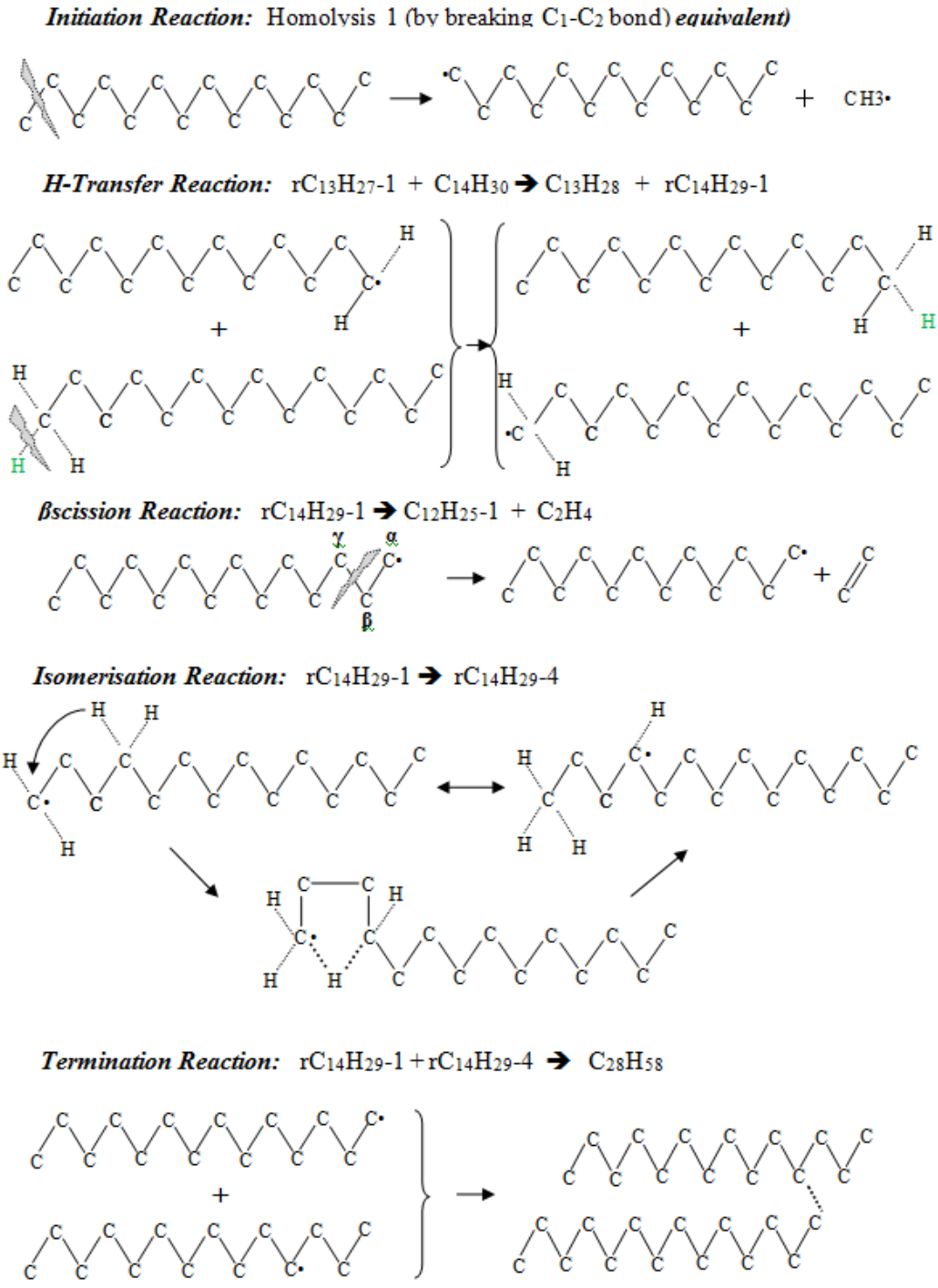

Figure 2-4. Some example of every step reactions from the detailed mechanism of thermal cracking of n-Tetradecane.

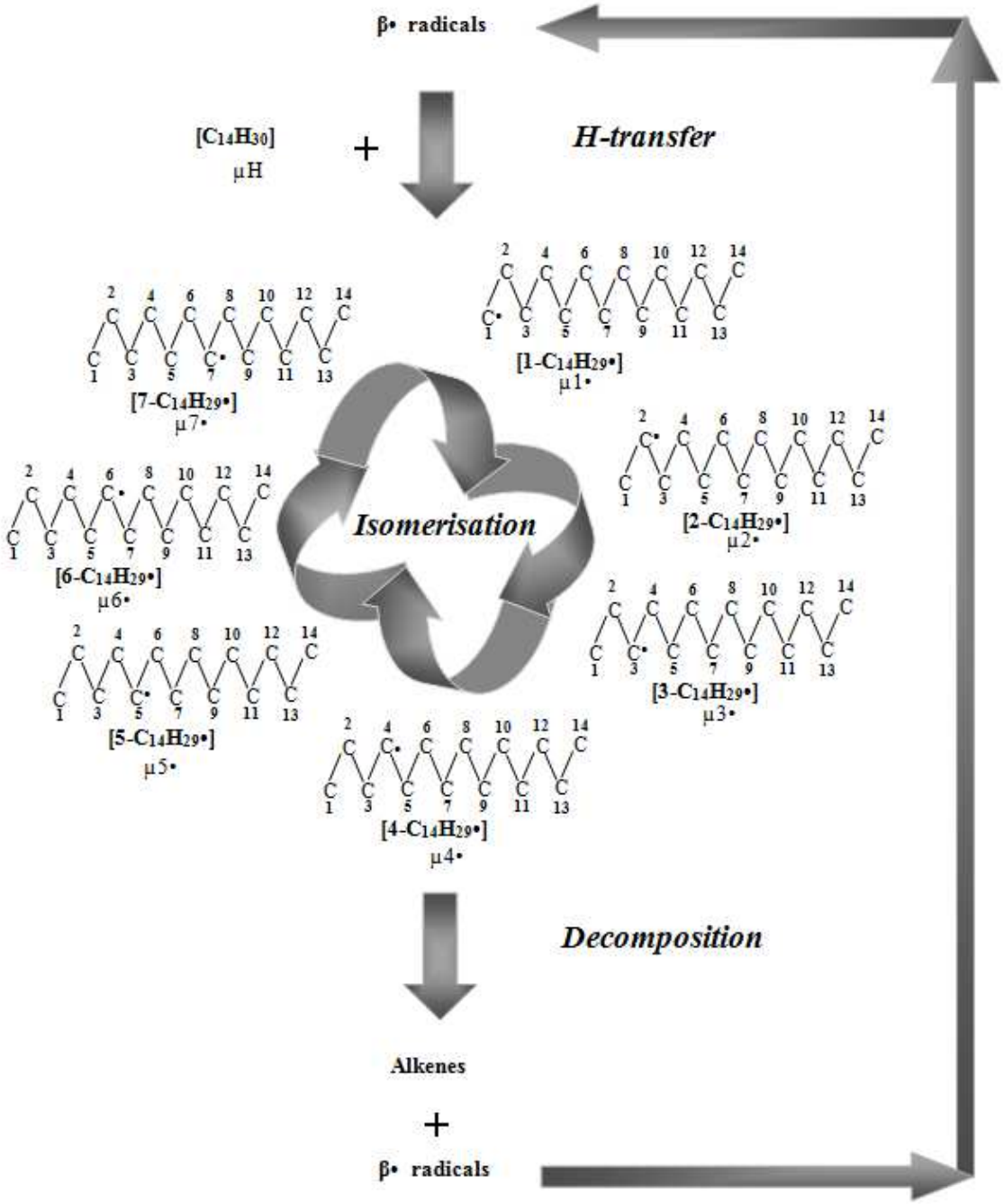

Figure 2-5. Scheme of the propagation chain of the pyrolysis of $nC_{14}H_{30}$.

2.5.Reduction of the free radical kinetic mechanism of the pyrolysis of $nC_{14}H_{30}$

In this thesis two methods of reduction have been used, based on chemical considerations [11]: *Lumping of chemical species* involves grouping all of the isomers of a radical, so that the number of species, and consequently the number of reactions, strongly decreases. This reduction is based on the fact that isomerisation reactions are

much faster than the propagation reaction, and hence the re-partitioning between isomers can be calculated independently [11] as depicted in Figure 2-5. Two indistinguishable lumped species are used: “radicals” (formed in the initiation reaction), and “alkanes” (formed in the decomposition reactions).

The second type of reduction used is the *Lumping of Reactions*, where all reactions of a given type are lumped together, so that the size of the mechanism is drastically reduced, with loss of molecular weight distribution but preservation of distribution between the families of products such as alkanes / alkenes.

The rate of lumped reaction needs to be equal to the sum of the rates of every detailed reaction in order to maintain equivalence. A summary of lumped rates is compiled in Table 2-2. In summary, the entire kinetic reduced mechanism includes 119 reactions (Table 2-3).

Reaction	Lumped Rate Constant
Initiation	$K\text{-}L_I$ = (# C-C homolysis)* $K\text{-}_I$
H-transfer	$K\text{-}L_{H\text{-}T} = n*K(s,s)$. (Table.1)
Decomposition	$K\text{-}L_D = K\text{-}_D* (1/n)$
Termination “μ•+μ•”	$K\text{-}L_T = K\text{-}_T* (n+1)/(2*n)$
Termination “β•+ β•”	$K\text{-}L_T = K\text{-}_T* (n+1)/(2*n)$
Termination “β•+ μ•”	$K\text{-}L_T = K_T$
n: number of μ• radicals	

Table 2-2. Summary of lumped rate constant.

Free-radical mechanism of $nC_{14}H_{30}$		
Reaction	**Detailed**	**Reduced**
Initiation	7	1
H-transfer	336	13
Decomposition	78	78
Termination “μ•+μ•”	28	1
Termination “β•+ β•”	134	13
Termination “β•+ μ•”	336	13
Isomerisation	80	0
Total	999	119

Table 2-3. Summary of detailed and reduced free-radical mechanism of $nC_{14}H_{30}$

2.6. Validation of the Kinetic Mechanisms for $nC_{14}H_{30}$, $nC_{16}H_{34}$ and $nC_{25}H_{52}$ with experimental published data.

In this Section, a comparison of the conversion of $nC_{14}H_{30}$, $nC_{16}H_{34}$ and $nC_{25}H_{52}$ is carried out, between the simulated results obtained from the Lumped Kinetic Models and the experimental results reported by Song et al. (1994) [13], Jackson et al. (1995) [14], and Behar et al.(1996) [15] respectively. In the case of $nC_{14}H_{30}$, a further comparison has been carried out, taking into account the simulated results obtained from the Detailed Kinetic Model.

2.6.1. Validation of the Reduced Kinetic Model of n-Tetradecane ($nC_{14}H_{30}$)

In order to validate the developed model for the pyrolysis of n-tetradecane at low conversion, the results obtained in this chapter are compared with corresponding experimental pyrolysis data published by Song et al. (1994) [13]. This experiment was conducted at 450 °C for 6-480 min, under an initial pressure of 0.69 MPa of ultra-high-purity (UHP) N_2 in 25 ml of an agitated, batch micro-reactor (micro-autoclave) using a 5 ml sample. An initial heating period of 6 minutes was required before the reaction temperature was reached, and based on the temperature profile published in the literature, the temperature ramp necessary to simulate the whole experiment was correlated.

As shown in Figure 2-6, very good agreement was achieved between the detailed, developed thermal cracking model of $nC_{14}H_{30}$ and the experimental data published by Song et al. (1994) [13], with an average error of 3.8%. A conversion of 0.5% of $nC_{14}H_{30}$ at 427°C was obtained at 3.43 minutes with the correlated ramp, and 4.5% conversion at 450°C (at 6.03 minutes). In comparison, the experimental data [13] reported a conversion of 3.98% at 450°C (at 6 minutes).

It is important to note that no adjustments of any kind were made to the kinetic parameters, and that the simulated results presented have been derived using only the kinetic data-set shown in Table 2-1.

It should be recalled that the good agreement between the developed model and the experimental data is due to the fact that the former is based on the molecular phenomenology of the thermal cracking mechanism. However, it is important to bear in

mind that at this stage the model caters only for the primary mechanism, and requires to be further developed to cover the secondary chain reaction mechanism in order to reliably represent the whole conversion, and more precisely the evolution of the concentration of the decomposition products.

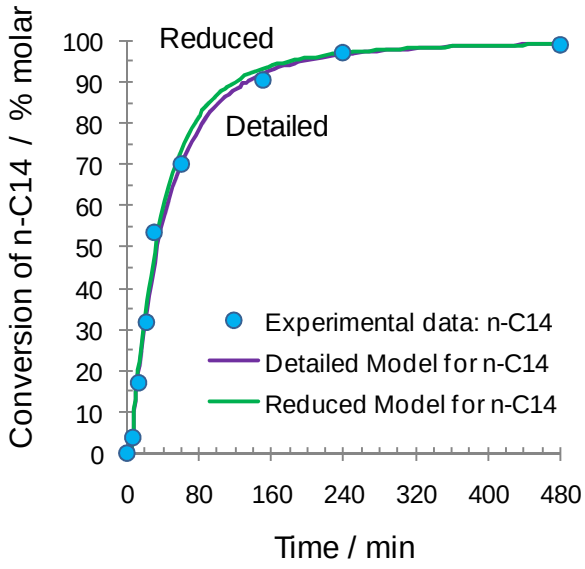

Figure 2-6. Comparison of the reduced thermal decomposition model developed for $nC_{14}H_{30}$, and the thermal decomposition experiments of Song et al. (1994) [13], until 100% conversion.

Regarding the *reduced model* developed for thermal cracking of $nC_{14}H_{30}$, very good agreement was also found (preserving the physical meaning of the thermal cracking) with the experimental data of Song et al. [13], with an average error of 5.4%, compared with an average error of 3% for the developed *detailed model*. (Figure 2-6).

It is important to point out that it is valid to use a *lumped mechanistic kinetic model* for extrapolated predictions in a wide range of temperature, because it is based on physico-chemical phenomena and also that this model has been neither optimized nor adjusted.

Moreover, the pyrolysis model developed in this thesis, not only yield information on the conversion of the reactant, but also give information of the production of pyrolysis products, during the thermal cracking of the reactants, which have to be approach very carefully, since in this work only a primary mechanism has been developed.

Because of the excellent agreement between the developed *Reduced* and *Detailed Models*, only the *Lumped Kinetic Model* of n-hexadecane ($nC_{16}H_{34}$) and n-Pentacosane ($nC_{25}H_{52}$) were developed, without the need to develop corresponding *Detailed Models*.

Thus, in the case of $nC_{16}H_{34}$ and $nC_{25}H_{52}$ a comparison of its conversion was carried out between the *Lumped Kinetic Model* and the corresponding experimental data from Jackson et al. (1995) [14] and Behar and et al.(1996) [15] respectively.

2.6.2. Validation of the Reduced Kinetic Model of n-Hexadecane ($nC_{16}H_{34}$)

The directly developed *Reduced Kinetic Model* of $nC_{16}H_{34}$ features 152 reactions: 1 initiation reaction; 1 H-transfer feeding reactions; 14 H-transfer reactions; 105 decomposition reactions; 1 "μ•+μ•" termination reaction; 15 "μ•+β•" termination reactions; and 15 "β•+ β•" termination reactions. The whole mechanism has 65 different species: 16 alkanes formed, 14 alkenes formed, 16 intermediate species (radicals), 17 final products, and 2 lumped species: "radicals" and "alkane".

Regarding the validation for $nC_{16}H_{34}$, results were compared for the reduced model with the experimental results published by Jackson et al. (1995) [14], who used a gold (Au) bag reaction vessel in their study. After loading 70 g of hexadecane solution, N_2 was applied initially to remove reactive gases, such as O_2, and then pressurized until the N_2 gas in the headspace was expelled, leaving only the hexadecane solution.

Good agreement was obtained for the conversion of $nC_{16}H_{34}$ (Figure 2-7) with the two isothermal experiments at 370°C and 353°C, with a relative average error of 17.9% and 17.4% respectively.

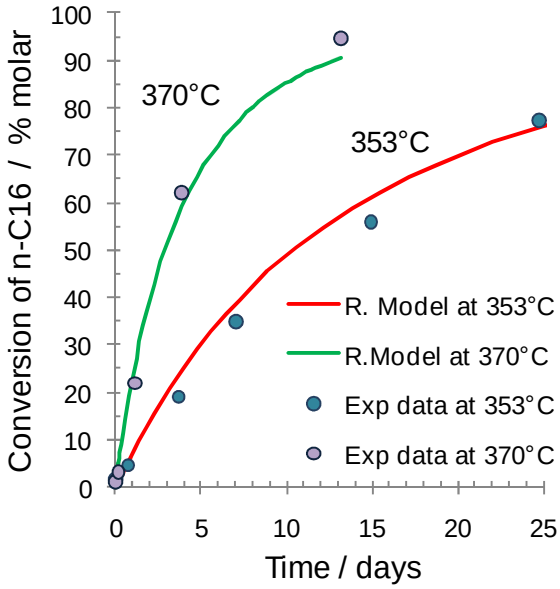

Figure 2-7. Validation of the reduced thermal decomposition model developed for $nC_{16}H_{34}$, and the thermal decomposition experiments of Jackson et al.(1995) [14].

Another important aspect of the validation is the lack of information on the accuracy of the literature experimental data which entails an important error, highlighting the need for developing and undertaking specific experiments which will provide reliable data for which the analytical accuracy is known.

2.6.3. Validation of the Reduced Kinetic Model of n-Pentacosane ($nC_{25}H_{52}$)

The directly developed *Reduced Kinetic Model* of n-pentacosane ($nC_{25}H_{52}$), has 350 reactions: 1 initiation reaction; 1 H-transfer feeding reaction; 23 H-transfer reactions; 276 decomposition reactions; 1 "μ•+μ•" termination reaction; 24 "μ•+β•" termination reactions; and 24 "β•+ β•" termination reactions. The whole mechanism has 101 different species: 25 alkanes formed; 23 alkenes formed; 25 intermediate species (radicals), 26 final products, and 2 lumped species: "radicals" and "alkane".

Lastly, we have validated the results of the reduced developed model for n-pentacosane ($nC_{25}H_{52}$) with the experimental data published by Behar and et al. (1996) [15]. In this publication, a gold (Au) reaction tube was used (40mm*5mm*0.1mm) under an Argon atmosphere, containing between 50 and 100 mg of $nC_{25}H_{52}$. For the comparisons, an average value of 75 mg of $nC_{25}H_{52}$ was assumed (or 0.96 ml), equivalent to 99.15% nC_{25} and 0.85%(molar) of Ar.

As can be observed in Figure 2-8, very good agreement was obtained between the conversion of $nC_{25}H_{52}$ with the two isothermal experiments at 375 °C and 400 °C, with a relative error average of 6.7% and 7.0% respectively compared to the results obtained by Behar et al. (1996) [15].

As a global conclusion, the developed *Lumped Mechanistic Kinetic Model* for every hydrocarbon preserves the physical meaning of thermal cracking in a wide range of temperatures, as was the case with $nC_{14}H_{30}$, $nC_{16}H_{34}$ and $nC_{25}H_{52}$, without any previous optimization or adjustments made. And similarly, very good agreement was achieved in the three cases studied, even when using the developed *Reduced Model*.

Whilst the mechanistic, *Kinetic Reduced Model* has proved reliable in the case of long chain hydrocarbons, such as $nC_{14}H_{30}$, $nC_{16}H_{34}$ and $nC_{25}H_{52}$, it would be interesting, nevertheless to undertake validation of longer chain hydrocarbons, such as $nC_{40}H_{82}$ and $nC_{60}H_{122}$, for which lumped mechanistic kinetic model has been developed in this thesis. This subject may therefore be examined in a future work.

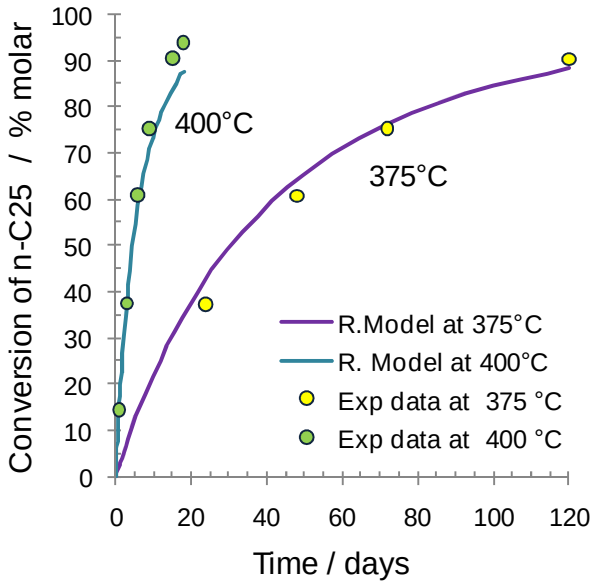

Figure 2-8. Validation of the reduced thermal decomposition model developed for $nC_{25}H_{52}$, and the thermal decomposition experiments of Behar et al.(1996) [15].

	Single Component		Final Mixture of heavy n-alkanes
	$nC_{14}H_{30}$		$C_{14}+C_{16}+C_{20}+C_{25}+\ldots+C_{80}$
	Detailed	Reduced	Reduced
Reactants	1	1	15
Reactions	999	119	7055
Species	96	57	336
Molecules	41	43	242
Radicals	55	14	94

Table 2-4. Summary of size of the mechanistic kinetics models developed.

Finally, a *reduced mechanistic kinetic model* was developed for each n-alkane hydrocarbon in the mixture comprising: $nC_{14}H_{30}$, $nC_{16}H_{34}$, $nC_{20}H_{42}$, $nC_{25}H_{52}$, $nC_{30}H_{62}$, $nC_{35}H_{72}$, $nC_{40}H_{82}$, $nC_{45}H_{92}$, $nC_{50}H_{102}$, $nC_{55}H_{112}$, $nC_{60}H_{122}$, $nC_{65}H_{132}$, n $C_{70}H_{142}$, $nC_{75}H_{152}$, $nC_{80}H_{162}$. This model of the final mixture of n-alkanes accounts for: 15 reactants; 7055 reactions; 336 species; 242 molecules; and 94 radicals (Table 2-4).

2.7.Preliminary modelling of thermal cracking of heavy alkanes at GC (P&T) conditions

This model has been used at specific conditions of temperature, pressure, volume and concentration of the heavy hydrocarbon mixture in the carrier gas (He) of a gas chromatographic column, in order to obtain a better understanding of its thermal cracking behaviour and stability.

As described in the previous sections, thermal cracking decomposition is a function of temperature and residence time. Therefore, in order to obtain a more precise knowledge of the behaviour of n-alkane samples (i.e. nC_{14}, nC_{16}, nC_{25} mixtures) as a function of temperature and time, several simulations were made at various isothermal temperatures, examining the exposure-time limits, and temperature at which n-alkanes start to crack at GC conditions.

Using a column with the following dimensions: length = 30m, internal diameter = 0.25mm, stationary phase thickness = 0.5µm, the empty column volume is 1.46 cm^3, for which a system pressure of 2 bars was assumed.

2.7.1. Preliminary Modelling of $nC_{40}H_{82}$ at constant temperatures

The concentration of n-alkanes sample diluted in helium at the moment of injection in the inlet varies with the level of CS_2 dilution applied, the flow of carrier gas (helium), and the split-ratio used with the capillary column. We have therefore studied the conversion of $nC_{40}H_{82}$ at two concentration levels, of 4% and 46% of sample in helium, in order to analyze the influence of the concentration of the sample on the rate of thermal decomposition.

Figure 2-9 shows that for $nC_{40}H_{82}$, at a lower concentration of 4% molar in helium, at 350 °C and 360 °C, the thermal cracking starts at 35 min and 15 min respectively, at a very low rate. However, at 370 °C, 380 °C and 400 °C, the residence times necessary to initiate thermal decomposition are only 7.5 min, 3.7 min and 0.9 min respectively, with corresponding times of 50 min, 23 min and 6 min respectively for achieving 1% conversion.

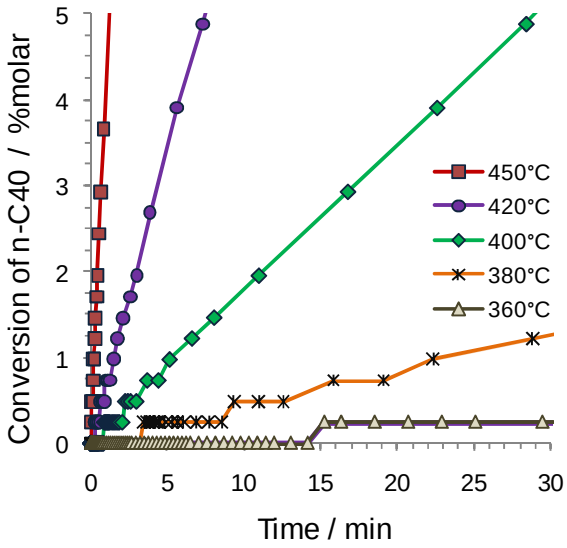

*Figure 2-9. Thermal cracking of $nC_{40}H_{82}$ at 5 constant temperatures. Column: (30m*0.25mm*0.5µm). (Molar concentration: 4% in helium).*

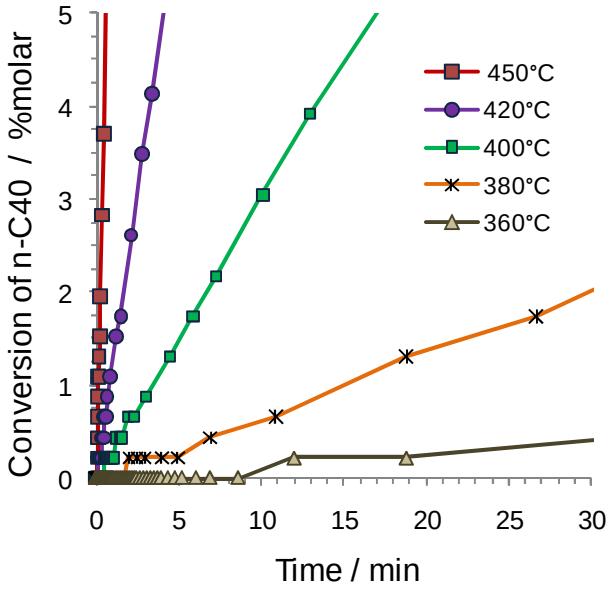

*Figure 2-10. Thermal cracking of $nC_{40}H_{82}$ at 9 constant temperatures. Column: (30m*0.25mm*0.5µm). (Molar concentration: 46% in helium).*

At temperatures of 420°C, 430°C, 440°C and 450°C the residence times required to trigger thermal degradation of $nC_{40}H_{82}$ at 4% molar concentration in helium , fall to less than 1 min, namely 16 s, 9 s, 5 s and 3 s respectively. And after exposure of 5 minutes to these temperatures the corresponding levels of thermal degradation increase to 3.5%, 6.3%, 11%, and 19.5% molar.

Temperature (°C)	$nC_{40}H_{82}$ (n-Tetracontane)			
	4% in Helium		46% in Helium	
	time	% degradation	time[=] min	% degradation
350	35min	0.24	23min	0.22
360	15min	0.24	12min	0.22
	115min	1	78min	1
370	7.5min	0.24	3.8min	0.22
	50min	1	32min	1
380	3.7min	0.24	2min	0.22
	23min	1	15min	1
400	53sec	0.24	26sec	0.22
	6min	1	5min	1.5
420	16sec	0.24	7sec	0.22
	5min	3.5	5min	6
430	9sec	0.24	4sec	0.22
	5min	6.3	5min	11
440	5sec	0.24	2sec	0.22
	5min	11	5min	20
450	3sec	0.24	1sec	0.22
	5min	19.5	5min	33.5

Table 2-5. Residence times and corresponding % thermal decomposition of nC_{40} (Tetracontane) under 9 isothermal temperatures, at 4% & 46% (molar) in helium.

Figure 2-10 shows the predictions for $nC_{40}H_{82}$ at 46% molar concentration in helium, where the predicted initiation times for thermal degradation are only 23 min at 350°C and 12 min at 360°C, but at very low rates. In the case of 370°C, 380°C and 400°C, the necessary residence times are 3.8 min, 2 min and 0.4 min respectively, to trigger thermal decomposition of $nC_{40}H_{82}$, achieving 1% molar degradation at 32 min, 15 min and 5 min. Increasing the temperatures further, to 420°C, 430°C, 440°C and 450°C, residence times of less than one minute are sufficient to initiate degradation of $nC_{40}H_{82}$; 7 s, 3.8 s, 2 s and 1.2 s respectively, with corresponding thermal degradation levels after 5 minutes exposure of 6%, 11%, 20%, and 33.5% molar.

Table 2-5 summarizes residence times, and the corresponding percentage of thermal decomposition of nC_{40}, for 4% and 46% molar concentrations in helium, for exposure at 9 isothermal temperatures.

2.7.2. Preliminary modelling of heavy n-alkanes mixtures using a temperature ramp

The thermal stability of three long-chain hydrocarbon mixtures (equimolar, light, and heavy) at 46% molar dilution in helium, has been modeled at 2 bars and for a temperature programmed analysis ($T_{initial}$=10 °C, ramp=15C/min, T_{final}= 425 °C). Compositional details of each of the mixtures are shown in Table 2-6.

%molar of Heavy Hydrocarbon Mixtures			
Heavy HC	**Equimolar**	**Heavy**	**Light**
$nC_{14}H_{30}$	14.29	2.04	26.53
$nC_{16}H_{34}$	14.29	6.12	22.45
$nC_{20}H_{42}$	14.29	10.2	18.37
$nC_{25}H_{52}$	14.29	14.29	14.29
$nC_{30}H_{62}$	14.29	18.37	10.2
$nC_{35}H_{72}$	14.29	22.45	6.12
$nC_{40}H_{82}$	14.29	26.53	2.04

Table 2-6. Molar compositions of synthetic heavy n-alkanes mixtures: ($nC_{14}H_{30}$ - $nC_{40}H_{82}$) for modeling.

Initially only the conversion of the heaviest and lightest hydrocarbons; $nC_{40}H_{82}$ and $nC_{14}H_{30}$ respectively, were studied as a function of exposure time in the above three mixtures comprising seven n-alkanes in the range of ($nC_{14}H_{30}$- $nC_{40}H_{82}$) at the given temperature program described above.

Figure 2-11 shows that the first heavy hydrocarbon to thermally crack is $nC_{40}H_{82}$, but requiring less time to crack in a heavy mixture than in an equimolar and a light mixture, and the last hydrocarbon to crack in the same mixtures is $nC_{14}H_{30}$, as expected, because of the greater number of moles in the heavy mixture. Hence at a given conversion, $nC_{40}H_{82}$ will crack first in the heavy mixture, then in the equimolar mixture and finally in the light mixture, since the rate of thermal cracking of the whole mechanism is related proportionally to the square root of concentration of reactant by the following equation [11]:

$$r_{global} = r_D \times [\mu^{\bullet}] = k_D \times \left(\frac{k_I}{k_T}\right)^{1/2} \times \sqrt{\mu H}$$

Equation 2-1

Conversely, $nC_{14}H_{30}$ in the heavy mixture is the hydrocarbon which takes longest to crack due to having the greatest rate of production by $nC_{40}H_{82,}$ which acts as a buffer to the rate of decomposition.

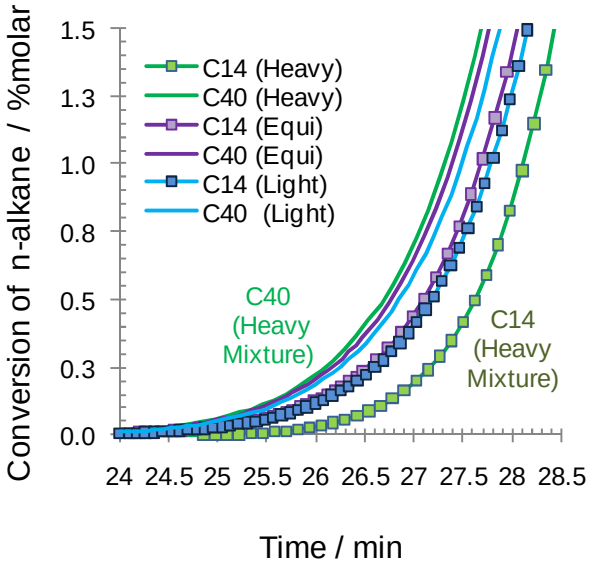

Figure 2-11. Thermal cracking conversion of $nC_{14}H_{30}$ & $nC_{40}H_{82}$ in three heavy n-alkanes mixtures (light, Equimolar, heavy) dissolved at 46% molar in He.

Secondly, the effect of the molar concentration of helium in three mixtures composed this time of fifteen n-alkanes in the range of: ($nC_{14}H_{30}$ - $nC_{80}H_{162}$), is studied as a function of the cracking time at 0.1% molar of conversion at the aforementioned temperature program. Compositional details of each of the mixtures are shown in Table 2-7.

Figure 2-12 shows, as expected that the greater the concentration of sample in He, the lower is the cracking time required in all of the cases studied. It should be noted that $nC_{14}H_{30}$ is not shown in this figure, since its rate of decomposition is far exceeded by its rate of production from partial decomposition of the heaviest hydrocarbons of the mixture: $nC_{80}H_{162}$.

Thus, in the case of $nC_{16}H_{34}$ it is evident that the same behavior is occurring; but since $nC_{16}H_{34}$ is also producing $nC_{14}H_{30}$ its decomposition rate is greater than in the case of $nC_{14}H_{30}$, presenting the longer time to crack among the n-alkanes in the mixture, in all the concentration of sample in He.

%molar of Heavy Hydrocarbon Mixtures			
Heavy HC	**Equimolar**	**Heavy**	**Light**
$nC_{14}H_{30}$	9.09	0.83	17.36
$nC_{16}H_{34}$	9.09	2.48	15.70
$nC_{20}H_{42}$	9.09	4.13	14.05
$nC_{25}H_{52}$	9.09	5.79	12.40
$nC_{30}H_{62}$	9.09	7.44	10.74
$nC_{35}H_{72}$	9.09	9.09	9.09
$nC_{40}H_{82}$	9.09	10.74	7.44
$nC_{50}H_{102}$	9.09	12.40	5.79
$nC_{60}H_{122}$	9.09	14.05	4.13
$nC_{70}H_{142}$	9.09	15.70	2.48
$nC_{80}H_{162}$	9.09	17.36	0.83

Table 2-7. Molar compositions of synthetic heavy n-alkanes mixtures: ($nC_{14}H_{30}$ - $nC_{80}H_{162}$) for modelling.

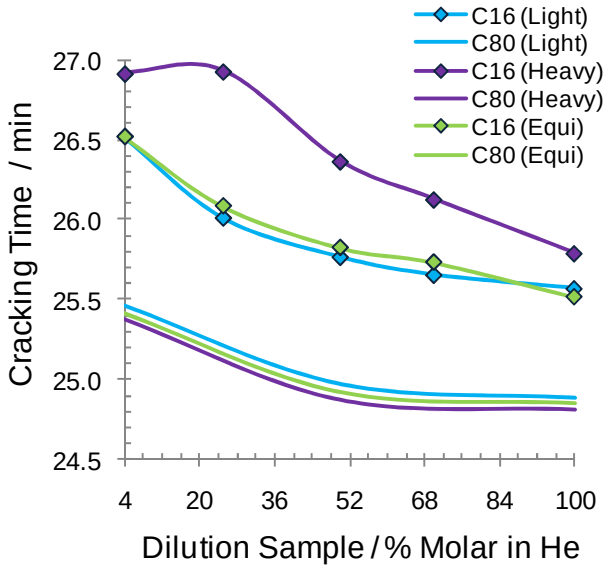

Figure 2-12. Thermal cracking of nC_{16}, nC_{30} & nC_{80} in three heavy n-alkanes mixtures (light, Equimolar, heavy) at 46% molar in He.

On the contrary, in the case of $nC_{80}H_{162}$ it is possible to discern that the ascending order of cracking time is guided by the number of moles in the mixture, as explained earlier, so that $nC_{80}H_{162}$ will crack first in a heavy mixture, then in the equimolar mixture; and finally in the light mixture, since no production of the heavier hydrocarbon is expected to take place.

2.8.Preliminary calculation of the minimum Single Carbon Number (SCN) at possible risk of thermal cracking at GC (P&T) conditions

In order to determine the lightest hydrocarbon at risk to crack inside a GC column, a new approach is introduced and proposed in this thesis, based on the calculation of the intercept between the retention time curve of n-alkanes standard mixtures [$nC_{10}H_{22}$-$nC_{75}H_{152}$] in an HT5 column and some low iso-conversion (0.1%, 1% and 7%) curves describing the minimal time required to trigger the thermal decomposition in the same range of SCN. To that end, the developed pyrolysis model was applied to the n-alkanes above mentioned in equimolar mixtures at three different dilutions in He, of 4% and 95% molar.

According to Figure 2-13, for the whole range of n-alkanes, the greater the concentration of sample in Helium, the lower the pyrolysis time required at a given conversion, as depicted for all the iso-conversion curves at 95% molar in Helium relative to the ones at 4% molar in Helium.

As far as the iso-conversion curves are concerned, the greater the conversion of any of the n-alkanes studied, the greater the exposure time required. Hence, a lower pyrolysis time is obtained when the molar conversion of 0.1% is achieved, and a greater residence times are required at the molar conversion of 7%, as expected.

The intercept between the pyrolysis iso-conversion and the GC retention time curves represents the minimum n-alkane which will thermally crack before eluting from the GC column. Therefore, $nC_{50}H_{102}$ reaches a molar conversion of 0.1% before eluting the GC column, in the studied conditions.

Almost at about the same time (with a difference of seconds) all the heavier n-alkanes than $nC_{50}H_{102}$ reach the same pyrolysis conversion at 25 minutes and 380°C(in agreement with Schwartz et al.(1987) [1] , but their residence times inside the GC column are much longer, allowing them to reach greater pyrolysis conversion before eluting, as in the case of $nC_{72}H_{146}$ whose elution time is 34 minutes, and therefore can thermally decompose at 7% of molar conversion before eluting the GC column.

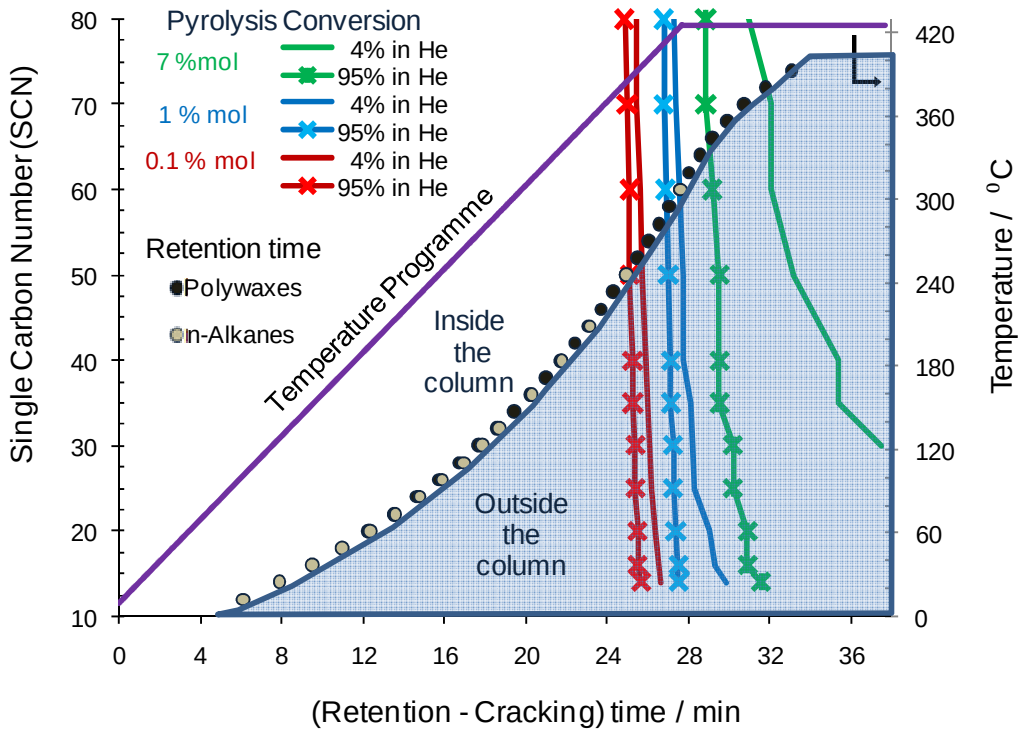

Figure 2-13. Retention time vs Cracking time as a function of single carbon number (SCN), for preliminary determination of the minimum SCN at risk to thermal crack in a GC column.

As a global conclusion, in the studied case, thermal cracking at 0.1 % of molar conversion occurs inside the GC column, at a concentration of 95% of sample in Helium for all the heavy n-alkanes greater than $nC_{50}H_{102}$, and at a concentration of 4% of sample in Helium, from $nC_{52}H_{104}$.

In the case of 1% molar conversion, the thermal cracking occurs from $nC_{55}H_{112}$ and $nC_{57}H_{116}$ at a concentration of 95% and 4% of sample in Helium respectively, before eluting the GC column.

2.9.Conclusions

This thesis provides a first insight into the limitations in the practice of high temperature gas chromatography (HTGC), regarding the dilution in carrier gas, residence time and maximal temperature conditions for a given sample, based on a developed mechanistic kinetic thermal cracking model, covering the range of n-alkanes

hydrocarbons: $nC_{14}H_{30}$, $nC_{16}H_{34}$, $nC_{20}H_{42}$, $nC_{25}H_{52}$, $nC_{30}H_{62}$, $nC_{35}H_{72}$, $nC_{40}H_{82}$, $nC_{45}H_{92}$, $nC_{50}H_{102}$, $nC_{55}H_{112}$, $nC_{60}H_{122}$, $nC_{65}H_{132}$, $nC_{70}H_{142}$, $nC_{75}H_{152}$, $nC_{80}H_{162}$.

A new approach for determining the minimum SCN undergoing pyrolysis inside the GC column has been introduced, based on the intercept of the thermal cracking and residence time curves, showing that for the cases studied in this chapter, the heavy hydrocarbons greater than nC_{50}-nC_{52} will crack before eluting from an HT5 column, in a mixture containing up to $C_{80}H_{162}$ at 0.1% of conversion, and from nC_{55}-nC_{57} at 1% of conversion. It should be noted that these results have been obtained only for the studied conditions presented throughout the chapter, and further studies will be required in order to obtain a better understanding on the limitation of HTGC practice in the analysis of heavy ends hydrocarbons.

Thus, future work on this subject may focus on the experimental validation of the pyrolysis model for heavy n-alkanes greater than $nC_{25}H_{52;}$ the modeling of the Gas chromatography migration and separation; and finally a coupled model (Pyrolysis + GC migration) and its respective GC validation.

2.10. References

[1] Schwartz, H.E., et al., *Simulated distillation of high-boiling petroleum fractions by capillary supercritical fluid chromatography and vacuum thermal gravimentric analysis.*, Analytical Chemistry, **59**(10), 1393-1401 (1987)

[2] Snijders, H., H.G. Janssen, and C. Cramers, *Optimization of temperature-programmed gas chromatographic separations .1. Prediction of retention times and peak widths from retention indices*, Journal of Chromatography A, **718**(2), 339-355 (1995)

[3] Rice, F.O. and K.F. Herzfeld, *The Thermal Decomposition of Organic Compounds from the Standpoint of Free Radicals. VI. The Mechanism of Some Chain Reactions*, Journal of the American Chemical Society, , **56**(2), 284-289 (1934)

[4] Oganesova, E.Y. and A.N. Rumyantsev, *Mechanism of pyrolysis of n-alkanes .4. Selectivity of interaction of hydrogen-atoms with c-h bonds at primary and secondary carbon-atoms,* Chemistry and Technology of Fuels and Oils, **23**(7-8), 342-345 (1987)

[5] Savage, P.E., *Mechanisms and kinetics models for hydrocarbon pyrolysis*, Journal of Analytical and Applied Pyrolysis, **54**(1-2), 109-126 (2000)

[6] Kee, R.J., F.M. Rupley, and J.A. Miller, Sandia National Laboratories Report, SAND89-8009, (1989)

[7] Benson, S.W., *Thermochemical Kinetics: Methods for the Estimation of Thermochemical Data and Rate Parameters*, 2nd ed, New York: Wiley-Blackwell, (1976)

[8] Bounaceur, R., et al., *Modelling of hydrocarbons pyrolysis at low temperature. Automatic generation of free radicals mechanism*, Journal of Analytical and Applied Pyrolysis, **64**, 103-122 (2002)

[9] Warth, V., et al., *Computer-aided derivation of gas-phase oxidation mechanisms: Application to the modeling of the oxidation of n-butane*, Combustion and Flame, **114**(1-2), 81-102 (1998)

[10] Bloch-Michel, V., *Logiciel d'estimation de paramètres cinétiques de processus élémentaires en phase gazeuse*,PhD thesis, l'Institut National Polytechnique de Lorraine, ENSIC: Nancy, France, (1995)

[11] Bounaceur, R., *Modélisation cinétique de l'évolution thermique des pétroles dans les gisements, « Kinetic modeling of the thermal evolution of crude oil in sedimentary basins* PhD thesis, l'Institut National Polytechnique de Lorraine, ENSIC: Nancy, France., (2001)

[12] Domine, F., et al., *Up to what temperature is petroleum stable? New insights from a 5200 free radical reactions model*, Organic Geochemistry, **33**(12), 1487-1499 (2002)

[13] Song, C.S., W.C. Lai, and H.H. Schobert, *Condensed-phase pyrolysis of n-tetradecane at elevated pressures for long-duration - product distribution and reaction-mechanisms*

Industrial & Engineering Chemistry Research, **33**(3), 534-547 (1994)

[14] Jackson, K.J., et al., *Temperature and pressure dependence of n-hexadecane cracking*, Organic Geochemistry, **23**(10), 941-953 (1995)

[15] Behar, F. and M. Vandenbroucke, *Experimental determination of the rate constants of the n-C-25 thermal cracking at 120, 400, and 800 bar: Implications for high-pressure/high-temperature prospects*, Energy & Fuels, **10**(4), 932-940 (1996)

CHAPTER 3 – MIGRATION & SEPARATION GAS CHROMATOGRAPHY MODELLING

3.1.Introduction

Reservoir fluid characterization by high-temperature gas chromatography (HTGC) extends the range of single carbon number (SCN) groups in oil analyses by temperature programming up to 450°C. However, the reliability of HTGC analyses is questionable for two main reasons: possible pyrolysis of the injected oil inside the GC column which could induce over-estimation of light and intermediate fractions; and secondly, possible incomplete elution of heavy fractions, which in turn would induce under-estimation.

The former, has been treated in CHAPTER 2 –[1], which focused on predicting the pyrolysis temperature of n-alkanes ($nC_{14}H_{30}$-$nC_{80}H_{162}$) at GC conditions. The latter is the focus of this chapter which introduces a gas chromatography migration and separation model for the n-alkane range $nC_{12}H_{26}$–$nC_{62}H_{126}$ in an HT5 column, using as main input the in-house distribution factors derived from isothermal GC retention time measurements.

On the basis of the developed model, the concentration and velocity of the above n-alkanes were determined at every point and time throughout the GC column, for typical temperature-programmed analyses.

Retention times were then predicted, and validated against experimental values, with an overall relative error within 2%. This chapter gives an insight into the components' behaviour throughout the GC column, allowing preliminary assessment of elution, by proposing a new approach for determining the non/incomplete elution of every component by introducing: the degree of elution, defined as the amount of component which has been eluted in relation to the amount injected. Thus, the degree of elution of each of the heavy n-alkanes studied in this chapter: ($nC_{12}H_{26}$–$nC_{62}H_{126}$) has been calculated for a typical temperature programmed.

This new approach can be applied, in order to determine the analytical conditions required for ensuring maximum elution of a given component, with the possibility of improving the practice of HTGC by optimizing the separation process.

3.2.Basic approach and terms in gas chromatography

Capillary gas chromatography is a well-established technique for separating constituent components in a mixture between two phases: a gaseous “mobile phase” assumed to behave ideally in most GC applications [2]; and a “stationary phase” consisting of a liquid bonded to, and distributed on the interior surface of the open tubular column. The mobile phase transports the mixture downstream within the column, while each component re-equilibrates between the two phases, after every displacement at a given temperature and pressure. The differences in the components’ partitioning ratios thus permit their separation.

When the separate analytes elute from the column in combination with the mobile phase, the mixture passes through a detector (generally a flame-ionization detector (FID)) generating a response which indicates the presence of the solute. The FID response to each solute should be ideally proportional to the solute amount or concentration, which is normally the case for hydrocarbons.

Ideally the chromatograms (plot of detector signal) should represent each solute as a vertical line, but as it migrates along the column it instead occupies a zone (or band) whose width gradually increases with time due to the dispersion of the component in the mobile and stationary phases.

Blumberg [3] has well explained two important approaches that will be used in the next section of this document: the solute zone, which corresponds to the space occupied by a solute migrating in a column; and the solute peak, which corresponds to the time that the solute zone will take for eluting from the column.

Ideally, using the probability theory, a solute injected very sharply (as a delta function), under the action of molecular diffusion, migrates in accordance with the random walk model, which states that at every time-step, each particle will travel the same space-step, either forward or backward with equal probability.

Then, at the limit of many steps, using the Central Limit Theorem the probable location of each particle approaches a normal distribution. Thus, the distribution of molecules along the column may be represented by a Gaussian zone (particles/ unit length) which elutes from the column as a nearly Gaussian peak (particles/unit time).

Therefore, the width of the solute zone and solute peak may be described by its standard deviations measured in units of length and time, respectively.

The specific moles profile (particles/unit length) [3-4] for every analyte can be obtained from the Gaussian distribution of the analytes through the column [5-6] (probability density function [particles/unit length]) and, yielding at (t=0) the Equation 3-1:

$$Molar\ Distribution\ = \frac{N(x, t_o)}{\sigma \cdot \sqrt{2\pi}} \exp\left[-\frac{(x - x_o)^2}{2\sigma^2}\right]$$

Equation 3-1

Here, σ corresponds to the standard deviation (in space units) of the amount of component throughout the GC column, x_0 corresponds to the centroid of its Gaussian distribution and x corresponds to the position of the component's dispersal around the centroid $x_{0.}$

Since the analytes initially present in the mixture injected into the GC column will not only diffuse but travel at the flow velocity of the carrier gas by advection throughout the column, the concentration profile of the analytes will vary with time and space according to the convection/diffusion conservation of mass equation, explained in the following section.

3.3.Mass balance (Diffusion-Convection) Equation in Gas Chromatography

Zone broadening under time-variant and non-uniform conditions (coordinate dependent: such as the density gradient of the carrier gas caused by the pressure drop), which change from the inlet to the outlet of the column can be described by a one-dimensional convective-diffusion mass-balance equation, after the Taylor [7] reduction of the cylindrical co-ordinate, mass-conserving equation for solute migrating in a capillary tube. [6] As such, the resulting equation is applicable to either isothermal or temperature programmed gas chromatography.

This approach was developed by Golay [4], taking into account the presence of a retentive layer, and became the most widely used equation in the theoretical analysis of chromatography in a non-uniform time-invariant linear medium. The non-uniformity in a chromatographic medium was considered a few years later by Giddings [8-11] by

dividing a column into small, equal segments, and assuming that the local conditions within each approach uniformity. They are then represented with any required precision when the number of segments becomes sufficiently large [9]. The mass balance of the solute[2-3] in an infinitely thin slice of column is described by Equation 3-2.

Here, $N_G(x,t)$ and $N_S(x,t)$ correspond to the moles per unit length in the gas phase and stationary phase respectively.

$$\frac{\partial N_G(x,t)}{\partial t} = -\frac{\partial}{\partial x}[N_G(x,t)\cdot \upsilon_M(x,t)] + \frac{\partial}{\partial x}\left[D(x,t)\cdot\frac{\partial N_G(x,t)}{\partial x}\right] - \frac{\partial N_S(x,t)}{\partial t}$$

Convection Diffusion Absorption

D represent the dispersion coefficient (assumed to be of physical interest only in the x-direction [4]) which represents all factors causing dispersion in a zone [12] (See Equation 3-7); and v_M is the velocity of migration of the carrier gas (see Equation 3-16).

The Absorption term, which describes the change with time of the moles in the stationary phase, can be expressed in terms of the moles in the gas phase by using the retention factor (ratio of moles of solute in the stationary phase to moles in the mobile phase), as follow:

$$\frac{\partial N_S(x,t)}{\partial t} = k\frac{\partial N_G(x,t)}{\partial t}$$

Therefore, by substituting the above expression as follow

$$\frac{\partial N_G(x,t)}{\partial t} = -\frac{\partial}{\partial x}[N_G(x,t)\cdot \upsilon_M(x,t)] + \frac{\partial}{\partial x}\left[D(x,t)\cdot\frac{\partial N_G(x,t)}{\partial x}\right] - k\frac{\partial N_G(x,t)}{\partial t}$$

$$(1+k)\frac{\partial N_G(x,t)}{\partial t} = -\frac{\partial}{\partial x}[N_G(x,t)\cdot \upsilon_M(x,t)] + \frac{\partial}{\partial x}\left[D(x,t)\cdot\frac{\partial N_G(x,t)}{\partial x}\right]$$

By rearranging, we obtain:

$$\frac{\partial N_G(x,t)}{\partial t} = -\frac{\partial}{\partial x}\left[N_G(x,t)\cdot\frac{\upsilon_M(x,t)}{(1+k)}\right] + \frac{\partial}{\partial x}\left[\frac{D(x,t)}{(1+k)}\cdot\frac{\partial N_G(x,t)}{\partial x}\right]$$

Where, "1/(1+k)" represents the frontal ratio or fraction of molecules in the mobile phase to those in the stationary phase, and v_{eff} and D_{eff} represent the effective cross-

sectional average velocity and dispersion coefficient obtained after multiplying the original values of v_M and D by "1/(1+k)".

$$\upsilon_{eff}(x,t) = \frac{\upsilon_M(x,t)}{(1+k)}$$

And

$$D_{eff}(x,t) = \frac{D(x,t)}{(1+k)}$$

Finally, by substituting the above expression, we finally obtain :

$$\frac{\partial N_G(x,t)}{\partial t} = -\frac{\partial}{\partial x}[N_G(x,t)\cdot\upsilon_{eff}(x,t)] + \frac{\partial}{\partial x}\left[D_{eff}(x,t)\cdot\frac{\partial N_G(x,t)}{\partial x}\right]$$

Equation 3-2

The separation is assumed to be linear, i.e., the diffusivity and velocity of the solute are independent of concentration [13]. Another consequence of the linearity assumption is the possibility of treating individually, each component of a complex mixture, enabling its migration to be studied separately. [13]

Although both the velocity of the analyte and its dispersion at each specific location are functions of the coordinate of the location, the distance travelled, *x* is insufficient for prediction purposes as the mass balance will not be conservative. Therefore a general theory of chromatography in a non-uniform, time-variant medium has been introduced, based on a more general equation of convective diffusion in a one-dimensional medium. [5, 13]

The relationship of band broadening to the kinetics of mass transfer in gas chromatography, has been described and validated in open tubular columns by Golay [4], who expressed the column plate height (H(x,t)) as a spatial rate of dispersion of a zone (Equation 3-3), and the apparent diffusivity D, as a representation of the zones' temporal dispersion rate. (Equation 3-4).

$$\frac{d\sigma^2}{dx} = H(x,t)$$

Equation 3-3

$$\frac{d\sigma^2}{dt} = H(x,t) \cdot \upsilon_M(x,t) = \ 2 \cdot D(x,t)$$

Equation 3-4

Thus, Golay [4] derived an exact equation to relate the band broadening and the kinetics of mass transfer in gas chromatography for open tubular columns with a smooth retentive coating, in very good agreement with experimental results.

$$H(x,t) = 2 \cdot \frac{D_M(x,t)}{\upsilon_M(x,t)} + \ \upsilon_M(x,t) \left\{ \left[\frac{1 + 6 \cdot k\big(T(t)\big) + 11 \cdot k(T(t))^2}{24 \cdot [1 + k\big(T(t)\big)]^2} \cdot \frac{{r_o}^2}{D_M(x,t)} \right] + \left[\frac{2 \cdot k\big(T(t)\big)}{3 \cdot [1 + k\big(T(t)\big)]^2} \cdot \frac{w^2}{D_s(x,t)} \right] \right\}$$

Equation 3-5

Golay [4], compared his chromatographic expression for a column plate height of circular cross-section and for coated tubular columns (Equation 3-5), with the van Deemter equation of the HETP (Height Equivalent to a Theoretical Plate) of packed columns (Equation 3-6). The Eddy-diffusion term, A which represents the diffusion caused by the multiple paths taken by the carrier gas flowing through a packed column is eliminated, there being but a single flow-path option in a coated tubular column.

$$H(x,t) = A + \frac{B}{\upsilon_M(x,t)} + \ C \cdot \upsilon_M(x,t)$$

Equation 3-6

The first term corresponds to the B term in the van Deemter equation (Equation 3-6), which represents the static longitudinal diffusion; the second term related to D_M (Diffusivity in the mobile phase)is absent in the van Deemter equation (Equation 3-6), and represents the dynamic diffusion of the sample; and the last term, related to Ds represents the mass transfer, and corresponds to the C term.

Golay [4] called this term the “hysteresis diffusion” of the sample, representing the diffusion of the sample between the gas-liquid interface and within the liquid phase. [4]

Therefore, by virtue of (Equation 3-4 and Equation 3-5) it is possible to derive the local dispersion term (Equation 3-7)which depends on the static longitudinal diffusion, the dynamic diffusion and the diffusion by forward mass transfer in the stationary phase:

$$D(x,t) = D_M(x,t) + \frac{v_M(x,t)^2}{2}\left\{\left[\frac{1+6\cdot k\big(T(t)\big)+11\cdot k(T(t))^2}{24\cdot[1+k\big(T(t)\big)]^2}\cdot\frac{{r_o}^2}{D_M(x,t)}\right] + \left[\frac{2\cdot k\big(T(t)\big)}{3\cdot[1+k\big(T(t)\big)]^2}\cdot\frac{w^2}{D_s(x,t)}\right]\right\}$$

Equation 3-7

In summary, the gas chromatographic migration and separation of a sharply injected sample can be described by the diffusion-convection mass balance equation (Equation 3-2). The variables required are: the effective diffusion and effective velocity of the sample, and the column specification.

3.4.Iterative Retention Time Prediction by Convective Migration Only

The use of discretization methods for calculating the retention times has been introduced by Snijders. [14] In his approach the diffusion effects are considered to be negligible in determining the peak position, enabling it to be described only by convection. [15]

The convection can be expressed by the effective velocity of the analyte in the carrier gas (Equation 3-18), which leads to:

$$v_{eff,i}(x,t) = \frac{dx}{dt} = v_M(x,t)\cdot\frac{N_{i,M}}{N_{i,M}+N_{i,S}} = \frac{v_M(x,t)}{1+\frac{K_i\big(T(t)\big)}{\beta}}$$

Equation 3-8

Then, discretization of the velocity into finite time-steps leads to (Equation 3-9) ,which can be used to track the average position of the analyte at every time step, and hence prediction of the retention time of the analyte, when it reaches the column outlet.[14]

$$x_{i+1} = x_i + \frac{v_M(x_i, t_i)}{1 + \frac{K_i\left(T(t_i)\right)}{\beta}} \cdot \Delta t$$

Equation 3-9

3.5.Time & Coordinate-Dependent Parameters in GC Calculations

The application and solution of the transient diffusion-convection mass balance (Equation 3-2) for temperature-programmed gas chromatography require that all the parameters involved previously should be expressed as a function of time and coordinate. [16] The calculation of these parameters is treated in the following section.

In all of the simulations carried out, each of the parameters has been related to the two main dependent variables, time and x-coordinate.

3.5.1. Coordinate-dependent pressure

By virtue of Boyle's Law the average carrier gas flow velocity under steady state (constant mass flow of carrier gas through any cross-section of the column at any given time interval), can be expressed as:

$$P(x = 0) \cdot v_M(x = 0, t) = P(0) \cdot v_M(0, t) = P(x) \cdot v_M(x, t)$$

Equation 3-10

The steady-state motion of the carrier gas in capillary gas chromatography is described by the differential form of the Hagen–Poiseuille equation (left-hand part of (Equation 3-11) [17-18]. It is obtained by relating the carrier gas velocity at any position in the column, to the pressure gradient at that point [19] by a proportional constant q. Substituting the expression of velocity (v_M) from (Equation 3-10) into the left-hand part of (Equation 3-11), we obtain the right-hand part of (Equation 3-11) which relates the local pressure drop at position x, with the initial value of velocity and pressure:

$$\frac{dP(x)}{dx} = -q \cdot v_M(x, t) = -q \cdot \frac{P(0) \cdot v_M(0, t)}{P(x)}$$

Equation 3-11

Thus, the Hagen-Poiseuille equation can be applied to a differential element in gas chromatography by the assumption of incompressibility of the gas in such an element at position x, due to its extremely low pressure drop [18].

By integrating (Equation 3-11), in the inlet and outlet position, with P_{in} and P_{out} respectively and rearranging we obtain the expression (Equation 3-12) which permits calculation of pressure at any position in the column:

$$P(x) = \sqrt[2]{{P_{in}}^2 - \left({P_{in}}^2 - {P_{out}}^2\right) \cdot \frac{x}{L}}$$

Equation 3-12

For the purpose of this thesis, an SGE HT5 column of 12 m has been used (Table 3-1). The profile of pressure drop with x-coordinate has been calculated assuming the outlet pressure to be atmospheric and the inlet pressure has been set to be 119.6 ± 0.5 kPa, in accordance with gas hold-up time measurements, t_0 for methane.

SGE HT5 Column		
Lengh	12	m
diameter	0.53	mm
film thickness	0.15	µm

Table 3-1. Column Dimensions of the in-house HTGC

3.5.2. Time-dependent Temperature

For a temperature programmed analysis, Equation 3-13 describes the temperature ramp followed by the GC oven.

$$T(t) = To + rampT \cdot \Delta t$$

Equation 3-13

This has been used for the purpose of the simulations presented in this article, e.g. the basic temperature program shown in Table 3-2.

To (°C)	10
Hold at To (min)	0
ramp of T (°C/min)	15
Tmax (°C)	425
Hold at Tmax (min)	12

Table 3-2. Temperature Programming

3.5.3. Viscosity of the carrier gas (η_m)

The carrier gas viscosity can be assumed to be dependent only on temperature and therefore independent of pressure as long as density changes caused by the pressure drop are negligible.

The expression used in the case where the carrier gas is helium, has been introduced by Kestin [20] and simplified by Hawkes [21], giving the viscosity in μPa·s.

This algorithm can be applied for temperatures above 104 K (-169 °C), where viscosity predictions for the HTGC temperature range show a maximum deviation of about 0.5%.

However, a correction can be made when using this equation in the range of (300-700) K [21] The derived values from Equation 3-14 may be optimized by multiplying a correction factor,$\{0.995+(T-300)\cdot 2.5\cdot 10^{5}\}$, to match experimental data within 0.1%. [21]

$$\eta\big(T(t)\big) = 0.7840374 \cdot T(t)^{\frac{1}{2}} \cdot \frac{f}{\Omega}$$

$$f = 1 + \frac{3}{196} \cdot (8 \cdot 10^{-7})^2$$

$$\alpha = 13.65299 - Ln(T^*)$$

$$T^* = (T(t))/10.4$$

$$a = -0.126516$$

$$b = -1.230553$$

$$c = 2.171442$$

$$E = 1 + \frac{1}{4 \cdot \Omega}\left\{\frac{-2 \cdot \Omega}{\alpha} + 0.00635209 \cdot \alpha^2 \cdot \left[\frac{-2 \cdot a}{Ln(T^*)^3} - \frac{3 \cdot b}{Ln(T^*)^4} - \frac{4 \cdot c}{Ln(T^*)^5}\right]\right\}$$

$$\Omega = 0.00635209 \cdot \alpha^2 \cdot \left[1.04 + \frac{a}{Ln(T^*)^2} + \frac{b}{Ln(T^*)^3} + \frac{c}{Ln(T^*)^4}\right]$$

Equation 3-14

The carrier gas viscosity is a function of temperature, which in turn is a function of time when temperature programming is involved (Table 3-2). Figure 3-1 illustrates the increase in viscosity of Helium with temperature and therefore with time, using a temperature ramp of 15 °C/min. Its viscosity increases from $19.4 \cdot 10^{-6}$ Pa.s at 10 °C (at time 0) reaching a maximum of $36.3 \cdot 10^{-6}$ Pa.s at the upper temperature limit of 425 °C (27.67 min).

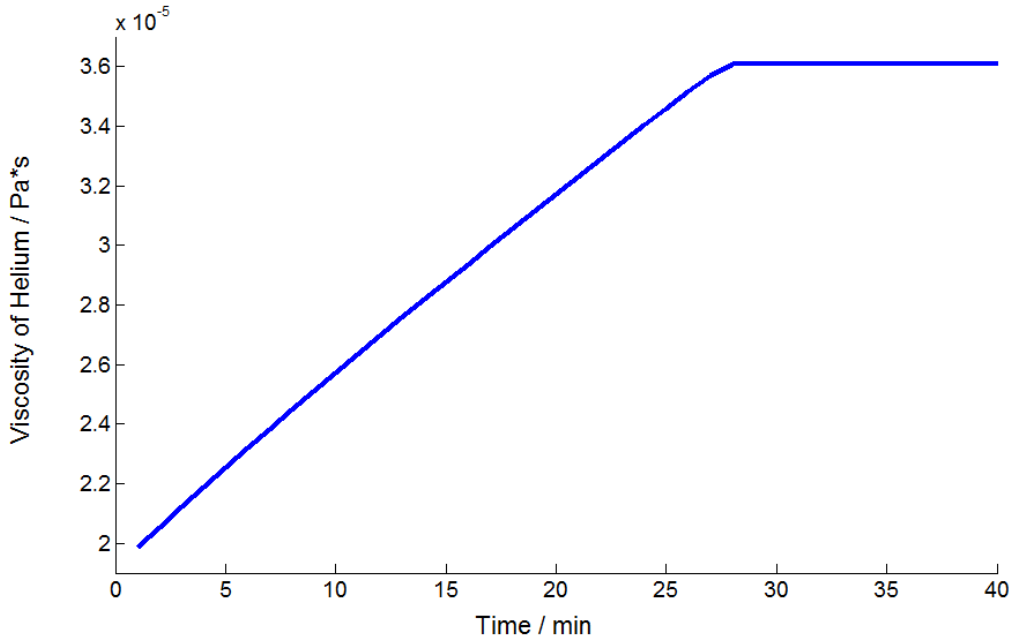

Figure 3-1. Viscosity of Helium as a function of time. (Temperature programming (Table 3-2): (From 10°C to 425°C, ramp of temperature:15C/min).

3.5.4. Velocity of the mobile phase (V_M)

The proportionality constant q of (Equation 3-11) for circular cross-section columns[4] is:

$$q = \frac{8 \cdot \eta\big(T(t)\big)}{{r_o}^2}$$

Equation 3-15

Then by integrating Equation 3-11 from the inlet to the outlet and using Boyle's Law (Equation 3-10) we obtain an expression describing the velocity profile of the mobile phase as a function of temperature, and therefore of time; and also as a function of pressure, and therefore of the x-coordinate position. [2, 16-19]

$$v_M(x,t) = \frac{{r_o}^2 \cdot \left({P_{in}}^2 - {P_{out}}^2\right)}{16 \cdot \eta\big(T(t)\big) \cdot L \cdot P(x)}$$

Equation 3-16

Based on the data in Table 3-1, the pressure has been calculated as a function of x-coordinate for the 12 m, HT5 column; and similarly the viscosity has been expressed as a function of temperature and hence time, using temperature programming (Table 3-2).

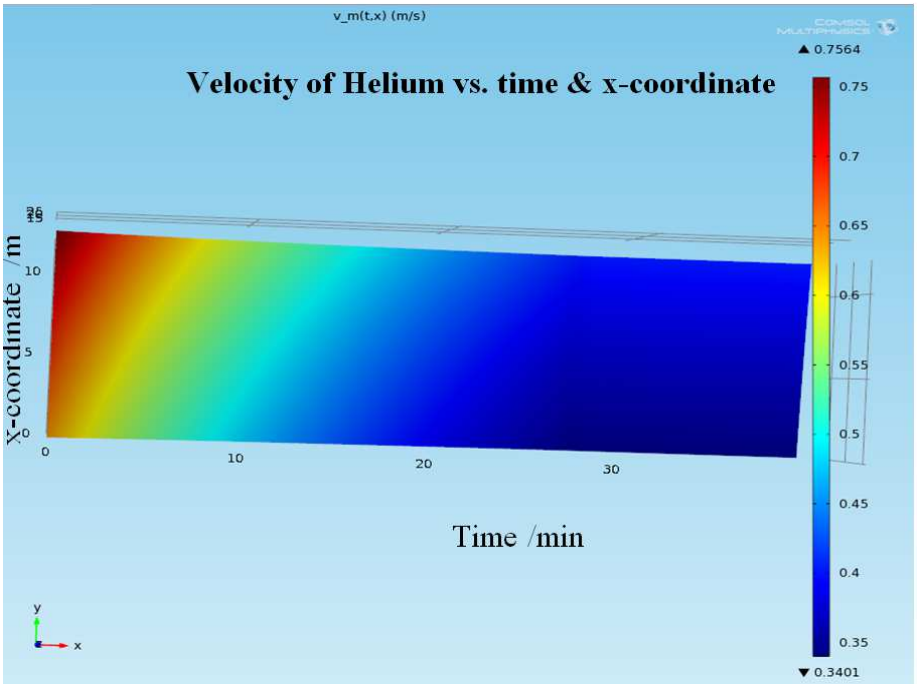

Figure 3-2. Velocity of Mobile phase as a function of time and x-coordinate (Temperature programming (Table 3-2): (From 10°C to 425°C, ramp of temperature:15C/min).

In relation to temperature, the maximum velocity of the mobile phase (helium) is found at the lowest values, and hence at the earliest times in the temperature program since the velocity is inversely proportional to its viscosity, which in turn increases with temperature (Equation 3-14).

In relation to the x-coordinate (i.e. distance travelled in the column), maximum velocity of the mobile phase is found at the highest value, at the column outlet, i.e., at. x = L. This is because velocity is also inversely proportional to the pressure (Equation

3-16), and the pressure drop is at maximum at the outlet of the column, at atmospheric pressure.

Thus, the velocity may vary from 0.35 m/s at the highest temperature (latest time) and the highest pressure (at the GC column inlet, and therefore the highest pressures) to 0.76 m/s at the lowest temperatures and lowest pressures, approaching the column outlet, as shown in Figure 3-3.

Therefore carrier gas velocity at the column inlet decreases as temperature increases with analysis time, a consequence of which is that the rate of desorption of the heavier components retained at the column inlet reduces as the analysis proceeds.

3.5.5. Diffusion constant, mobile phase (D_M)

The diffusion constant in the mobile phase may be calculated from the empirical method of Fuller, Schettler, and Giddings. [22]

$$D_M(x,t) = D_{AB}(x,t) = \frac{0.00100 \cdot T(t)^{1.75} \cdot \sqrt[2]{\frac{1}{MW_A} + \frac{1}{MW_B}}}{P(x) \cdot [(\sum v_A)^{1/3} + (\sum v_B)^{1/3}]^2}$$

Equation 3-17

Here, MW_A and MW_B are the molecular weight of the component in the sample, and of the carrier gas respectively, and υ_A and υ_B are the special atomic diffusion volumes calculated as a sum of all the atomic diffusion volumes increments (reported by Fuller et al. [22]) of the atoms involved in the molecule of interest. Thus, the greater the number of carbon atoms, the greater is the value of atomic diffusion volume.

The variation of the diffusivity in helium of n-alkanes; $nC_{20}H_{42}$ and $nC_{60}H_{122}$, has been analyzed under the temperature program described in Table 2-2.

According to Equation 3-17, the greater the temperature, the greater is the diffusivity of n-alkanes in helium; and conversely, the greater the pressure, and the heavier the n-alkane, the lower is the diffusivity in helium.

Therefore, the highest values of diffusivities apply to the lightest n-alkanes, at the highest temperatures (latest elution times) and the lowest pressures (approaching the GC column outlet), as shown in Figure 3-4.

Thus, $nC_{20}H_{42}$ at 425 °C (time>27.67 min) and atmospheric pressure (when approaching the GC column outlet) has the highest diffusivity of $6.06 \cdot 10^{-5}$ m^2/s; whereas $nC_{60}H_{122}$ has the lowest diffusivity value of $7.85 \cdot 10^{-6}$ m^2/s at the lowest temperature of 10 °C (initial time) and greatest pressure, at the GC column inlet.

Nevertheless, temperature is the most influential factor in the diffusivity of n-alkanes in He, as can be seen in Figure 3-4, where at the lowest temperature of 10 °C there is little evidence of variation of diffusivity with pressure and SCN (single carbon number) groups, compared with higher temperatures.

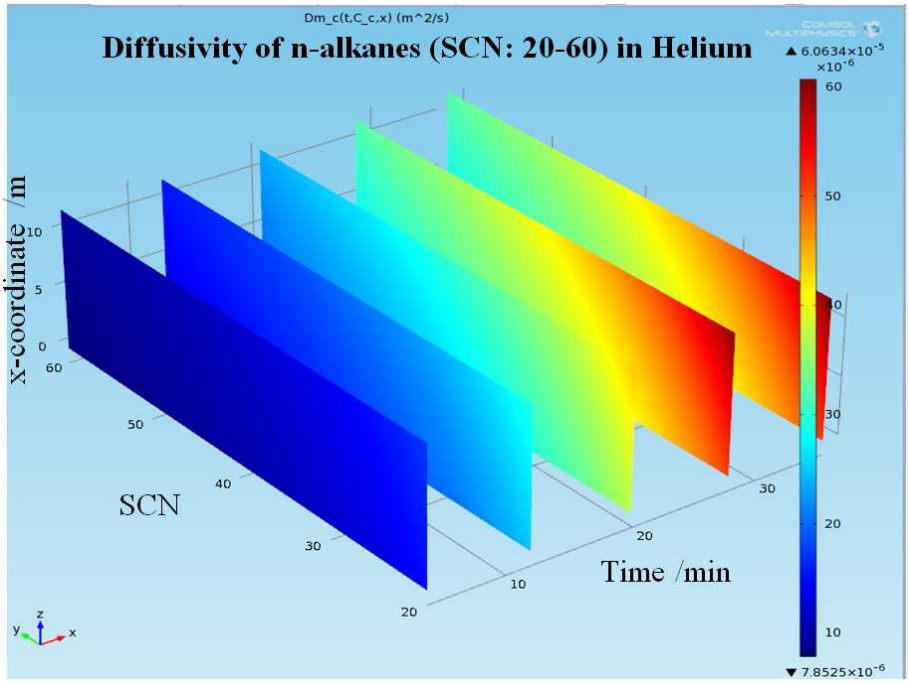

Figure 3-3. Diffusivity of n-alkanes (SCN: 20-60) in Helium (Temperature programming (Table 3-2): (From 10°C to 425°C, ramp of temperature:15C/min).

3.5.6. Diffusion constant, stationary phase (D_s)

The diffusion constant in the stationary phase is a very important parameter in gas chromatography, even although there is no model, to date, providing good accuracy for all systems which include a liquid solvent [16]. For that reason an approximate value is calculated from its relationship with the diffusion constant in the mobile phase [14] by the following expression:

$$D_S(x,t) = \frac{D_M(x,t)}{5 \cdot 10^4}$$

Equation 3-18

Accordingly, the diffusivity of n-alkanes in the stationary phase is directly proportional to their diffusivity in helium, and therefore the same correlations apply with temperature, the x-coordinate, and SCN.

The highest value of diffusivity in the stationary phase is $1.21 \cdot 10^{-9}$ m^2/s and corresponds to $nC_{20}H_{42}$ at 425 °C (time > 27.67 min), and atmospheric pressure (approaching the GC column outlet).

Thus, the lowest value of diffusivity in the stationary phase is $1.57 \cdot 10^{-10}$ m^2/s, corresponding to $nC_{60}H_{122}$ at the lowest temperature (at initial time), and greatest pressure (approaching the GC column inlet).

3.5.7. Effective Velocity (v_{eff})

The effective velocity is an average of the fraction of sample which flows in the mobile phase, equal to 1/(1+k), and moving at the velocity of the mobile phase v_M, and the fraction of sample which has been retained by the stationary phase with zero velocity, equal to k /(1+k).

$$v_{eff,i}(x,t) = \frac{v_M(x,t)}{1 + k_i\,(T(t))}$$

Equation 3-19

The effective velocities of $nC_{20}H_{42}$ and $nC_{60}H_{122}$, have been analyzed under the temperature program shown in Table 3-2.

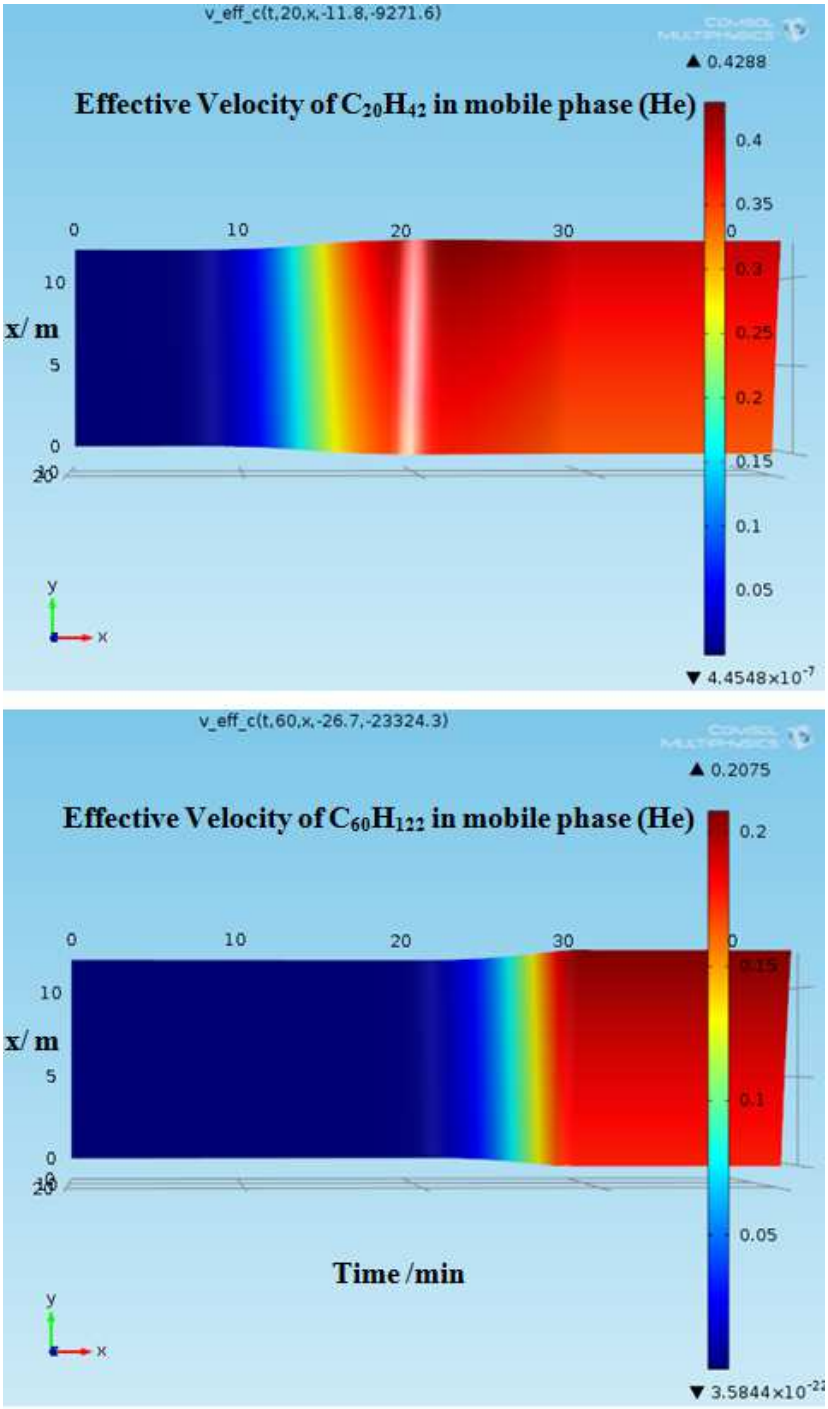

Figure 3-4. Effective Velocity of $nC_{20}H_{42}$ and $nC_{60}H_{122}$ in (He) in a 12m x 0.53mm x 0.15µm HT5 column. (Temperature programming (Table 3-2): (From 10°C to 425°C, ramp of temperature:15C/min).

Figure 3-5, clearly shows that the effective velocity has a low dependency on pressure and therefore on the x-coordinate. This contrasts with its high dependency on temperature, and therefore time, due to the retention factor being a function only of temperature (time). Consequently, its values are high compared with the values of velocity of mobile phase, which are a function of both pressure and temperature.

Thus, temperature is the predominant influential variable on a component's effective velocity in the mobile phase because of its powerful effect on retention factor.

The retention factor of a component determines its effective velocity, since the fraction of the component moving at the velocity of the mobile phase is given by the former. Therefore, at a given temperature, the greater the retention factor of a compound, the more strongly it will be retained in the stationary phase, and therefore the lower will be its fractions in mobile phase, making the effective velocity lower.

This explains why $nC_{20}H_{42}$ achieves a higher effective velocity at a lower temperature more quickly than $nC_{60}H_{122}$, as shown in *Figure 3-4*.

3.5.8. Effective Diffusivity (D_{eff})

In order to obtain the effective diffusivity (Equation 3-20), an analogous averaging method is used as in the case previously explained for V_{eff}. The effective diffusivity corresponds to the fraction of sample which is found in the mobile phase, equal to 1/(1+k), with a local dispersion D. The local dispersion takes into account its static longitudinal diffusion, the dynamic diffusion and the diffusion by mass transfer forwards the stationary phases according to (Equation 3-7):

$$D_{eff,i}(x,t) = \frac{D(x,t)}{1 + k_i(T(t))}$$

Equation 3-20

The effective diffusivities of two n-alkanes: $nC_{20}H_{42}$ and $nC_{60}H_{122}$ have been analyzed under the temperature program described in Table 3-2.

As in the case of the effective velocity, Figure 3-6, shows that the effective diffusivity exhibits a low dependency on pressure, and therefore on the x-coordinate, compared with its high dependency on temperature and therefore time.

Nevertheless, the local dispersion *D* (Equation 3-7), is not the same for every component, as is the case of the effective velocity, where the velocity of the mobile phase is independent of the proportion of the components flowing throughout the

column. Rather, local dispersion takes into account the diffusivity of every component in both the mobile and stationary phases, resulting in large variations between different components, depending on temperature, and hence retention factor.

Similarly to the effective velocity, the effective dispersion depends on the fraction of component which dwells in the mobile phase "1/(1+k)". Since this fraction is greater for the lightest components at a given temperature, then the effective dispersion will also be greater.

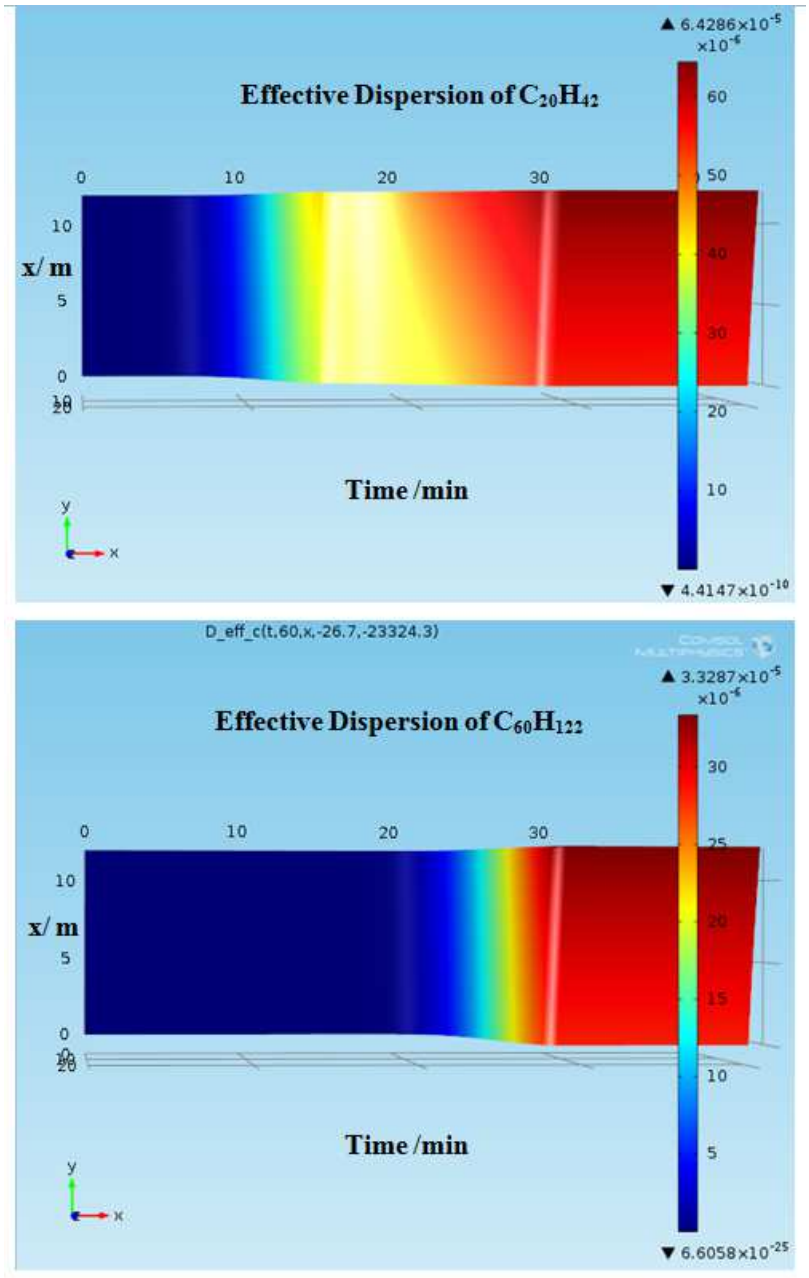

Figure 3-5. Effective Dispersion of $nC_{20}H_{42}$ and $nC_{60}H_{122}$ in (He) in a 12m x 0.53mm x 0.15µm HT5 column.(Temperature programming (Table 3-2): (From 10°C to 425°C, ramp of temperature:15C/min).

Thus, the heavier the component, the lower is the fraction of component which dwells in the mobile phase "1/(1+k)" at a given temperature, and the higher is the fractions which dwells in the stationary phase " k /(1+k)". Thus, the heavier components are longer retained in the stationary phase, until they reach a minimum temperature at which they start to be released from the stationary phase. Therefore, the retention times of the heavier components are greater than those of the lighter components. This, explains why $nC_{60}H_{122}$ takes longer to elute than $nC_{20}H_{42}$, since a higher temperature is required to release it from the stationary phase.

It is interesting to analysis that in spite of the fact that the effective dispersion (D(x,t)/1+k)) reaches lower values at a given temperature for the heavier components than for lighter components (see Figure 3-5), the peaks of the heavier components are broader than those of the lighter components.

The main reason of this lies in the fact that, the lighter components reach the column outlet quicker than the heavier components thanks to its higher effective velocity, therefore when $nC_{20}H_{42}$ reach the GC outlet at 11.2 minutes, its effective dispersion reach just a value of $4.41 \cdot 10^{-10}$ m^2/s, whereas when $nC_{60}H_{122}$ reach the GC outlet, at about 28.2 minutes, its effective dispersion reach a value of $1.3 \cdot 10^{-5}$ m^2/s.

On top of this, the final zone's variance is calculated as the summation of all the local contributions of zone variance (See Equation 5-7 in CHAPTER 5 –) during the time interval that each component takes inside the GC column. Therefore, since the heavier components spend more time inside the column than the lighter components, the final zone's variance (i.e. the peak width) is likewise greater for the heavier components than for the lighter components.

The large difference in the effective dispersion between that observed for $nC_{20}H_{42}$ compared with $nC_{60}H_{122}$, simply reflects the fact that $nC_{60}H_{122}$ is retained longer on the stationary phase with significant vaporization not occurring until temperature is close to the isothermal maximum temperature (Table 3-2).

As a result, smoother changes in diffusivity are evident. Conversely, large changes occur in greater measure in the case of $nC_{20}H_{42}$, where the temperature at which the stationary phase starts to release the component is achieved during the temperature ramping period.

3.5.9. Retention and Distribution Factor

Knowledge of how the distribution factor varies with temperature is an essential requirement in gas chromatography when temperature-programming is the most common practice in order to accelerate analysis of solutes with a wide range of boiling points.

Application of a time-dependent function of distribution factor enables calculation of retention factors, and hence prediction of retention times [23] (Equation 3-9). It also permits simulation of the concentration profile inside the column by solving (Equation 3-2), and therefore optimization of the separation of complex mixtures.

3.5.10. Thermodynamic equilibrium of the solvation in GC

The solvation of a solute in the solvent [10] can be expressed at thermodynamic equilibrium by the logarithm of the solute molecule's numerical density ratio in both phases [24-25]:

$$Ln\left[\frac{{}^{L}\rho_A}{{}^{G}\rho_A}\right] = Ln\,K = -\frac{\Delta G(T)}{R \cdot T}$$

Equation 3-21

The distribution coefficient *K* involves the ideal behaviour of the gas phase at infinite dilution, with assumptions of negligible interaction between solute-solute and solute-carrier gas, with the main interaction occurring between the solute and stationary phase. In addition, interfacial and extra-column effects on the mass transfer, which lead to non-equilibrium conditions, are expected to be negligible. [26]

Under the above conditions, the isothermal retention times can be expressed by Equation 3-22, where the distribution factor has been replaced by the first two terms of

the Taylor series expansion which has been treated in terms of thermodynamic properties by Castells et al. [27] yielding a semi-empirical model. [17, 28]

Here, *ΔH* and *ΔS*, represent the changes in enthalpy, and entropy associated with the transfer of solute from the stationary phase to the mobile phase at a given temperature (T).

$$t_{r,i} = t_M \cdot \left[1 + \frac{K_i(T)}{\beta}\right] = t_M + \frac{t_M}{\beta} \cdot \left(a_0 + a_1 \cdot \frac{1}{T(t)}\right)$$

$$a_0 = \frac{\Delta S(T)}{R}; \qquad a_1 = -\left(\frac{\Delta H(T)}{R}\right)$$

Equation 3-22

Aldaeus [15] has proposed two retention mechanisms according to the nature of the separation hold between the analyte and the stationary phase, based on the semi-empirical values of the thermodynamic properties of Equation 3-22.

The entropy-driven mechanism (e.g. size exclusion chromatography), is dominated by the loss of the molecules' translational, rotational, and vibrational degrees of freedom, being retained in the absence of proper interaction by the stationary phase. However, the enthalpy-driven mechanism (e.g. partition chromatography) is dominated by the difference between the dissolution energies of the analyte in the mobile phase and stationary phase.

The GC modelling implemented in this chapter, uses as main input the distribution factors *K*, for the n-alkanes in the range of $nC_{12}H_{26}$–$nC_{64}H_{130,}$ reported in CHAPTER 4 – [23], (*Figure 3-6*). The distribution factors have been obtained by linear fitting of numerous isothermal measurements carried out at temperatures up to 430°C in an HT5 GC column, corresponding to Equation 3-22.

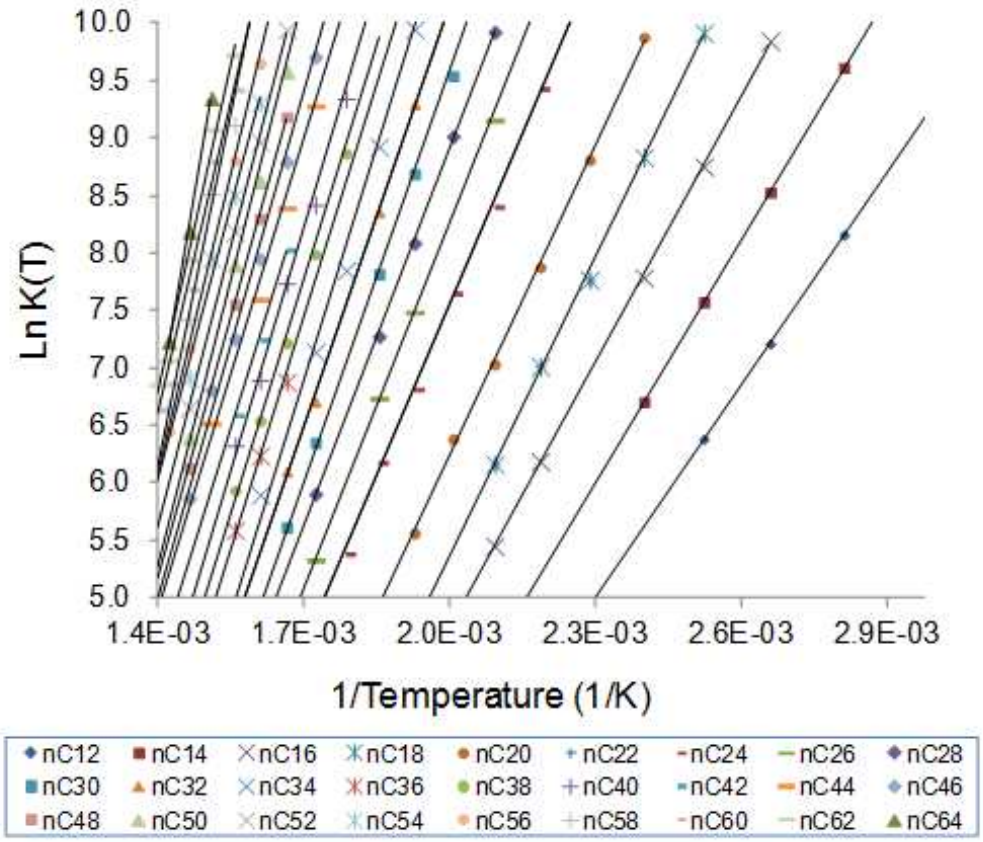

Figure 3-6. Distribution factors in a HT5 capillary column, based on the retentions times of every compound and hold-up time for every constant temperature in the range of temperature 80-430 °C, using $Ln((t_r/t_m-1)\cdot\beta) = Ln(K(T))$.

3.6.Validation of the predicted retention times.

A model in MATLAB R2010bSP1 has been developed for predicting retention times, (Equation 3-9) which contains the distribution coefficients of every compound [23] and the corresponding equations for the calculations of viscosity, pressure, and velocity through the GC column, as explained in the previous sections.

It is important to note that all GC analyses have been carried out using constant flow mode for the column carrier gas supply, and therefore the algorithm used calculated the variation of the inlet pressure required for maintaining the flow constant at reference conditions, while the temperature increased, and carrier-gas viscosity did likewise.

Validation of this model has been carried out using both literature solvation thermodynamic properties of a series of n-alkanes from $C_{12}H_{26}$-$C_{40}H_{42}$, and PAH's from

$C_{10}H_{24}$-$C_{22}H_{46}$ in a DB-1 and a DB-5 column [17], and the thermodynamic properties obtained with the in-house experimental data (*Figure 3-6*), for an HT-5 capillary column [23] for $C_{12}H_{26}$ to $nC_{62}H_{126}$ n-alkanes.

For the DB-1 column, average deviations of 1.9% for n-alkanes and 2.0% for PAH's were obtained between the published [17] measured retention and the retention times predicted with the developed model (*Figure 3-7*).

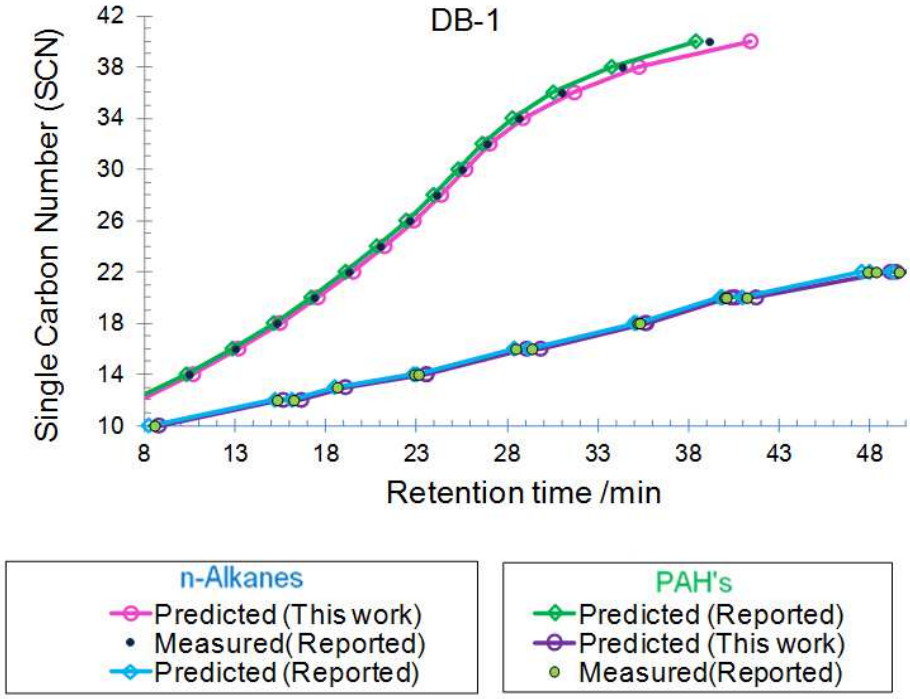

Figure 3-7. Validation of the retention times predicted with the in-house model developed, compared with literature data (Aldaeus [17]) in a DB-1 column for PAH's (from $C_{10}H_{24}$-$C_{22}H_{46}$) and n-alkanes (from $C_{12}H_{26}$-$C_{40}H_{42}$), using their retention factors.

In the case of the DB-5 column, the average deviations in retention times [17] with the in-house model predictions were 2.2% for n-alkanes and 2.6% for PAH's; and for the predicted retention times published [17], the corresponding errors were 0.8% for n-alkanes and 0.3% for PAH's (*Figure 3-8*).

Figure 3-10 shows a comparison of the retention times predicted by the in-house model and the in-house experimental values obtained with an HT5 column, based on the

temperature program shown in (Table 3-2), but also applying ramp rates of 10°C/min and 20°C/min..

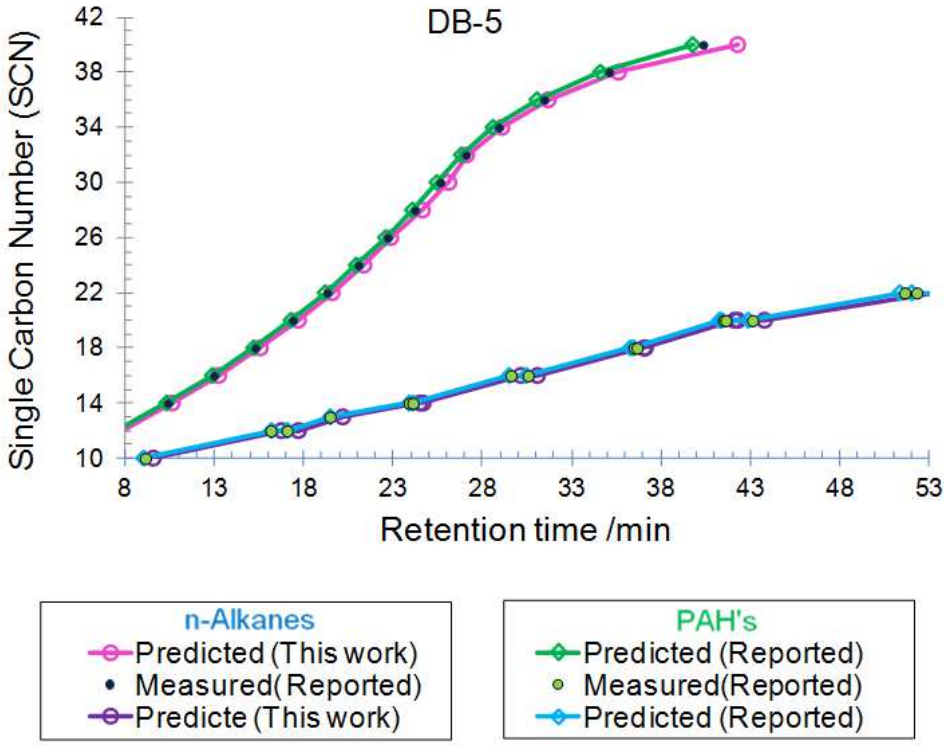

Figure 3-8. Validation of the retention times predicted with the in-house model developed, compared with literature data (Aldaeus [17]) in a DB-5 column for PAH's(from $C_{10}H_{24}$-$C_{22}H_{46}$) and n-alkanes (from $C_{12}H_{26}$-$C_{40}H_{42}$), using their retention factors.

The average deviations with the in-house model, were 1.3%, 1.1% and 2.2% for a temperature ramp of 10°C/min, 15°C/min and 20°C/min respectively.

As seen in Figure 3-9, for the data relating to the lowest ramp rate(10°C/min) the five highest retention times are over-predicted; and secondly, for the highest ramp rate(20°C/min) virtually all measured retention times are greater than predicted. Two distinct reasons are suggested for these observations.

In the case of the over-predicted retention times at the lowest ramp rate, the measured hold-up times in the region of the upper temperature limit are subject to higher

deviations as temperatures increased, affecting both the back calculated inlet pressure and the calculated distributions factors for the associated alkanes.

And in the case of the under-predicted retention times for the highest ramp rate of 20°C/min, it is certain that the true column temperature is lagging behind the apparent ramp set-point value. (As such, the effect could be confirmed by applying a higher ramp rate of say 25°C/min, in which case even larger deviations would be evident).

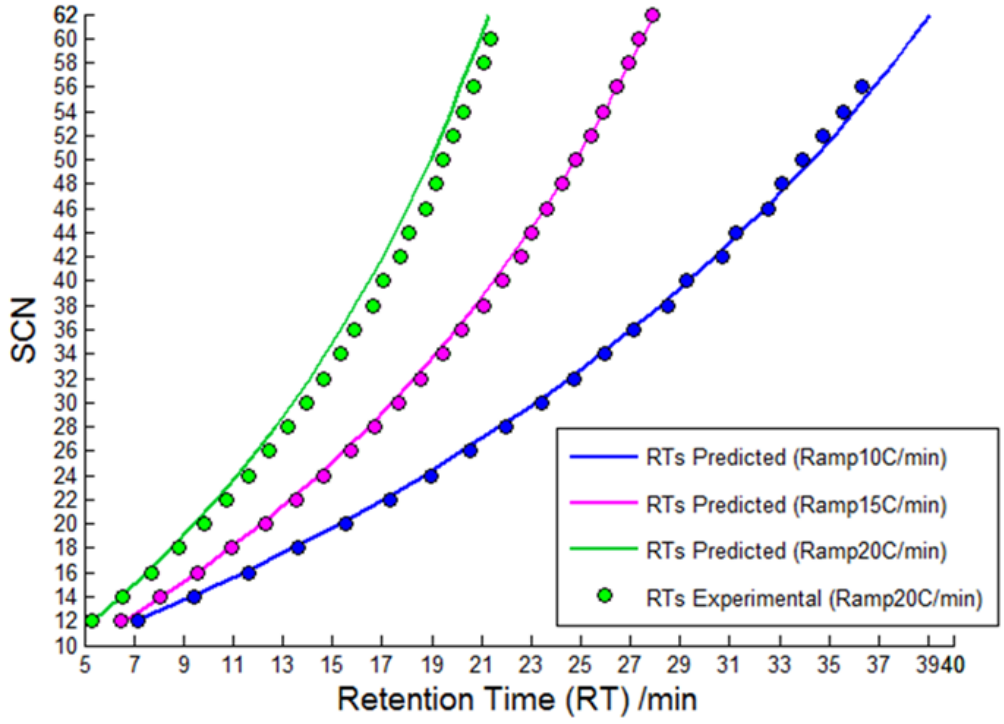

Figure 3-9. Validation of the model developed with in-house experimental data for Alkanes in a HT5 column, using three ramps of temperatures 10, 15 & 20 °C/min in the range of 10-430 °C.

However, means exist for correcting for such temperature differentials, and can be applied retrospectively and for future work.

Finally, accurate retention time predictions have been obtained for the three temperature ramps, which started from 10 °C up to 430 °C, even when the temperature

range for which the distribution factors have been derived, related to isothermal measurements in the range 80 °C to 430 °C.

3.7.Measurement of n-Alkane Isothermal Retention Times (RT)

In isothermal gas chromatography, components of a homologous chemical family exhibit a rapid increase in retention time and peak width with increasing boiling point, in a generally linear plot of log(RT) vs Carbon Number. As a consequence, only a limited number of alkanes' isothermal RTs can be reliably measured from a single injection at a given temperature (because of peak broadening and no-realistic retention time).

Another constraint is that single alkanes above nC_{40} are not readily commercially available with adequate purity with the exception of nC_{44}, nC_{50} and nC_{60} and Polywaxes are generally utilized for retention time measurements to generate boiling-point/RT calibration plots for HTGC analyses.

However, the latter are mixtures comprising polyethylene oligomers of even carbon number intervals, and are qualitative mixtures only. Hence the weight fraction of each oligomer in a particular Polywax distribution is not readily known, although accurate estimation is possible if the complete distribution can be chromatographed and total elution of the sample can be demonstrated, e.g., by spiking.

Whilst qualitative alkane or Polywax mixtures or a combination of the two are suitably adequate for both isothermal and temperature programmed retention time measurements, gravimetric dilutions in CS_2 of the ASTM D5442 Linearity Standard [29] were also used in this chapter, covering the alkanes nC_{12}-nC_{14}-nC_{16}-nC_{18}-nC_{20}-nC_{22}-nC_{24}-nC_{26}-nC_{28}-nC_{30}-nC_{32}-nC_{36}-nC_{40}-nC_{44}-nC_{50}-nC_{60}.

In such cases, fairly accurate calculations are possible of the molar quantities of each alkane injected in a given volume. However, this is not the case when a gravimetric blend of this standard is made with a Polywax solution in CS_2 except for those alkanes which elute before the lightest oligomers present in the Polywax range.

The injection technique used was FVI (Flash Vaporization Injection), in order to have the same conditions in all isothermal injections at the GC column inlet.

3.8.Degree of Elution

The *degree of elution* is defined as the amount of component which has been eluted in relation to the amount injected. Its calculation is based on the retention factors of every component, 'i' which represent the ratio of moles of "i" in the stationary phase to the moles of "i" in the mobile phase for a given temperature.

In order to determine the degree of elution of every component, their retention factors have been analyzed during a GC analysis using the temperature-program of Table 3-2. (T_{max} 425°C).

During the migration of a component, two periods have been defined: the period of movement and the period of elution.

Initially, when the components first establish equilibrium with the stationary and the gas phase, the components are trapped in the stationary phase, until a minimum temperature is reached. At this temperature equilibrium is re-established, increasing the amount of moles available in the gas phase and therefore increasing its effective velocity, for them to start moving through the GC column.

The period of movement has been defined as the time elapsing from the moment at which a component starts to travel through the GC column, until the time when the component is completely eluted as it reaches the column outlet and achieves 100% elution. (Equation 3-24)

The minimum effective velocity at which a component starts to move has been set here at 0.25 mm/sec, corresponding to 1 mm/°C if using a ramp of 15°C/min of temperature programming.

During the period of movement depicted in Figure 3-10 to Figure 3-11, each component "i" travels through the GC column, increasing the number of moles in the gas phase by re-establishing their equilibrium with the increasing temperature (lower

retentions factors) and changing their effective velocity with the decreasing pressure, until all the components are eluted, reaching the GC column outlet.

Secondly, the period of elution is defined as the time elapsing from the first moment where some molecules of a given component pass the GC outlet, to the time when all the molecules of the given component has entirely eluted.

Figure 3-10 depicts the period of movement of n-alkanes in the range $nC_{12}H_{26}$ through $nC_{62}H_{126}$ as each travels through the GC column, with the rose colored band depicting their retention factors during that interval. The band shows that the round average, minimum retention factor to initiate movement for the n-alkanes studied is 2000 [moles "i" in the stationary phase per moles "i" in the gas phase].

The round average elution retention factor is 2 over the $nC_{12}H_{26}$- $nC_{62}H_{126}$ range, being lower for the heaviest component since they elute at higher temperatures, and therefore their solubility in the stationary phase is lower at elution.

Nevertheless, it is important to note that the elution temperature of these components is lower than the maximum temperature (T_{max}, 425 °C) reached in the GC column. This means that components heavier than $nC_{62}H_{126}$ which elute at T_{max} will re-establish equilibrium until total elution occurs during the final isothermal period and therefore with a constant retention factor. Conversely, during the temperature ramping period the greater the temperature the lower is the retention factor.

Making use of retention factor during the moving period of a component inside the GC column until elution, the mole fraction remaining in the gas phase relative to the total amount of moles injected, can be determined by Equation 3-23.

$$(X_i) = \frac{1}{1 + k_i\,(T(t))} = \left[\frac{(moles\ "i")^M}{(moles\ "i")^{S+M}}\right]$$

Equation 3-23

Figure 3-11 depicts (in green) the fraction of each component in the gas phase during its moving period until elution; and (in black), the fraction of component in the gas phase during its elution period.

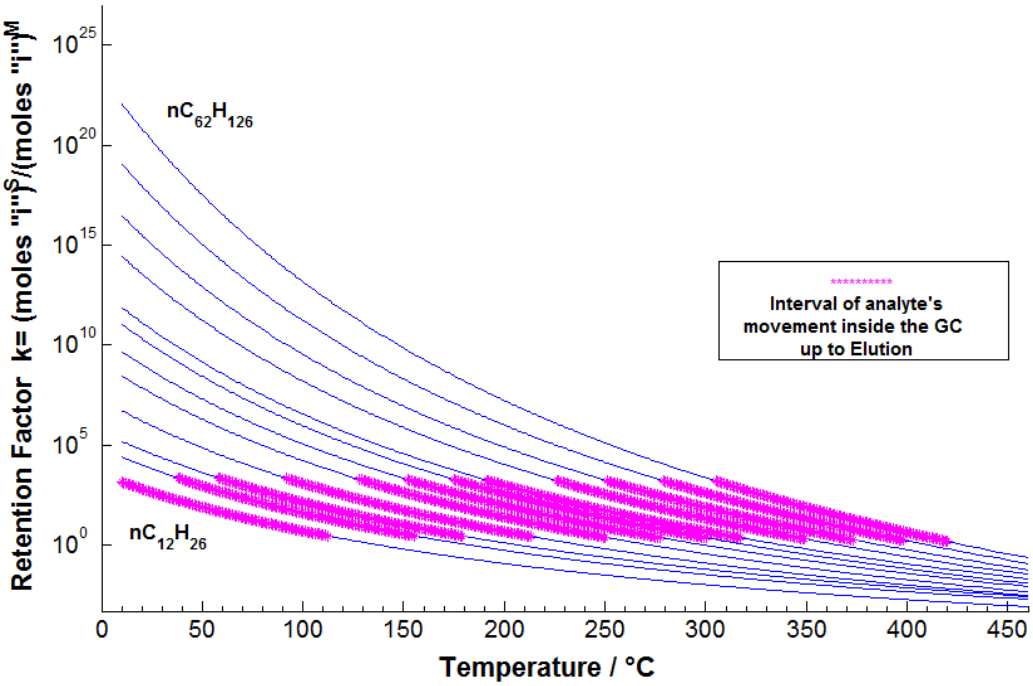

Figure 3-10. Retention Factor vs Temperature (blue), Interval of Retention Factors, which allows movement to every analyte until its elution, reaching the GC outlet (pink) for the n-alkanes from $nC_{12}H_{26}$- $nC_{62}H_{126}$ in a HT5 capillary GC column, under a temperature-programmed 15 °C/min in the range of 10-425 °C.*

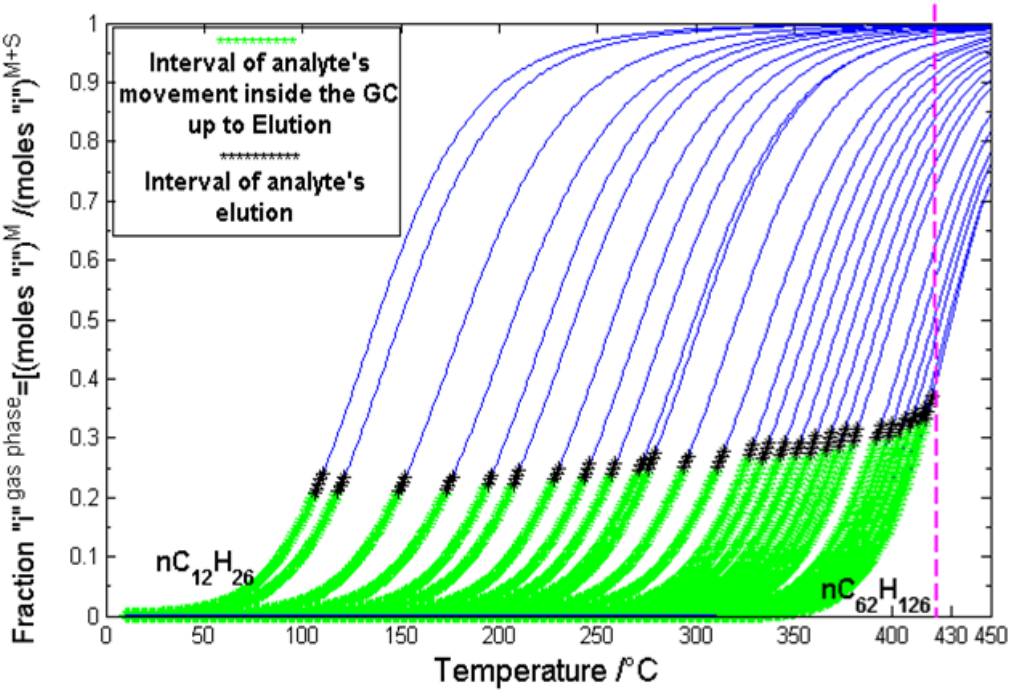

Figure 3-11. Fraction of moles of "i" in mobile phase to the total moles of "i" vs. temperature (blue) covers all the range of temperature, (green) covers the

temperature up to elution temperature of every component "i". The component "i", corresponding the n-alkanes with Single Carbon Number (SCN) from $nC_{12}H_{26}$ *to* $nC_{62}H_{126}$

The average initial elution fraction of the studied n-alkanes, relative to the corresponding amount injected is 0.3 moles in the gas phase at elution per total moles injected. The lowest values occur with the most volatile components since they elute at lower temperature, where solubility in the stationary phase is still considerable, in relation to those eluting at higher temperatures, but below the maximum for the analysis.

Therefore from Figure 3-11 only a fraction of respectively 0.24 at 110 °C and 0.35 at 420 °C of injected moles of nC_{12} and nC_{62} are in the gas phase available to elute initially, and only the percentage which passes the GC outlet, will elute at that temperature.

Thus, the number of moles remaining inside the column can be re-calculated, being the difference between moles injected and moles eluted at the given temperature. (However, it should be recalled that estimated concentrations have been applied here for the alkanes which are not present in the ASTM D5442 linearity standard, as these components derive from a qualitative Polywax standard, or a blended mixture of one with the ASTM standard).

At the next time step, (1 °C higher from the initial elution temperature), the retention factor of each component decreases (lower retention in the stationary phase), and the fraction in the gas phase increases in relation to the amount of moles remaining in the column.

Again, only a percentage of the moles available will pass the GC outlet, and the total amount of component remaining can again be recalculated, as before.

Thus, the equilibrium is re-established at every time step (i.e., per °C from initial elution) and the amount of moles inside the column is re-calculated, until total elution for each component. The degree of elution can then be calculated at every time step using Equation 3-24.

$$Degree\ of\ Elution = \left[\frac{\sum(moles\ "i")^{elute}\left(T(t)\right)}{(moles\ "i")^{injected}}\right]$$

$$(moles\ "i")^{elute}\left(T(t)\right) = \frac{1}{1 + k_i\left(T(t)\right)} \cdot (moles\ "i")^{inside} \cdot\ \%Moles\ Elute\left(T(t)\right)$$

Equation 3-24

Figure 3-12 depicts the degree of elution of every component studied, using the temperature program of Table 3-2, as a function of time, showing that all components from nC_{12} to nC_{62} completely elute from the GC column, reaching 100% of degree of elution before the end of the GC analysis time.

It is important to note, that the degree of elution increases sharply once the elution starts, producing sharp peaks during the temperature programmed used.

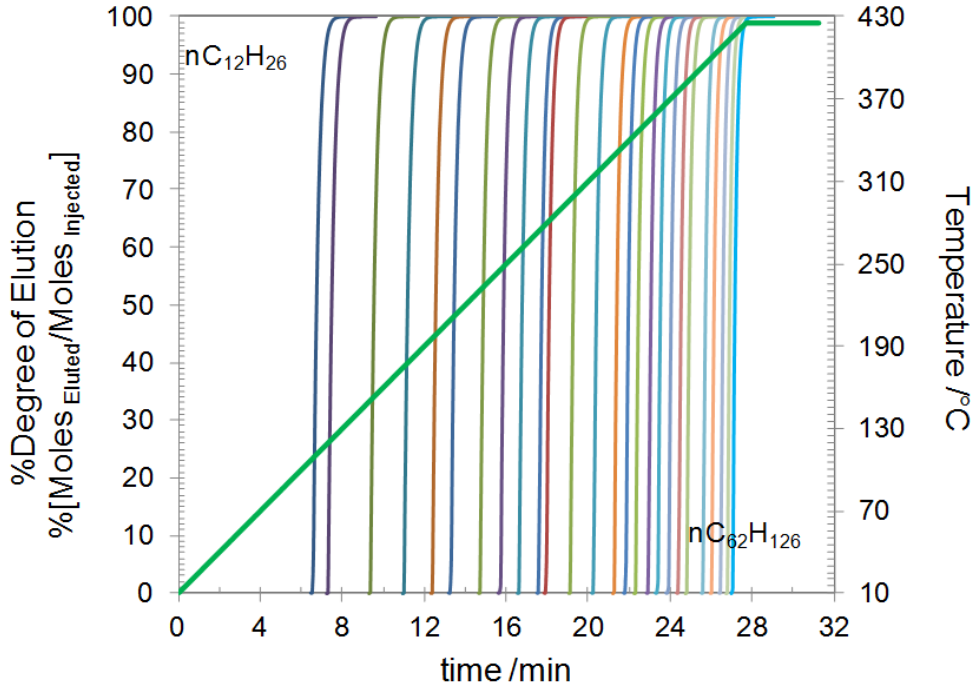

Figure 3-12. Degree of Elution vs time of each component "i" :n-alkanes in the range of $nC_{12}H_{26}$ to $nC_{62}H_{126}$. Degree of Elution= Moles of "i" inside the GC column at time (t) /Moles injected of "i".

Knowing the retention factors of components heavier than nC_{62}, whose elution is very difficult to identify in a chromatogram, will allow the determination of their degree of elution, as well as the extent of non-elution of the components which are unable to elute

completely. This subject is treated in CHAPTER 5 –, covering an analysis extended to much heavier n-alkanes.

3.9.Concentration & Temperature Profiles

By solving Equation 3-1 and Equation 3-2, it is possible to determine the distribution (assumed to be normal Gaussian), of moles of each component during the GC analysis, taking account the temperature increase the pressure decrease and movement of the component through the column. In this way the dispersion and movement of the components at every moment can be described by their standard deviations and centroid, respectively.

Figure 3-13, shows the position of the centroid of every component with the variation of temperature, using the temperature-program of Table 3-2. It is noticeable that every component remains at the column inlet until it reaches a minimum temperature at which the stationary phase starts to release it.

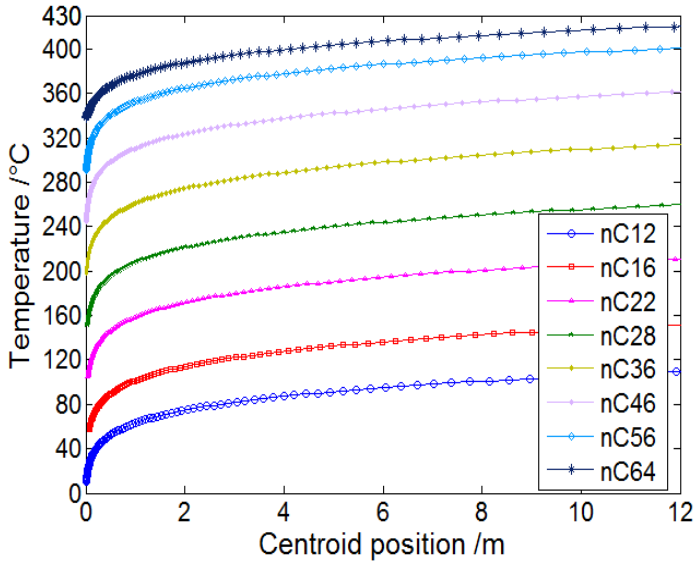

Figure 3-13. Centroid Position of every component "i" vs Temperature up to elution from the GC column, using the temperature programmed of Table 3-2.

The minimum temperatures can be seen clearly in this figure. For $nC_{12}H_{26}$, the movement starts from the beginning of the analysis at 10 °C, and for $nC_{64}H_{130}$ it starts is about 330 °C. It is evident as expected that the heavier the component, the higher its elution temperature, and the higher the minimum temperature to initiate the movement inside the GC column.

In order to calculate the total moles of gas phase (carrier gas + component “i”) which occupies a volume covering 95% of the component in the gas, ideal gas behaviour is assumed and the percentile equivalence of normal Gaussian distributions, which states that 95% of a distribution occupies *(4·σ(T(t)))*. Thus, the volume where 95% of molecules of component “i” are located, mixed with carried gas, can be calculated, multiplying the cross sectional area of the tube (ignoring the retentive layer) by four times the standard deviation at the given temperature.

The gas molar fraction of “i” and the distribution of moles of component “i” inside the GC column are depicted in Figure 3-14 and Figure 3-15 respectively.

Therefore, the molar fraction of component “i” available in the gas phase relative to the total number of moles of gas phase(carrier gas + component “i”) depicted in Figure 3-14, has been determined, based on the total amount of moles of ideal gas in the corresponding volume, equal to *4·σ(T(t))·Free Transverse Area*, and calculating the amount of moles of component “i” in the gas phase at the given temperature as: Moles Injected· *(1/(1+k(T)))*.

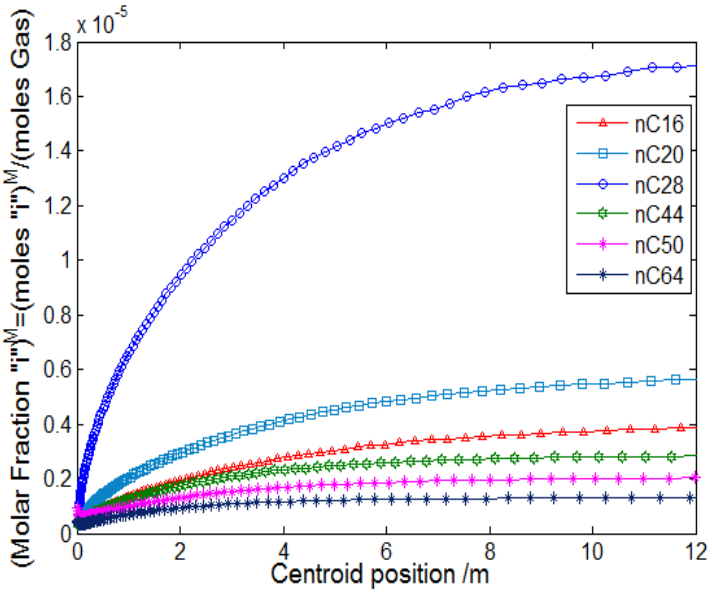

Figure 3-14. Molar fraction of component “i” in the gas phase vs centroid position of the moving component “i”, using the temperature programmed of Table 3-2. The period depicted correspond at the time before elution.

The higher molar fraction is found before the beginning of the interval of elution of every component, as the molecules of the component have not started to be released from the column outlet. Hence the higher the temperature, the greater the fraction of component available in the gas phase relative to the moles injected, as explained previously by Equation 3-23 and Figure 3-11.

Thus, $nC_{20}H_{42}$ shows the higher value of c.a. $1.8 \cdot 10^{-5}$ moles in the gas phase per total moles of gas, and a lower corresponding value is seen for $nC_{64}H_{130}$ of ca. $0.18 \cdot 10^{-5}$ moles. These proportions correspond to those of their injected values according to Table 3-3. This confirms that their elution fractions retain the same proportion as when injected.

Finally, Figure 3-15, depicts the distribution of moles [mol/m], with time and position throughout the GC column, showing that $nC_{12}H_{26}$ starts to move from the beginning of the analysis, and elutes at about 6 minutes, when $nC_{20}H_{420}$ has barely started to move and elute after about 12 min; while $nC_{30}H_{62}$ has just started to move at this time and elute at about 17 min. Movement starts for $nC_{44}H_{90}$ at about16 min and elution at about 23 min. $nC_{50}H_{102}$ starts to move at about 19 min, when $nC_{44}H_{90}$ is located at about 1m from the GC inlet; and at 24 min, $nC_{64}H_{130}$ is 1 m away from the GC inlet, when $nC_{50}H_{102}$ starts to elute. Finally, $nC_{64}H_{130}$ starts to elute at about 27 min.

It is important to note that every component travels individually, and there is no mixing of components through the GC column, since they travel the same distance, and pass through the same positions but at different times, and hence do not meet each other during their journey. In this way good separation of the components occurs during the analysis.

It may be seen that the amount of moles per unit length of column increases in the case of $nC_{12}H_{26}$, $nC_{20}H_{42}$, and $nC_{30}H_{62}$, but decreases in the case of $nC_{44}H_{90}$, $nC_{50}H_{102}$ and $nC_{64}H_{130}$, which corresponds to the expected behaviour, retaining the same proportion as the corresponding amount injected, as described in Table 3-3.

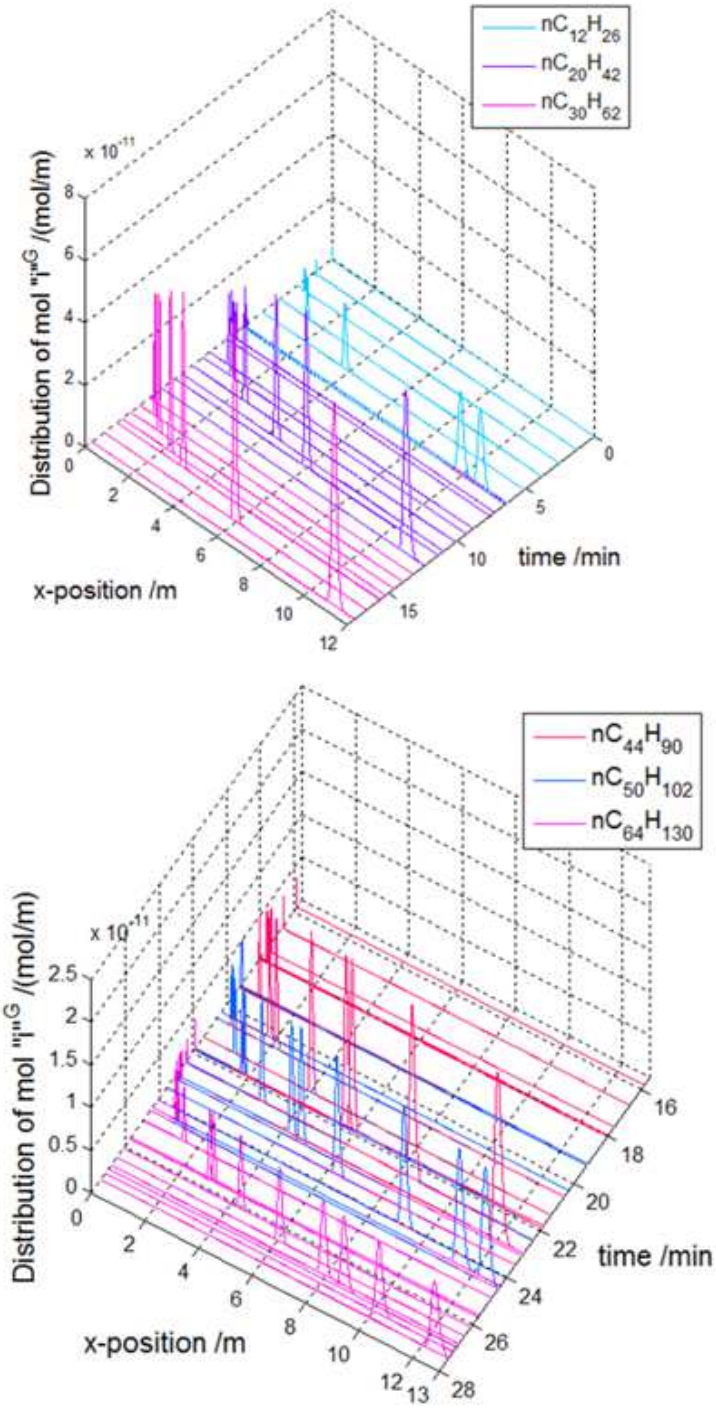

Figure 3-15. Distribution of moles of component "i" per unit of length regarding the position inside the GC column, and the analysis time until elution, using the temperature programmed of Table 3-2.

Compound	Moles Injected	Compound	Moles Injected
nC12	3.65E-11	**nC40**	2.75E-11
nC14	4.69E-11	**nC42**	2.75E-11
nC16	5.47E-11	**nC44**	2.00E-11
nC18	6.09E-11	**nC46**	2.00E-11
nC20	6.58E-11	**nC48**	2.00E-11
nC22	7.98E-11	**nC50**	1.32E-11
nC24	9.15E-11	**nC52**	1.32E-11
nC26	1.69E-10	**nC54**	1.32E-11
nC28	1.61E-10	**nC56**	1.32E-11
nC30	7.34E-10	**nC58**	1.32E-11
nC32	5.50E-11	**nC60**	7.36E-12
nC34	5.50E-11	**nC62**	7.36E-12
nC36	3.67E-11	**nC64**	7.36E-12
nC38	3.67E-11		

Table 3-3. Composition of injected n-alkanes (Mixture of ASTM 54179 and Polywax, assumed values for calculation purposes only) in 0.3µL.

As expected, the standard deviations of every component, and therefore their dispersion, increase with time, and therefore temperature through the column, from the inlet to the outlet. The sharper the eluting peak, the lower the dispersion.

3.10. Conclusions

This chapter provides further insight into the limits of high temperature gas chromatography (HTGC), proposing a new approach for determining the non/incomplete elution of every component by introducing: the degree of elution, defined as the amount of component which has been eluted in relation to the amount injected.

The degree of elution of the n-alkane hydrocarbons in the range, $nC_{12}H_{28}$ to $nC_{62}H_{126}$ has been calculated based on the continuous equilibrium re-established during the interval of elution for every component, using their corresponding retention factors, and assuming no cracking inside the GC column.

This new approach is applied in CHAPTER 5 –, for n-alkanes heavier than $nC_{62}H_{126}$ in order to determine the analytical conditions required for ensuring maximum elution

of a given component, allowing the possibility of improving the practice of HTGC by optimizing the separation process.

The chapter introduces a preliminary method of calculating, at each moment during a temperature-programmed analysis, the molar fraction of the components in the gas phase, in accordance with the standard deviations of their Gaussian distribution at the point where 95% of the molecules are travelling through the column.

The pyrolysis model developed in the previous CHAPTER 2 – [45] and the gas chromatography migration and separation model developed in this chapter, are combined in CHAPTER 5 –, in order to complete the analysis of the cracking risk of heavy n-alkanes.

This chapter also provides a deeper understanding of the separation of components in a gas chromatographic column, and provides a basis for further analysis of non-elution of components heavier than $nC_{62}H_{126}$, which will be treated in a later publication.

3.11. References

[1] Hernandez-Baez, D.M., et al., Establishing the Maximum Carbon Number for Reliable Quantitative Gas Chromatographic Analysis of Heavy Ends Hydrocarbons. Part 1: Low-Conversion Thermal Cracking Modeling, Energy & Fuels (2011)

[2] Guiochon, G. and C.L. Guillemin, Book Title: Quantitative Gas Chromatography for Laboratory Analysis and On-lin Control: ELSEIVER, Amsterdam, (1988)

[3] Blumberg, L.M., Book Title: Temperature-Programmed Gas Chromatography: WILEY-VCH Verlag GmbH & Co. KGaA, Weinheim, (2010)

[4] Golay, M.J.E., ed. Theory of chromatography in open and coated tubular columns with round and rectangular cross-sections. 1958. 36–53.

[5] Blumberg, L.M., Variance of a zone migrating in a linear medium .2. Time-varying nonuniform medium,Journal of Chromatography, 637(2), 119-128 (1993)

[6] Thewalim, Y., F. Aldaeus, and A. Colmsjo, Retention time prediction of compounds in Grob standard mixture for apolar capillary columns in temperature-programmed gas chromatography, Anal Bioanal Chem, 393(1), 327-34 (2009)

[7] Taylor, G., Dispersion of Soluble Matter in Solvent Flowing Slowly through a Tube, Proceedings of the Royal Society of London. Series A. Mathematical and Physical Sciences, 219(1137), 186-203 (1953)

[8] Giddings, J.C., Plate Height of nonuniform chromatographic columns (Gas compresion effects, coupled columns, and analogous systems), Analytical Chemistry, 35(3), 353-356 (1963)

[9] Giddings, J.C., Journal of Gas Chromatography, 2, (1964)

[10] Giddings, J.C., Par I, Principles and theory., in Dynamics of chromatography, Edward Arnold, (Publisher, London), Marcel Dekker, Inc., : New York, (1965)

[11] Giddings, J.C., et al., Plate Height in gas chromatography, Analytical chemistry, 32(8), 867-870 (1960)

[12] Taylor, G., Dispersion of soluble matter in solvent flowing slowly through a tube, Proceedings of the Royal Society of London. Series A. Mathematical nd Physical Sciences., 219(1137), 186-203 (1953)

[13] Blumberg, L.M. and T.A. Berger, Variance of a zone migrating in a nonuniform time-invariant linear medium, Journal of Chromatography, 596(1), 1-13 (1992)

[14] Snijders, H., H.G. Janssen, and C. Cramers, Optimization of temperature-programmed gas chromatographic separations .1. Prediction of retention times and peak widths from retention indices, Journal of Chromatography A, 718(2), 339-355 (1995)

[15] Aldaeus, F., New tools for trapping and separation in gas chromatgorahpy and dielectrophoresis (Improved performance by aid of computer simulation), Doctoral thesis in analytical chemistry, Stockholm University, (2007)

[16] Aldaeus, F., Y. Thewalim, and A. Colmsjo, Prediction of retention times and peak widths in temperature-programmed gas chromatography using the finite element method, Journal of Chromatography A, 1216(1), 134-139 (2009)

[17] Aldaeus, F., Y. Thewalim, and A. Colmsjo, Prediction of retention times of polycyclic aromatic hydrocarbons and n-alkanes in temperature-programmed gas chromatography, Analytical and Bioanalytical Chemistry, 389(3), 941-950 (2007)

[18] Gonzalez, F.R. and A.M. Nardillo, Retention index in temperature-programmed gas chromatography, Journal of Chromatography A, 842(1-2), 29-49 (1999)

[19] Davankov, V.A., The true physical meaning of the corrected retention volumes in GC, Chromatographia, 44(5-6), 279-282 (1997)

[20] Kestin, J., et al., Equilibrium and trasport properties of the noble gases and their mixtures at low density, Journal of Physical and Chemical Reference Data, 13(1), 229 (1984)

[21] Hawkes, S.J., Viscosities of carrier gases at gas-chromatograph temperatures and pressures, Chromatographia, 37(7-8), 399-401 (1993)

[22] Fuller, E.N., P.D. Schettler, and J.C. Giddings, A new method for prediction of binary gas-phase diffusion coefficients, Industrial and Engineering chemistry, 58(5), 19-27 (1966)

[23] Hernandez-Baez, D.M., et al., Establishing the Maximum Carbon Number for Reliable Quantitative Gas Chromatographic Analysis of Heavy Ends Hydrocarbons. Part 3. (Determination of Distribution Factors (nC12-nC98) in an HT5 GC column), in Unpublished manuscript. 2013.

[24] Gonzalez, F.R., J.L. Alessandrini, and A.M. Nardillo, Revision of a theoretical expression for gas-liquid chromatographic retention, Journal of Chromatography A, 852(2), 583-588 (1999)

[25] Ben Naim, A., Solvation Thermodyanmics, Plenum Press, New York, (1987)

[26] Gonzalez, F.R., Interpreting the gas chromatographic retention of n-alkanes, Journal of Chromatography A, 873(2), 209-219 (2000)

[27] Castells, R.C., E.L. Arancibia, and A.M. Nardillo, Regression against temperature of gas-chromatographic retention data, Journal of Chromatography, 504(1), 45-53 (1990)

[28] Gonzalez, F.R., Considerations on the temperature dependence of the gas-liquid chromatographic retention, Journal of Chromatography A, 942(1-2), 211-221 (2002)

[29] ASTM® 5442 (C12-C60) Quantitative Linearity Standard 0.01 % (w/w) each component in cyclohexane, analytical standard, in ASTM Analytical standard (http://www.sigmaaldrich.com/catalog/product/supelco/502235?lang=en&region=GB).

CHAPTER 4 – DETERMINATION OF DISTRIBUTION FACTORS (nC_{12}-nC_{98}) IN AN HT5 GC COLUMN

4.1.Introduction

This chapter is focused on extending the data set of n-alkane distribution factors (K values) from $nC_{12}H_{26}$ through $nC_{98}H_{198}$ in an SGE HT-5 GC column. The measurement procedures and data treatment are explained in detail in this chapter.

For this purpose, numerous isothermal gas chromatography injections have been carried out in the temperature range from 80°C to 420°C, at 20°C intervals and 430°C.

In this chapter, two complementary HTGC methods have been applied, both using wide-bore HT5 columns (SGE UK, Ltd) of 0.53mm ID fused silica tubing, with aluminium coating. Both are rated to 460°C for isothermal analyses, or 480°C for temperature programmed use, but were constrained to 435°C in the study by the 450°C limit of the flame ionization detector, which require a temperature differential of 15°C-20°C to the maximum column operating temperature. Two modes of HTGC operation were applied:-

High-Efficiency Mode, with dimensions and flow parameters as follows:-

- HT5 Column: 12.0m x 0.53mm ID x 0.15mic film
- retention gap: 1.8m x 0.53mm ID of deactivated, uncoated, aluminium-clad fused silica.
- carrier gas (helium) flow: 6ml/min
- flow-control mode: constant inlet pressure
- n-alkanes elution range: to nC_{64}

SimDist(Low-Efficiency) Mode, with dimensions and flow parameters in accordance with ASTM D7169-11 [1], for low-resolution operation, reduced retention times, and extended elution of heavy alkanes:-

- HT5 Column: 5.0m x 0.53mm ID x 0.15mic film
- retention gap: None
- carrier gas (helium) flow: 20ml/min
- flow-control mode: constant flow rate

- n-alkanes elution range: to nC_{100}

In this chapter, the 5 m HT5 GC column was used to generate a database of isothermal retention times of n-alkanes for the range, and spanning the Single Carbon Number (SCN) group equivalent to nC12 through nC_{98}.

Based on the isothermal data, distribution factors for the n-alkanes have been determined and used as input data for the prediction of their corresponding retention times in Temperature Programmed Gas Chromatography (TPGC).

The in-house developed analytical model (CHAPTER 3 –) [2-3] was then used to predict retention times for HT5 analyses under three different ramps of temperature, for comparison with experimental retention times obtained from both modes of HTGC operation mentioned above.

This thesis reports values of the thermodynamic properties (distribution factors) for the n-alkanes in the range of $nC_{12}H_{26}$–$nC_{64}H_{130}$ under constant inlet pressure GC conditions; and in the range $nC_{12}H_{26}$–$nC_{98}H_{198}$ when constant flow rate mode was applied. For this purpose a linear fit of numerous isothermal measurements was carried out from 80-420°C, at 20°C intervals and at 430°C, with an HT5 column.

The retention times predicted for three different temperature ramps at constant flow rate yielded an average error of 4.4% when the data set of distribution factors obtained at constant flow rate were used. In the same way, the retention times predicted at constant inlet pressure yielded an average error of 1.5% when the data set of distribution factors obtained at constant inlet pressure were used.

Simulating a constant flow rate GC measurement as a constant inlet pressure measurement (with an average inlet pressure through the temperature program), has been shown to improve the accuracy of the predicted retention times, with a reduction in the deviation from 4.4% to 2.4%.

Knowledge of how the distribution factor varies with temperature is an essential requirement when temperature programming is conventionally applied to accelerate elution and reduce analysis time of samples with wide solute boiling point range. This

work is focused on the heavy ends hydrocarbons, covering the alkanes, $nC_{12}H_{26}$-$nC_{98}H_{198}$, which can be separated and detected using an HT5 column.

4.2.Distribution Factor Theory

Application of a time-dependent function of distribution factor enables calculation of retention factors, and hence prediction of retention times [4] (Figure 4-1). It also permits simulation of the concentration profile inside the column (CHAPTER 3 –) [2-3], and therefore optimization of the separation of complex mixtures.

4.2.1. Thermodynamic equilibrium of the solvation in GC

The solvation of a solute in the bulk [5] solvent can be expressed at thermodynamic equilibrium by the logarithm of the solute molecule's numeral density ratio in both phases [6-7]:

$$Ln\left[\frac{{C_i}^L}{{C_i}^G}\right] = Ln\,K = -\frac{\Delta\, G(T)}{R \cdot T}$$

Equation 4-1

Here ${C_i}^L$ and ${C_i}^G$ are the molar concentration of the solute in the stationary phase and mobile phase. The ratio of the molar concentration in the two phases is equal to the distribution coefficient K, representing the solvation thermodynamically. ΔG in the right hand side of (Equation 4-1) is the average Gibbs free energy related to the transfer of one solute molecule from the mobile phase (ideal gas) into a fixed position in the stationary phase (the bulk liquid solution).

The distribution coefficient, K involves the ideal behaviour of the gas phase at infinite dilution, with assumptions of negligible interaction between solute-solute and solute-carrier gas. It is assumed that the main interaction occurring is between the solute and the stationary phase. In addition, interfacial and extra-column effects on the mass transfer, which lead to non-equilibrium conditions, are expected to be negligible. [8]

Under the above conditions, the isothermal retention times can be expressed by,

$$t_r = t_M \left[1 + \frac{K(T)}{\beta}\right]$$

Equation 4-2

Where, tr, tm, and *K* correspond to retention time of the solute, hold-up time, distribution factor, and β is the phase ratio of the column. β may be calculated by Equation 4-3, with ro the inner radius of the column, and w the film thickness of the stationary phase.

$$\beta = \frac{(2r_o - 2w)^2}{2r_o{}^2 - (2r_o - 2w)^2}$$

Equation 4-3

Consequently, inserting Equation 4-1 in Equation 4-2, yield to (Equation 4-4) an expression for the retention time as a function of the hold-up time, tm (time required for traversing the column without permeating the stationary phase) and its solvation time, thermodynamically expressed by the Gibbs free energy at a given temperature:

$$t_r = t_M \left[1 + \frac{1}{\beta} \exp\left(-\frac{\Delta G(T)}{R\,T}\right)\right]$$

Equation 4-4

Replacing the Free Gibbs Energy in terms of ΔH and ΔS, which represent the changes in enthalpy and entropy associated with the transfer of solute from the stationary phase to the mobile phase at a given temperature T, leads to Equation 4-5 which corresponds to a semi-empirical model[9-10] developed by Castells et al [11]

$$t_{r,i} = t_M \left[1 + \frac{K_i(T)}{\beta}\right] = t_M + \frac{t_M}{\beta} \exp\left(a_0 + a_1 \frac{1}{T(t)}\right)$$

$$a_0 = \frac{\Delta S(T)}{R}; \qquad a_1 = -\left(\frac{\Delta H(T)}{R}\right)$$

Equation 4-5

Finally, by solving Equation 4-5 for the distribution factor(K) we obtain Equation 4-6, which leads to a temperature-dependent expression for K, which requires the calculation of β (Equation 4-3), andlinear fitting using a set of data for tm, tr, T from isothermal gas chromatographic measurements

$$K(T(t)) = \beta\left[\frac{t_r}{t_M} - 1\right] = \exp\left[a_0 + a_1\frac{1}{T(t)}\right]$$

Equation 4-6

Aldaeus [12] has proposed two retention mechanisms according to the nature of the separation hold between the analyte and the stationary phase, based on the semi-empirical values of the thermodynamic properties of Equation 4-5.

The entropy-driven mechanism (e.g. size exclusion chromatography), is dominated by the loss of the molecules' translational, rotational, and vibrational degrees of freedom, being retained in the absence of proper interaction by the stationary phase. However, the enthalpy-driven mechanism (e.g. partition chromatography, i.e: GC) is dominated by the difference between the dissolution energies of the analyte in the mobile phase and stationary phase.

Based on Equation 4-6 and isothermal experiments, it is possible to derive a temperature-dependent function of distribution factor which has been applied to a series of n-alkanes spanning (nC12-nC98) in this chapter, and is presented in the following sub-sections.

4.3.Iterative method for retention time prediction

The use of discretization methods for calculating the retention times has been introduced by Snijders. [13] This method considers the diffusion effects to be negligible in the determination of the peak position, which therefore may be described only by convection. [12]

The convection can be expressed by the effective velocity veff of the analyte in the carrier gas (Equation 4-7), which can be discretize into finite time-steps, allowing tracking of the position of the analyte until the time step when the peak reaches the column outlet [3, 12], as explained in Figure ***4-1***.

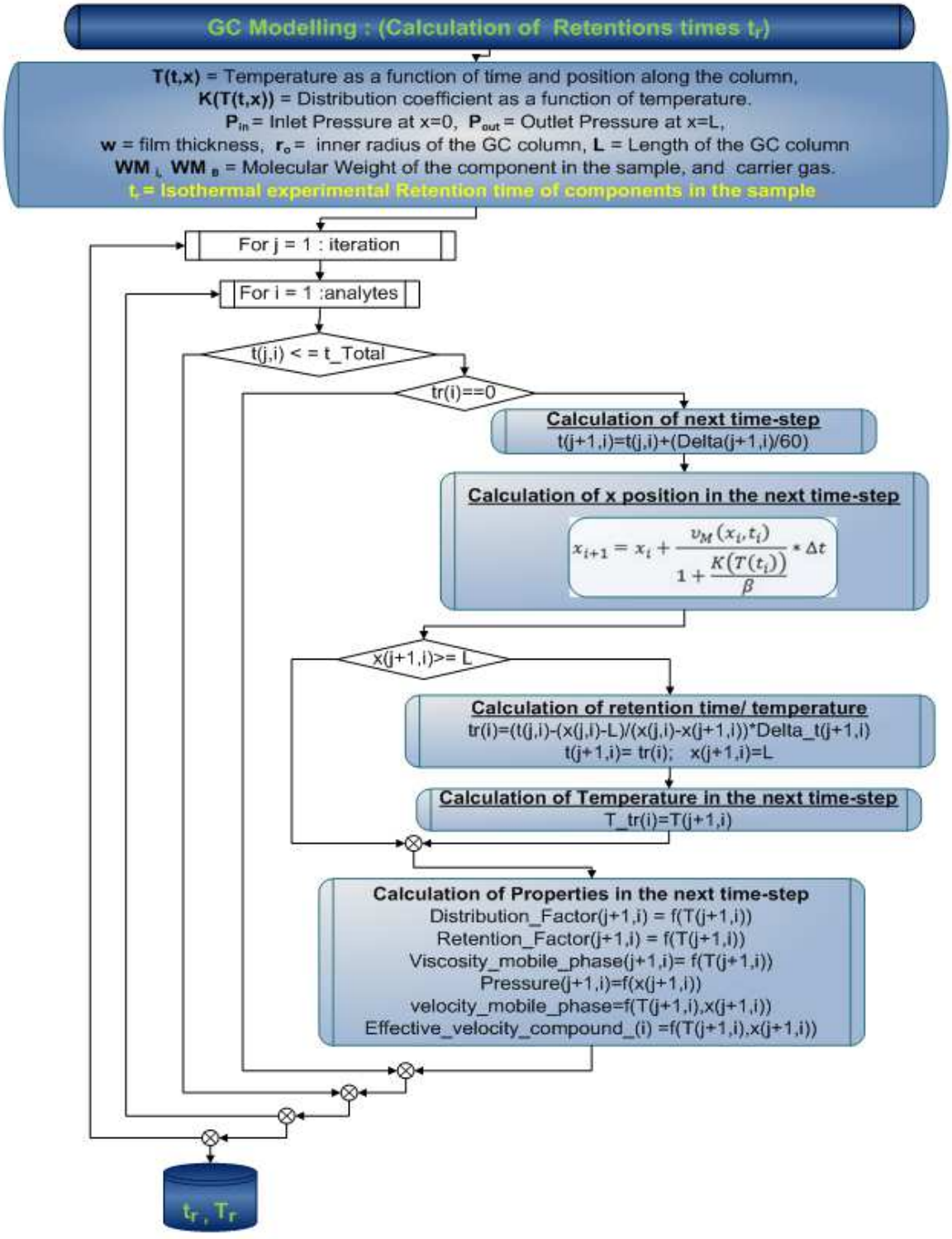

Figure 4-1. Calculation of Retention times – Algorithm

In Equation 4-7, K and β correspond to the distribution factor and phase ratio of the column, and v_m corresponds to the velocity of the mobile phase.

$$v_{eff,i}(x,t) = \frac{v_M(x,t)}{1 + \frac{K_i(T)}{\beta}}$$

Equation 4-7

v_m can be calculated by integration through the length of the column of the differential form of the Hagen-Poiseuille fluid mechanics equations [9, 14], which relate the carrier gas velocity at any position in the column, to the pressure gradient at that point [15] by a proportional constant for a column of circular cross-section [16], yielding:

$$v_M(x,t) = \frac{r_o{}^2 \cdot \left(P_{in}{}^2 - P_{out}{}^2\right)}{16 \cdot \eta\left(T(t)\right) \cdot L \cdot P(x)}$$

Equation 4-8

Here, η(T(t)) is the viscosity of the carrier gas (He in the study case), using the equation introduced by Kestin [17] and simplified by Hawkes [18]. (See the summarized equations in CHAPTER 3 –) [2-3]. P_{in} and P_{out} correspond to the inlet and outlet pressure of the GC column, respectively. P(x) corresponds to the pressure at position x, which can be calculated with Equation 4-9, and r_o is the inner radius of the column.

4.4.Calculation of the coordinate-dependent pressure

By integrating the Hagen-Poiseuille equation between the inlet and outlet position, of a differential element and assuming incompressibility of the gas in each element at position x (due to the extremely low pressure drop in gas chromatography [14]), the following expression is obtained (Equation 4-9) which allows the calculation of pressure at any position in the column:

$$P(x) = \sqrt[2]{P_{in}{}^2 - \left(P_{in}{}^2 - P_{out}{}^2\right)\frac{x}{L}}$$

Equation 4-9

Different column configurations can be used in Gas Chromatography, such as inserting a retention gap of deactivated fused silica tubing before the main GC column, to prevent non-volatile residues being deposited in the stationary phase at the column inlet. In the case of GC-1 an uncoated retention gap was used, with dimensions shown

in Table 4-1. Its presence was taken into account in the GC calculations as its effect can be significant depending on the chosen experimental method.

It is therefore necessary to calculate the internal pressure at each capillary union, such as the retention gap to column inlet (as in this case), or for the connection between the GC column outlet and a length of capillary restrictor before the detector (FID) inlet.

	GC-1		GC-2	
	Retention Gap	SGE HT5 GC Column	SGE HT5 GC Column	
Length	1.8	12	5	m
diameter	0.53	0.53	0.53	mm
film thickness		0.15	0.15	µm

Table 4-1. Column configuration & dimensions of the two in-house HTGC used.

As gas chromatography measurements can be carried out either using constant flow rate measured at ambient conditions, or using constant inlet pressure throughout the temperature program used. In both cases the GC calculation requires to be done by steps as explained in the next subsections.

4.4.1. Pressure at point x, using constant flow rate and a Retention Gap

In this case, two variables are known: the outlet pressure of the GC column (Ambient Pressure), and the flow rate (constant throughout the temperature program). However, both the GC column inlet pressure and the inlet pressure of the retention gap are unknown.

Therefore, the inlet pressure of the GC column has been calculated first, knowing the flow rate; and the outlet pressure by using Equation 4-8, transformed to flow rate. The inlet pressure of the retention gap is then calculated, knowing its outlet pressure, which equals the inlet pressure of the GC column; and knowing the flow rate by using Equation 4-8 transformed to flow rate.

4.4.2. Pressure at point x, using constant Inlet Pressure and Retention Gap

In this case, two variables are known: the outlet pressure of the GC column (Ambient Pressure), and inlet pressure of the retention gap (constant throughout the temperature

program) and two variables are unknown, the GC column inlet pressure and the flow rate, which will decrease with the increasing temperature according to Equation 4-8, transformed to flow rate.

Therefore, an average flow rate is calculated first, according to the average radius between the GC main column (which contains stationary phase) and the uncoated retention gap. The inlet pressure of the column is then calculated (which is the outlet pressure of the retention gap), knowing the flow rate and the outlet pressure of the GC column, by using Equation 4-8 transformed to flow rate.

4.5.Experimental procedure (measurement of n-Alkane isothermal retention times)

Two, SGE HT5 GC Capillary Columns [19] were employed in this chapter, with dimensions described in Table 4-1. Two methods have been used: (a) using conventional HTGC set-up conditions (long GC columns and low flow rates) eluting n-alkanes spanning the range of ($nC_{12}H_{26}$–$nC_{64}H_{130}$), under constant inlet pressure measurements conditions; and (b) using ASTM D7169-11[1] for extended SimDist analysis up to ~nC_{100} using a short column with a high flow rate, in 'constant flow' mode. (i.e for elution of alkanes spanning the range $nC_{12}H_{26}$–$nC_{98}H_{198}$.

In both columns, at least 3 isothermal GC measurements have been carried out at intervals of 20°C, from 80 to 420°C and at 430°C, using standard samples (ASTM D5442) containing n-alkanes ($nC_{12}H_{26}$-$nC_{60}H_{122}$) + Polywax 655, Polywax 850, Polywax 1000 as described in the next section.

4.5.1. Sample preparation

For various reasons it is not practicable to use a single, multi-component mixture of alkanes, with a wide carbon number range, for measurement of isothermal GC retention times:

i) retention increases rapidly with boiling point, in a generally linear plot of log(RT) vs Carbon Number.

ii) as a consequence of (i), only a limited number of alkanes' isothermal RTs can be obtained from a single injection at a given temperature.

As single alkanes above $nC_{40}H_{82}$ are not readily commercially available with adequate purity —with the exception of $nC_{44}H_{90}$, $nC_{50}H_{102}$ and $nC_{60}H_{122}$ — Polywaxes are generally utilized for retention time measurements to generate boiling-point/RT calibration plots for HTGC analyses.

However, the latter are mixtures comprising polyethylene oligomers of even carbon number intervals, and are qualitative mixtures only. Hence the weight fraction of each oligomer in a particular Polywax distribution is not readily known, although accurate estimation is possible if the complete distribution can be chromatographed and total elution can be demonstrated, e.g. by spiking.

Whilst qualitative alkane or Polywax mixtures – or a combination of the two -- are suitably adequate for both isothermal and temperature programmed retention time measurements, gravimetric dilutions in CS_2 of the ASTM D5442 Linearity Standard were also used in this chapter, covering the alkanes nC_{12}-nC_{14}-nC_{16}-nC_{18}-nC_{20}-nC_{22}-nC_{24}-nC_{26}-nC_{28}-nC_{30}-nC_{32}-nC_{36}-nC_{40}-nC_{44}-nC_{50}-nC_{60}.

In such cases, fairly accurate calculations are possible of the molar quantities of each alkane injected in a given volume. However, this is not the case where a gravimetric blend of this standard is made with a Polywax solution in CS_2 except for those alkanes which elute before the lightest oligomers present in the Polywax range.

Four main samples were prepared for the isothermal gas chromatography runs, one containing 25mg of $nC_{12}H_{26}$-$nC_{60}H_{122}$ (ASTM D5442) in 20ml of CS_2, and three others as suggested by ASTM D7169-11; 25 mg of Polywax, 10mg paraffin and 20ml CS_2.

Three different Polywax mixtures were used, with average molecular weights of 655, 850 and 1000, and for peak identification purposes three n-alkane blends in CS_2 dilution were prepared: nC_{28}, nC_{32}, nC_{34}, nC_{36}, nC_{40}; nC_{16}, nC_{20}, nC_{24}; and nC_{44}- nC_{50}- nC_{60}.

4.6.Experimental determination of constant inlet pressure using isothermal retention time measurements

The hold-up time can be calculated by integrating the inverse of the velocity of mobile phase (Equation 4-8), according to the coordinate x through the length of the column [9, 20]:

$$t_M = \int_0^L \frac{dx}{v_M(x,t)} = \frac{32\,\eta\big(T(t)\big)\,L^2}{3\,{r_o}^2} \cdot \frac{\big({P_{in}}^3 - {P_{out}}^3\big)}{\big({P_{in}}^2 + {P_{out}}^2\big)^2}$$

Equation 4-10

T (°C)	T(K)	tm (min) Experimental	μ He (Pa*s)	Pin calculated (kPa)	Gauge Pin (kPa)	tm (min) Calculated	tm % Relative Error
80	353.15	0.528	2.23E-05	119.6	18.28	0.542	2.7
100	373.15	0.55	2.32E-05	119.6	18.28	0.563	2.5
120	393.15	0.584	2.40E-05	119.6	18.28	0.584	0.0
140	413.15	0.596	2.49E-05	119.6	18.28	0.605	1.4
160	433.15	0.614	2.57E-05	119.6	18.28	0.625	1.8
180	453.15	0.63	2.65E-05	119.6	18.28	0.645	2.4
200	473.15	0.648	2.74E-05	119.6	18.28	0.665	2.6
220	493.15	0.663	2.82E-05	119.6	18.28	0.684	3.2
240	513.15	0.684	2.90E-05	119.6	18.28	0.704	2.9
260	533.15	0.702	2.98E-05	119.6	18.28	0.723	3.0
280	553.15	0.731	3.06E-05	119.6	18.28	0.742	1.6
300	573.15	0.742	3.13E-05	119.6	18.28	0.761	2.6
320	593.15	0.76	3.21E-05	119.6	18.28	0.78	2.6
340	613.15	0.766	3.29E-05	119.6	18.28	0.799	4.3
360	633.15	0.783	3.36E-05	119.6	18.28	0.817	4.4
380	653.15	0.804	3.44E-05	119.6	18.28	0.836	3.9
400	673.15	0.815	3.51E-05	119.6	18.28	0.854	4.8
420	693.15	0.833	3.59E-05	119.6	18.28	0.872	4.7
430	703.15	0.851	3.63E-05	119.6	18.28	0.881	3.5
							Average %Error
			Inlet Pressure	119.6	18.28		2.9

Table 4-2. Inlet Pressure calculation for HT5 column

Thus, in order to obtain the most accurate constant inlet pressure value for use in the in-house GC modelling (CHAPTER 3 –) [2-3], Equation 4-10 is solved simultaneously for every corresponding temperature in the range of (80-430)°C as shown in (Table *4-2*), assuming an ambient outlet pressure: 101.325 kPa, the dimensions of Column 1(see Table 4-1), and calculating the viscosity of the carrier gas (He in the study case),

using the equation introduced by Kestin [17] and simplified by Hawkes [18]. (See the summarized equations in CHAPTER 3 –) [2-3].

Whilst the indicated gauge inlet pressure for GC-2 was 20kPa, the calculated value using this approach is 18.3kPa, as shown in (*Table 4-2*), providing better precision for modelling purposes, and yielding an inlet pressure of 119.6kPa.

This approach has been described by Gonzalez [20] as insufficiently accurate for the determination of the hold-up time, tm "due to the intrinsic errors of measurement in the average internal column diameter, the carrier gas viscosity, or the flow-rate".[20] Nevertheless, since the objective is to obtain a more accurate inlet pressure than the integral GC gauge indication, for use as an average through the entire temperature range applied, this approach can be used, although introducing a tolerable error, as shown in Figure 4-2.

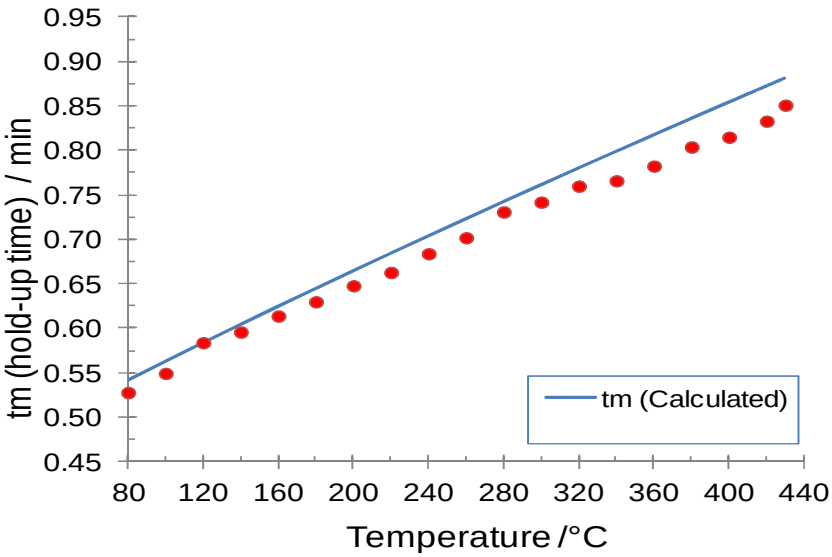

Figure 4-2. Comparison of Hold-up time(t_m) experimental and calculated. (HT5 column)

The largest deviations are found at temperatures greater than 300°C, with an average relative error of 2.9% as indicated in Table *4-2*. The higher the temperature, the higher is the viscosity of carrier gas (Helium), and therefore the lower is its velocity because of the increased resistance to flow within the column. These considerable discrepancies have been studied by Castello et al. [21]

Nevertheless the method does permit a more accurate input value to be obtained for the inlet pressure to be used analytically in the calculations of velocity of carrier gas, the effective velocity of each one of the analytes, and finally in the prediction of retention times, as will be shown in section 8, of this chapter.

4.7.Determination of distribution factors for an HT5 capillary column using in-house experimental data

On completion of the isothermal retention time measurements, all data were reviewed in order to identify any that were unreliable and which did not conform to expected behaviour. Suspect data could then be excluded, eliminating their potential to introduce a global error to the overall determination of the distributions factors.

This screening was important due to the large amount of data acquired, and it enabled identification of random errors such as misidentification of peaks, especially for the late eluting Polywax components, whose carbon numbers were greater than the highest available, heavy alkane, $nC_{60}H_{122}$, which served as a marker.

Two approaches were applied in assessing out-of-trend experimental data for deletion. The first was to plot $\log(t_r-t_m)$ vs SCN, which corresponds to a linear curve[22-24]. This graph has been plotted for each isothermal run, spanning 80°C-430°C with outliers of the regression line with a coefficient of correlation (r^2) of 0.999, excluded.

The second method of assessment was to plot $Ln((t_r-t_m)/t_m)$*Beta vs 1/T, which is based on Equation 4-2, relating K with t_r and t_m, and which behaviour is expected to be linear according to (Equation 4-1). [6-7] .

Plots of the screened retention data, after smoothing by reference to the linearity of the $\log(t_r-t_m)$ vs SCN relationship (Coefficient of correlation (r^2) of 0.999) are shown in Figure 4-3 for GC-1(12m column), for constant inlet pressure. Similarly smoothed data for GC-2(5m column) are shown in Figure 4-4, where constant flow rate conditions applied.

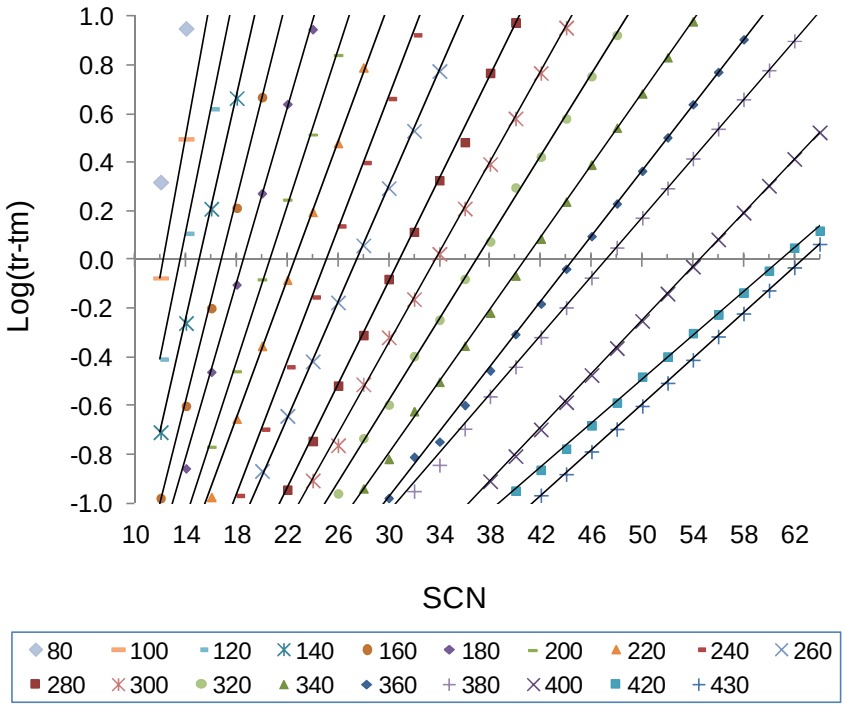

Figure 4-3. Log (t_r-t_m) vs SCN at 19 isothermal experiments in gas chromatography using constant inlet pressure of 18.3 kPa (gauge pressure), in GC-1 (Table 4-1).

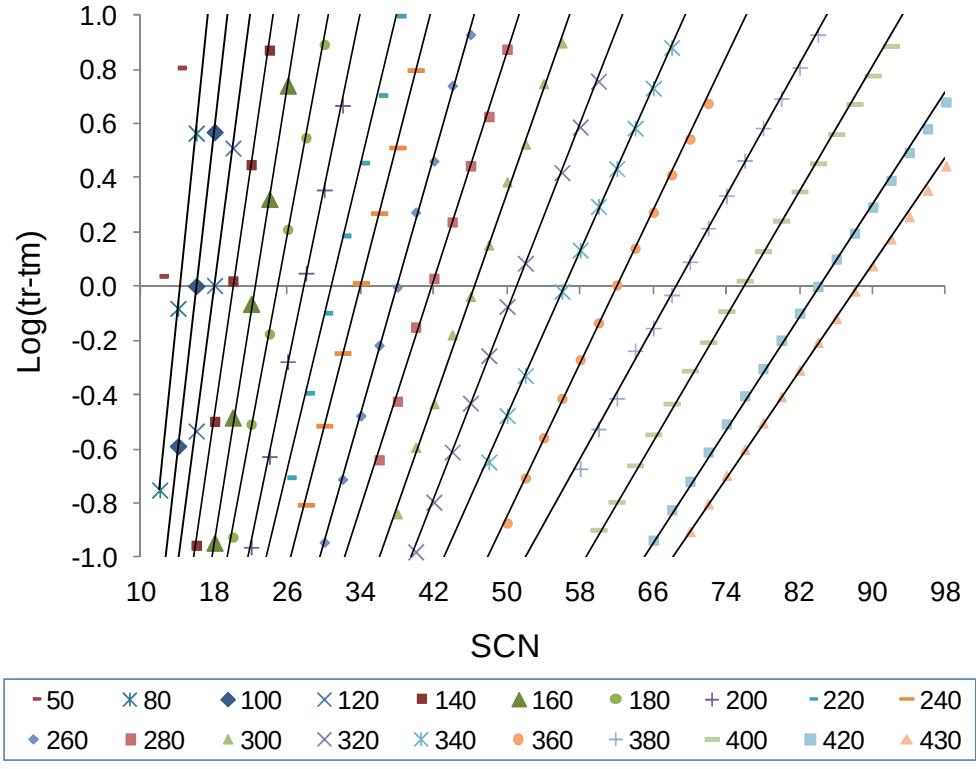

Figure 4-4. Log (t_r-t_m) vs SCN at 20 isothermal experiments in gas chromatography using constant flow rate of 20ml/min, in GC-2 (Table 4-1).

Plots of the screened retention data, after smoothing by reference to the linearity of the Ln(K(t)) as function of tr and tm (Equation 4-6) vs 1/T, are shown in Figure 4-5 for GC-1 (12m column), for constant inlet pressure; and similarly smoothed data for GC-2 (5m column) are shown in Figure 4-6(upper) for $nC_{12}H_{26}$ – $nC_{54}H_{110}$, and Figure ***4-6***(lower) for nC_{54} – nC_{98}, where constant flow rate conditions applied for both.

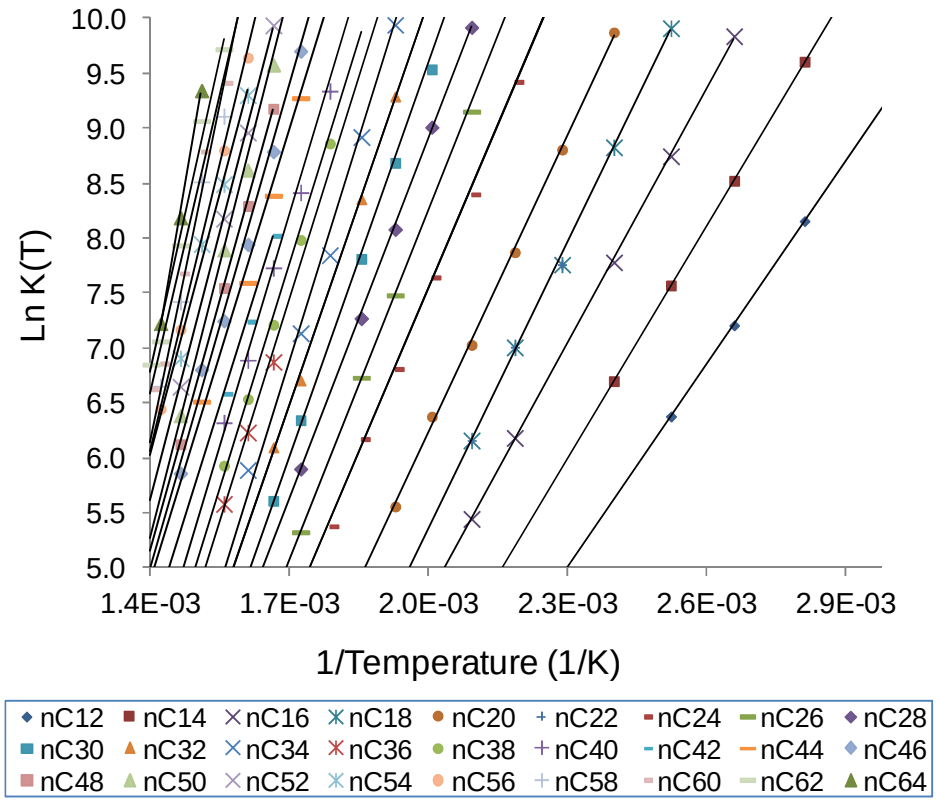

*Figure 4-5. (Ln (K(t)) = Ln((t_r/t_m-1)*β)) vs SCN, for n-alkanes ($nC_{12}H_{26}$ – $nC_{54}H_{110}$) at 20 isothermal chromatographic runs (80-430)°C using constant inlet pressure of 18.3 kPa (gauge pressure), in GC-1 (Table 4-1).*

Following the above data smoothing procedures, the reliable data were fitted to Equation 4-6 in order to obtain coefficients a0, and a1, which correspond to the thermodynamic values $\Delta S(T)/R$ and $\Delta H(T)/R$ respectively, according to Equation 4-5.

The values are temperature dependent, and are valid in the temperature range 10°C - 430°C, as the validation section will explain subsequently.

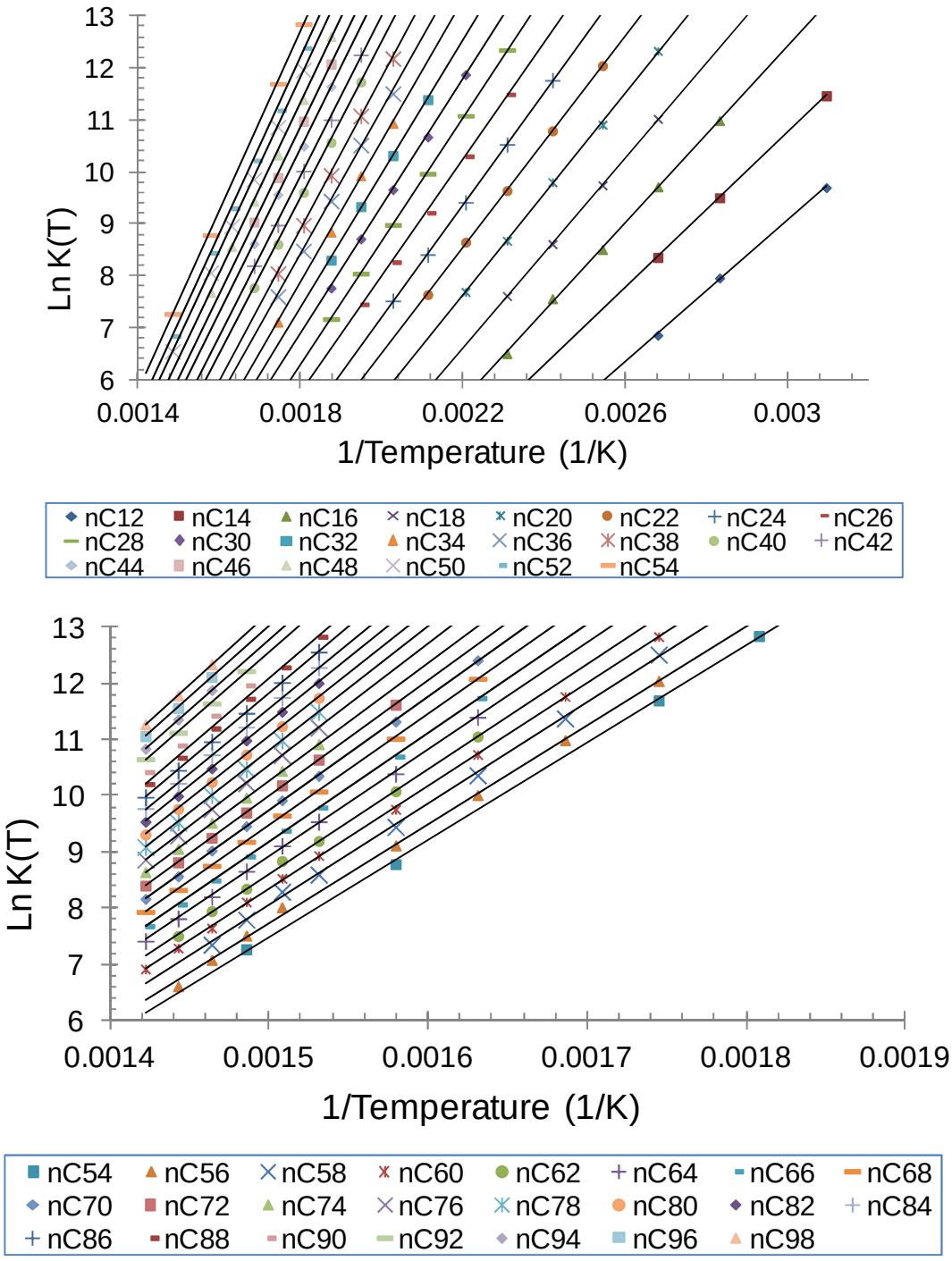

Figure 4-6. (Ln (K(t)) = Ln((t_r/t_m*-1)*β)) vs SCN, for n-alkanes (*$nC_{12}H_{26}$*-*$nC_{98}H_{198}$*) at 20 isothermal chromatographic runs (80-430)°C using constant flow rate of 20ml.min*$^{-1}$*, in GC-2 (Table 4-1)*

Data obtained for the 12m column (GC-1) using constant inlet pressure of 119.6 kPa, are summarized in Table 4-3 for the $nC_{12}H_{26}$-$nC_{64}H_{130}$ range of alkanes, with a coefficient of correlation (r^2) of 0.999.

Compound	a0=ΔS/R	a1=(-)ΔH/R	R^2
nC12	-9.3	6623.9	1.0
nC16	-9.8	7575.0	1.0
nC18	-10.4	8241.6	1.0
nC20	-11.8	9271.6	1.0
nC22	-12.4	9807.1	1.0
nC24	-13.3	10681.3	1.0
nC26	-14.2	11467.5	1.0
nC28	-14.7	12005.2	1.0
nC30	-15.0	12465.4	1.0
nC32	-15.9	13076.9	1.0
nC36	-16.8	14426.1	1.0
nC38	-18.9	15984.9	1.0
nC40	-19.0	16292.8	1.0
nC42	-19.7	16905.5	1.0
nC44	-20.4	17562.0	1.0
nC46	-21.0	18138.7	1.0
nC48	-21.7	18811.6	1.0
nC50	-22.1	19273.2	1.0
nC52	-23.0	20012.5	1.0
nC54	-24.3	21223.4	1.0
nC56	-24.9	21836.7	1.0
nC58	-25.2	22207.2	1.0
nC60	-26.7	23324.3	1.0
nC62	-27.6	24148.1	1.0
nC64	-30.2	26020.6	1.0

Table 4-3. Thermodynamic properties of n-alkanes ($nC_{12}H_{26}$-$nC_{64}H_{130}$) determined in the range of (80-430)°C using constant inlet pressure (gauge pressure=18.3 kPa) in GC-1 (Table 4-1).

Similarly, the corresponding data for the 5m column (GC-2), with a constant flow rate of 20ml.min-1, are summarized in Table 4-4 for the $nC_{12}H_{26}$-$nC_{98}H_{198}$ range.

It is important to note that with the high efficiency mode of HTGC column configuration of long column operated at low flow rate, the range of n-alkanes detected and suitable for determination of distribution factors, extended only to $nC_{64}H_{130}$. The range was limited by the greater retention times associated with the low flow-rate, which increased resolution but resulted in a lower cut-off for the heavy alkanes which elute at a given temperature.

Also, as every component has to be identified at least 3 isothermal gas chromatography runs were carried out in order to fit Equation 4-6, fewer alkanes could be validated by screening. For that reason it was necessary to adopt a short HT5 column configuration, operated at high flow rate for true SimDist conditions, based on ASTM D7169-11 [1], in order to increase the range of eluting n-alkanes for which distribution factors could then be determined.

Compound	a0=ΔS/R	a1=(-)ΔH/R	R^2	Compound	a0=ΔS/R	a1=(-)ΔH/R	R^2
nC12	-11.4	6826.3	1.0	**nC56**	-18.7	17624.7	1.0
nC14	-11.7	7501.6	1.0	**nC58**	-19.0	18053.3	1.0
nC16	-13.1	8522.5	1.0	**nC60**	-19.1	18323.7	1.0
nC18	-13.6	9190.1	1.0	**nC62**	-19.4	18682.2	1.0
nC20	-13.8	9751.5	1.0	**nC64**	-19.7	19044.8	1.0
nC22	-13.9	10204.4	1.0	**nC66**	-19.9	19364.1	1.0
nC24	-14.5	10830.1	1.0	**nC68**	-20.3	19826.6	1.0
nC26	-14.6	11273.3	1.0	**nC70**	-20.6	20234.2	1.0
nC28	-15.2	11905.5	1.0	**nC72**	-20.8	20556.7	1.0
nC30	-15.3	12299.2	1.0	**nC74**	-21.2	21000.8	1.0
nC32	-15.9	12918.7	1.0	**nC76**	-22.0	21677.5	1.0
nC34	-16.6	13598.6	1.0	**nC78**	-22.4	22128.9	1.0
nC36	-16.7	13923.8	1.0	**nC80**	-22.5	22400.5	1.0
nC38	-17.6	14673.8	1.0	**nC82**	-22.8	22757.5	1.0
nC40	-17.6	15059.3	1.0	**nC84**	-23.2	23150.6	1.0
nC42	-18.0	15475.1	1.0	**nC86**	-23.8	23771.8	1.0
nC44	-18.1	15840.4	1.0	**nC88**	-24.3	24230.5	1.0
nC46	-18.3	16170.4	1.0	**nC90**	-24.4	24449.6	1.0
nC48	-18.3	16450.2	1.0	**nC92**	-24.5	24717.3	1.0
nC50	-18.5	16814.7	1.0	**nC94**	-24.7	24977.2	1.0
nC52	-18.5	17058.0	1.0	**nC96**	-24.9	25260.9	1.0
nC54	-18.6	17351.9	1.0	**nC98**	-25.2	25662.1	1.0

Table 4-4. Thermodynamic properties of n-alkanes (nC_{12}-nC_{98}), determined in the range of (80-430)°C using constant flow rate of 6ml/min, in GC-2 (Table 4-1).

As distribution factors are a function of the phase ratio, β (Equation 4-6) but independent of column length, it was necessary that the 5m HT5 column for SimDist operating conditions should also have a film thickness of 0.15 microns*. (GC-2, Table *4-1*). (*A matching phase ratio can be assumed because of the tight manufacturing specifications achievable in modern capillary column manufacturing processes). In this way, the range of eluting alkanes was extended to $nC_{100}H_{202}$, enabling distribution

factors up to $nC_{98}H_{198}$ to be obtained, consistent with the earlier data derived from the 12m HT5 column (GC-1).

Both sets of data of *K*, have been applied to either mode of flow control, with tolerable errors as will be shown in the following section.

4.8.Validation of the predicted retention times (RTs)

The retention time prediction model, developed in MATLAB R2010bSP1, was described in CHAPTER 3 –[2-3]. It is based on Equation 4-7, and contains the corresponding equations for calculation of viscosity, pressure, and velocity through the GC column, for which the main input data requirement is the distribution coefficients of every compound, as explained earlier. (See Section 4.7).

The model has been validated using distribution coefficients obtained in this chapter for nC_{12}-nC_{64} (Table 4-3) and for nC_{12}-nC_{98} (Table 4-4), which were applied to analyses conducted under both modes of flow control --- constant inlet pressure, and constant flow rate. These analyses were conducted on both the 12m (GC-1), and the 5m HT5 column (GC-2), with 3 different temperature ramps applied as described in Table *4-5*. Validation of the model led to some interesting conclusions, which are discussed in the following sections.

	Ramp 1	Ramp 2	Ramp 3
T_o(°C)	10	10	10
Hold up time at T_o (min)	0	0	0
ramp of T (°C/min)	10	15	20
T_{max} (°C)	430	430	430
Final Hold at T_{max} (min)	12	12	12

Table 4-5. Temperature Programming

4.8.1. Validation of the model for predicted RTs at constant inlet pressure

Validation of this model has been carried out experimentally, using temperature ramps of 10°, 15°, and 20°C.min-1 (Table 4-5) for the analysis of a solution of Polywax 850 + $nC_{12}H_{26}$-$nC_{60}H_{122}$, described above. All analyses involved the 12m HT5 column (GC-1), operated under constant inlet pressure conditions, at an indicated 20kPa gauge

pressure, and producing a set of retention times for each ramp for the $nC_{12}H_{26}$-$nC_{60}H_{122}$ alkane range.

The experimental values obtained have been compared with the two data sets of distribution factors obtained using isothermal GC measurements at constant flow rate (Table 4-4), and at constant inlet pressure (Table 4-3). The calculated input value of 18.3kPa used in the model for the constant inlet gauge pressure has been obtained according to the experimental procedures explained above, as shown in Table 4-2.

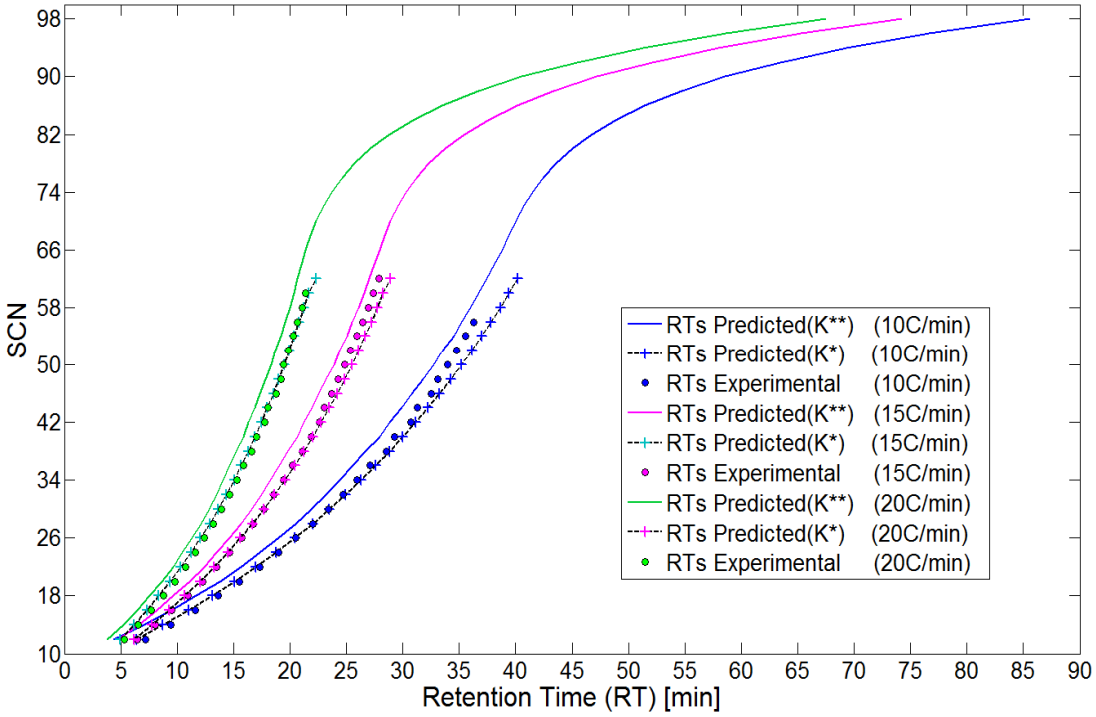

*Figure 4-7. Validation of the model developed with in-house experimental data for Alkanes, using the temperature programming (*Table 4-5*), for n-alkanes ($nC_{12}H_{26}$-$nC_{98}H_{198}$) at constant inlet pressure (Gauge pressure=18.3 kPa), in GC-1 (Table 4-1), using K** (Table 4-4) and K* (Table 4-3).*

Figure 4-7 shows the improved match of the model prediction with the experimental data, using the data set of distribution factors *K** (obtained with isothermal GC measurements under constant inlet pressure (Table 4-3), with an average deviation of 1.5% relative error. This finding was as expected, as the isothermal experiments and the 3 ramps of temperature were carried out using the same column configuration (Table *4-1*) and same constant inlet pressure.

The deviations resulting from the data set of distribution factors *K*** (obtained with isothermal GC measurements under constant flow rate) are shown in Table 4-4, with a higher average relative error of 4.8%. This also is to be expected due to the different conditions at which the distribution factors were obtained (constant flow rate), compared with those which applied to analyses involving the three different temperature ramps, where constant inlet pressure flow mode was applied.

4.8.2. Validation of the model for predicted RTs at constant flow rate

For the validation at constant flow rate, the same three ramps of temperature were applied for analyses of the solution of Polywax 850 + $nC_{12}H_{26}$-$nC_{60}H_{122}$, but using the 5 m HT5 column(GC2) at constant flow rate of 20 ml.min-1 as specified in ASTM D7169-11 [1]. A set of retention times for each ramp was thus obtained for the $nC_{12}H_{26}$-$nC_{98}H_{198}$ alkane range.

The experimental values have been compared with the same two data sets of distribution factors used in the case of constant inlet pressure, summarized in Table 4-3, obtained at constant inlet pressure, and in Table 4-4, at constant flow rate conditions.

The developed in-house model allows a choice between constant inlet pressure, and constant flow rate for intended calculations. When using the latter, the model calculates the variation of the inlet pressure required for maintaining the flow constant at reference conditions, as temperature increases and carrier-gas viscosity does likewise.

A third model was therefore used for predicting experimental retention times, by using the distribution factors obtained at constant flow rate, but using an average constant inlet pressure derived by algorithm, rather than recalculating the inlet pressure required to maintain constant flow.

The average inlet pressure used has been calculated as the average between the range of pressure required to maintain constant flow throughout the temperature program used. The lowest pressure required is at 10 °C, namely 115.5kPa; and the highest pressure required is at 430C: 133.9kPa (with an average value throughout the programming temperature of 124.7 kPa).

This model takes into account the average response of the flow controller during the temperature program, since no model exists for estimating the effect on inlet pressure of the lag in temperature between column and oven.

Figure 4-8 shows that at constant flow rate, and using the data set of distribution factors *K*** obtained at the same condition, and using the same column configuration as the 3 ramps of temperature, the model predictions produce an average relative error of 4.4%.

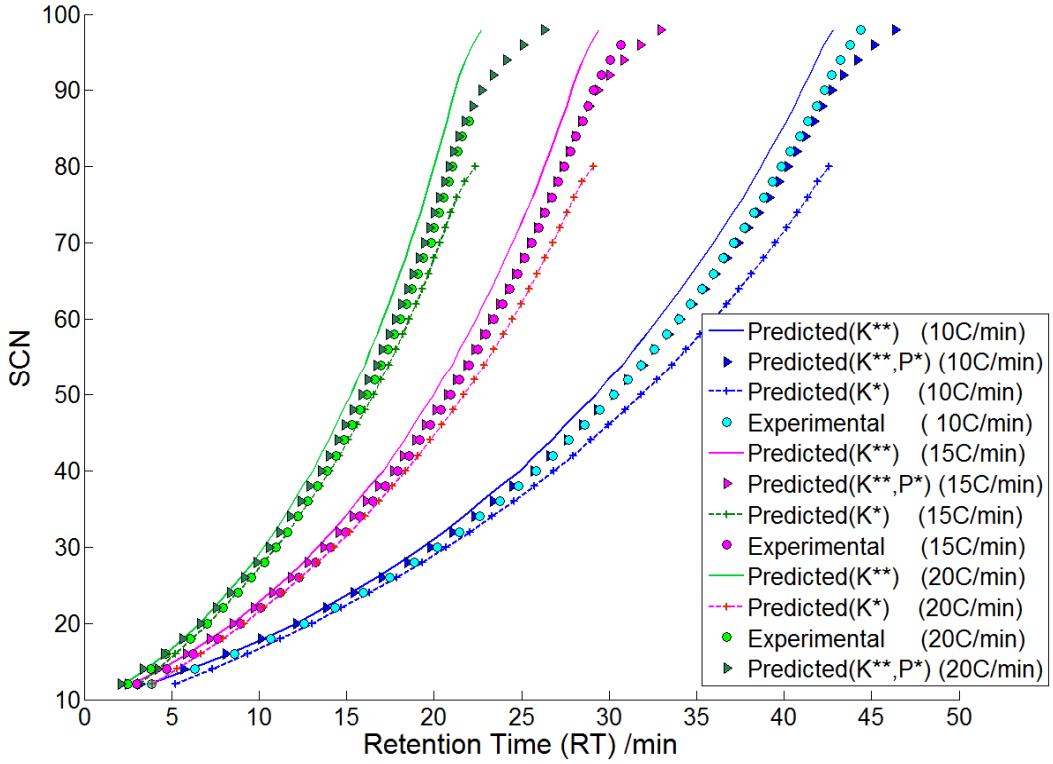

*Figure 4-8. Validation of the model developed with in-house experimental data for Alkanes, using temperature programming (Table **4-5**), for n-alkanes (nC_{12}-nC_{98}) at constant flow rate of 20ml.min-^{1}, in GC-2 (Table 4-1), using K** (Table 4-4) and K* (Table 4-3) and at constant inlet pressure (mean pressure = P*= 124.7kPa) using K** (Table 4-4).*

Figure 4-8 may reflect use of an ideal model, which produces an immediate change in the inlet pressure in response to the temperature program set-point, rather than the true column temperature. Therefore a model taking account of both the lag in temperature changes, and the lag in the response of the flow controller for changing the inlet pressure, would be required in order to improve the predictions, such as the one suggested by Conder [25].

The model providing the best match in Figure 4-8, with the experimental data is the third model (*K***,*P**) which used the data set of distribution factors obtained from the 5m HT5 column (GC-2), operated under the same conditions as the three ramps of temperatures, with constant flow rate of 20ml.min-1, but using the model at constant inlet pressure with an average value of 124.7kPa, which yielded an average relative error of 2.4%.

This outcome is as expected since an average value of the inlet pressure will represent an average change by the flow controller to the inlet pressure during the temperature changes, even with a lag in response.

The model producing the highest deviation is, as expected the one using the data set of distribution factors (*K***) obtained at different conditions from the one used for the three ramps of temperatures, as occurs with the validation at constant inlet pressure, described previously. Figure 4-8 depicts an average relative error of 9.2% when using the thermodynamic data obtained at constant inlet pressure, since the 3 ramps of temperature were carried out a constant flow rate.

Finally, it is notable that accurate retention time predictions have been obtained for the three temperature ramps which initiated from 10°C up to 430°C, even when the temperature range for which the distribution factors have been derived, related to isothermal measurements in the range 80°C to 430°C.

4.9.Conclusions

This chapter provides an extension of the data set of distribution factors for n-alkanes up to $nC_{98}H_{198}$ over the temperature range 10°C-430°C, based on isothermal gas chromatography measurements carried out at both constant inlet pressure and constant flow rate.

The former used the common HTGC configuration of a long column with low flow rate providing a data set of distribution factors for the n-alkane range spanning $nC_{12}H_{26}$-$nC_{64}H_{130}$.

As the purpose of this thesis is to analyze the GC limits for heavy n-alkanes, and since the extrapolation of the above distribution factors yielded poor predictions, this work proposed extension of the data set of *K* values(distribution factors) for $nC_{12}H_{26}$-$nC_{98}H_{198}$, by using a true SimDist configuration with a short HTGC column operated at high flow rate.

The distribution factors obtained in this chapter were used as the main input for the GC developed model for the prediction of retention times, which was introduced in CHAPTER 3 –. Its validation has been carried out using distribution factors obtained at both constant flow rate and constant inlet pressure operating conditions.

Two conventional HTGC configurations were applied: for efficient resolution with a long column operated at low flow rate; and true SimDist HTGC with a short column operated at high flow rate for inefficient resolution.

When the distribution factors used in the modelling have been obtained at the same conditions as the experimental data with which they are being compared, an average relative error of 1.5% was found for constant inlet pressure mode; and of 4.4% for constant flow rate mode.

Nevertheless, when the distribution factors used were obtained at different conditions, an average relative error of 4.8% was found (e.g. when distribution factors at constant flow mode were applied to measurements to be validated at constant inlet pressure). The average relative error increased to 9.2% when distribution factors obtained at constant inlet pressure were applied to experiments conducted at constant flow.

Finally, a model running at constant inlet pressure, using the average value through the temperature programming was used in order to improve the predictions when the experiments were carried out at constant flow rate, giving an average relative error of 2.35%.

This chapter also provides a basis for extending the analysis of non-elution using HTGC configurations (introduced in CHAPTER 3 –) for n-alkanes heavier than $nC_{62}H_{126,}$ which will be treated in CHAPTER 5 –.

4.10. References

[1] *ASTM D7169 - 11. Standard Test Method for Boiling Point Distribution of Samples with Residues Such as Crude Oils and Atmospheric and Vacuum Residues by High Temperature Gas Chromatography*: ASTM International,West Conshohocken, PA, ,(2010)

[2] Hernandez-Baez, D.M., et al., *Establishing the Maximum Carbon Number for Reliable Quantitative Gas Chromatographic Analysis of Heavy Ends Hydrocarbons. Part 2. (Migration & Separation Gas Chromatography Modelling)*, Energy & Fuels, (2013)

[3] Hernandez-Baez, D.M., et al., *Establishing the Maximum Carbon Number for Reliable Quantitative Gas Chromatography Analysis of Heavy Ends Hydrocarbons. Part 2. (Gas Chromatography Modeling by MATLAB-COMSOL)*, World Heavy Oil Congres 2012 (WHOC12). Abstract Submitted, (2012)

[4] Hernandez-Baez, D.M., et al., *Establishing the Maximum Carbon Number for Reliable Quantitative Gas Chromatographic Analysis of Heavy Ends Hydrocarbons. Part 3. (Determination of Distribution Factors (nC12-nC98) in an HT5 GC column)*, in *Unpublished manuscript*,(2013)

[5] Giddings, J.C., *Par I, Principles and theory.*, in *Dynamics of chromatography*, Edward Arnold, (Publisher, London), Marcel Dekker, Inc., : New York, (1965)

[6] Gonzalez, F.R., J.L. Alessandrini, and A.M. Nardillo, *Revision of a theoretical expression for gas-liquid chromatographic retention*, Journal of Chromatography A, **852**(2), 583-588 (1999)

[7] Ben Naim, A., *Solvation Thermodyanmics*, Plenum Press, **New York**, (1987)

[8] Gonzalez, F.R., *Interpreting the gas chromatographic retention of n-alkanes*, Journal of Chromatography A, **873**(2), 209-219 (2000)

[9] Aldaeus, F., Y. Thewalim, and A. Colmsjo, *Prediction of retention times of polycyclic aromatic hydrocarbons and n-alkanes in temperature-programmed gas chromatography*, Analytical and Bioanalytical Chemistry, **389**(3), 941-950 (2007)

[10] Gonzalez, F.R., *Considerations on the temperature dependence of the gas-liquid chromatographic retention*, Journal of Chromatography A, **942**(1-2), 211-221 (2002)

[11] Castells, R.C., E.L. Arancibia, and A.M. Nardillo, *Regression against temperature of gas-chromatographic retention data*
Journal of Chromatography, **504**(1), 45-53 (1990)

[12] Aldaeus, F., *New tools for trapping and separation in gas chromatgorahpy and dielectrophoresis (Improved performance by aid of computer simulation)*, Doctoral thesis in analytical chemistry, Stockholm University, (2007)

[13] Snijders, H., H.G. Janssen, and C. Cramers, *Optimization of temperature-programmed gas chromatographic separations .1. Prediction of retention times and peak widths from retention indices*, Journal of Chromatography A, **718**(2), 339-355 (1995)

[14] Gonzalez, F.R. and A.M. Nardillo, *Retention index in temperature-programmed gas chromatography*, Journal of Chromatography A, **842**(1-2), 29-49 (1999)

[15] Davankov, V.A., *The true physical meaning of the corrected retention volumes in GC*, Chromatographia, **44**(5-6), 279-282 (1997)

[16] Golay, M.J.E., *Theory of chromatography in open and coated tubular columns with round and rectangular cross-sections*, 36–53, (1958)

[17] Kestin, J., et al., *Equilibrium and trasport properties of the noble gases and their mixtures at low density*, Journal of Physical and Chemical Reference Data, **13**(1), 229 (1984)

[18] Hawkes, S.J., *Viscosities of carrier gases at gas-chromatograph temperatures and pressure*, Chromatographia, **37**(7-8), 399-401 (1993)

[19] *http://www.sge.com/products/columns/gc-columns/ht5*.

[20] Gonzalez, F.R. and L.G. Gagliardi, *Distribution coefficients of n-alkanes measured on wall-coated capillary columns*, Journal of Chromatography A, **879**(2), 157-168 (2000)

[21] Castello, G., S. Vezzani, and P. Moretti, *Theoretical calculation of gas hold-up time in capillary gas-chromatography - influence of column, instrument parameters and analysis conditions and comparison of different methods of dead-time determination*, Journal of Chromatography A, **677**(1), 95-106 (1994)

[22] Poole, C.F. and S.K. Poole, *Foundation of retention in partition chromatography*, Journal of chromatography A, **1216**, 1530-1550 (2009)

[23] Hawkes, S.J., *Slope of the log plot of adjusted retention time against carbon number for various homologues serices*, Chromatographia, **25**(12), (1988)

[24] Groenendijk, H. and A.W.C.v. Kemenade, *The linearity of the log-plot of adjusted retention times versus carbon number*, Chromatographia, **1**(11-12), 472-476 (1968)

[25] conder, J.R., *Correction of Gas chromatoraphic retention volumes for small temperature changes*, Journal of Chromatography, **248**, 1-6 (1982)

CHAPTER 5 – COUPLED PYROLYSIS-GC MODEL, DETERMINATION OF PYROLYSIS RISK INSIDE THE GC COLUMN AND INCOMPLETE ELUTION

5.1. Introduction

The objective of this chapter is to provide an in-depth analysis of the two main HTGC limitations for the analysis of heavy oil hydrocarbons. First, the pyrolysis risk inside the GC column; and secondly, the non/incomplete elution of heavy n-alkanes spanning the range from $nC_{14}H_{30}$ to $nC_{80}H_{162}$.

The large amount of species of the reduced free-radical pyrolysis model developed and explained in CHAPTER 2 –, has imposed the need to develop a reduced molecular pyrolysis model, comprising 11 n-alkanes ($nC_{14}H_{30}$, $nC_{16}H_{32}$, $nC_{20}H_{42}$, $nC_{25}H_{52}$, $nC_{30}H_{62}$, $nC_{35}H_{72}$, $nC_{40}H_{82}$, $nC_{50}H_{102}$, $nC_{60}H_{122}$, $nC_{70}H_{142}$, and $nC_{80}H_{162}$).

Similarly, the excessive computing time of the GC model developed in (COMSOL-MATLAB) and explained in detail in CHAPTER 3 –, for predicting the zone's variances while every component is migrating and partitioning between the stationary and the gas phases, has imposed the need to develop an analytical and more efficient GC model.

Thus, using these two efficient models, a Pyrolysis-GC coupled model has been developed in MATLAB, running at constant time-step, which enables isothermal conditions to be assumed at every time-step calculation. This model is capable of calculating the cumulative pyrolysis conversion and the degree of elution in order to determine the maximum single carbon number (SCN) which can be reliably quantified using HTGC analysis.

5.2. Reduction of the pyrolysis model

Simulation of large reaction mechanisms can result in excessive computational demands / processing time. Consequently it is necessary to reduce the size of the

reaction mechanisms to an almost equivalent, smaller computing model, several of which exist, mostly based on mathematical rather than chemical concepts. [1-2]

In CHAPTER 2 – [3] a reduced free radical primary pyrolysis mechanism has been developed for the n-alkanes, comprising $nC_{12}H_{30}$, $nC_{16}H_{34}$, $nC_{20}H_{42}$, $nC_{25}H_{52}$, $nC_{30}H_{62}$, $nC_{35}H_{72}$, $nC_{40}H_{82}$, $nC_{45}H_{92}$, $nC_{50}H_{102}$, $nC_{55}H_{112}$, $nC_{60}H_{122}$, $nC_{65}H_{132}$,$nC_{70}H_{142}$, $nC_{75}H_{152}$ and $nC_{80}H_{162}$. This model accounts for 15 reactants, 7055 reactions, 336 species, 242 molecules, and 94 radicals (Table 5-1).

	RADICALS	MOLECULAR
	Mixture of heavy Oils	
	$C_{14} + C_{16} + C_{20} + C_{25} + C_{35} + C_{40} + C_{45} + C_{50} + C_{55} + C_{60} + C_{65} + C_{70} + C_{75} + C_{80}$	
Reactants	11	
Reactions	7055	127
Species	336	
Molecules	242	17
Radicals	94	

Table 5-1. Summary of size of the mechanistic kinetics model developed. (See the free radical mechanism in CHAPTER 2 –)

Nevertheless, the large size of this model still represents a computing time constraint, when coupled to a GC migration/separation model, which is the ultimate purpose of this work.

A further reduction is therefore required of the free-radical pyrolysis model, when developing it into a molecular pyrolysis model. This new reduction process is based on knowledge of the thermal reactions' networks and the rates of the different pathways[4], and will be explained as follows.

The validation is based on the comparison of the results of simulations obtained from the reduced molecular mechanisms with those derived from the free radical mechanisms mixture model developed in CHAPTER 2 –[3], using a closed reactor at 1MPa and at 380 °C and 450 °C, with an initial equimolar composition of 9.09% molar for each of the 11-n-alkanes studied in this chapter ($nC_{12}H_{30}$- $nC_{80}H_{162}$) .

A generic reaction scheme of the thermal cracking at low conversion is depicted in Figure 5-1. The thermal cracking of an alkane (reactant: μH) is made up of chain

reactions leading to two cracking products, an alkane lighter: βH, with lower single carbon number (SCN) than μH, and an alkene.

		Kinetic
Initiation:	$\mu H \rightarrow \beta\bullet + \beta'\bullet$	K_I
H-Transfers:	$\mu H + \beta\bullet \rightarrow \mu\bullet + \beta H$	$K_{H\text{-}T}$
Decomposition:	$\mu\bullet \rightarrow \beta\bullet + \text{alkene}$	K_D
Termination:	$\mu'\bullet + \mu\bullet \rightarrow \text{Products}$	K_T
	$\mu + \beta\bullet \rightarrow \text{Products}$	K_T
	$\beta\bullet + \beta'\bullet \rightarrow \text{Products}$	K_T

Figure 5-1 Primary Reduced Reaction mechanism of thermal cracking of alkanes, for low-temperature and low conversion. (Reactant: μH), (radicals: μ•, β•), (alkanes: μH, βH).

The chain scheme uses the standard notation [5-6] to refer to the radicals, μ and β which react in a uni-molecular and bi-molecular propagation step, respectively. [7] The mechanism presented is based on the work of Bounaceur et al. [8]

The temperature range used in HTGC analysis is considered as low temperature for pyrolysis reactions, and therefore the propagation chain reactions control the whole pyrolysis mechanism. At these conditions the decomposition reaction is the limiting reaction (or limiting step) of the propagation chain [8], and therefore of the global rate of the reaction (for the whole mechanism). This is based on the Quasi-Stationary-State Approximation (QSSA) and the Long Chain Approximation (LCA). [8] (See CHAPTER 2 –[3])

5.2.1. Reduction of the radical pyrolysis model to a molecular pyrolysis model (stoichiometric lumping)

The size reduction from a radical mechanism to a stoichiometric mechanism is considerable, as will be presented in the next sub-sections. However, the approach required for building a molecular reduced mechanism is much less straightforward than the approach used for lumping radical reactions mechanism. Additionally the reactions

are not of first order but ½ orders, which are the main source of possible errors, and hence the technique should be applied to complex mixtures with extreme care.

The free-radical mechanism developed for the mixture spanning the range of alkanes , $nC_{14}H_{30}$- to $nC_{80}H_{162}$ (CHAPTER 2 –[3]), will be named "Original Mechanism", the reduction of which simplifies all of the radical species, according to the above mention simplification. Thus, the whole mechanism is reduced to the propagation chain only, which is much more significant than the initiation and termination reactions, due to the long chain simplification

In the first reduction step, all the decomposition and H-transfer reactions have been simplified into their corresponding molecular reaction (Figure 5-2). Since the rate limiting reaction is the decomposition, applying the Quasi-Steady State Approximation, its kinetic parameters have been calculated according to Equation 5-1. The rate constant parameters used come from the lumped initiation and termination reactions of all the n-alkanes considered (μH), considering all kind of μ or β radicals.

$$r_{STO} = r_{global} \quad ; \quad r_{global} = r_D = k_D[\mu\bullet] = k_D\sqrt{\frac{k_I}{k_T}}\sqrt{[\mu H]}$$

Equation 5-1

As the required reaction ($^1/_2$) order cannot be simulated by means of the software CHEMKIN II, it is considered to be a first order reaction, which may have chemical sense, since the temperature range used in this work is around 400°C, and according to Bounaceur [4] the global order of the reaction for n-alkane cracking at low temperature (~ 200°C) is equal to ½ and at high temperature (above 600 °C) is close to $^3/_2$.

Nevertheless, after comparing the original model and the first step reduced mechanism, a slight under-reactivity of the mixture has been observed for temperatures around 400°C. Therefore, the pre-exponential factors of all the molecular reactions have been multiplied by an arbitrary factor of 10 in order to increase the reactivity and reproduce the simulated values obtain with the original mechanism.

Finally, a reduced molecular model representative of the pyrolysis of the Original Model has been obtained, composed of 2935 reactions and 161 molecular compounds.

In order to reduce further the molecular model, a second step reduction has been applied, by lumping some species into the following 14 “classes” : alkene, CH_4, C_2H_6, C_3-C_5, C_6-C_{13}, $C_{15}H_{32}$, C_{17}-C_{19}, C_{21}-C_{24}, C_{26}-C_{29}, C_{31}-C_{34}, C_{36}-C_{39}, C_{41}-C_{49}, C_{51}-C_{59}, C_{61}-C_{69}, C_{71}-C_{79}, and keeping the 11 n-alkanes as reactants from the original model.

Thus, the class “C_{21}-C_{24}” represents the lumping of n-$C_{21}H_{44}$, n-$C_{22}H_{46}$, n-$C_{23}H_{48}$ and n-$C_{24}H_{50}$, and the class “alkene” represents the sum of all the alkenes included in the original model.

The reduction of the reaction and its corresponding kinetic data is required to be written step-by -step taking into account all kind of reactions in which the species belonging to the new class are included, and finally lumping all the reactions which are repeated.

In the case of the class “C_3-C_5”, the stoichiometric reduction of nC_5H_{12} accounts for 6 reactions (Figure 5-2.a), which required to be rewritten as described (Figure 5-2.b) and then rearranged, in order to obtain the 2 class lumped reactions.

When replacing every molecule by the corresponding class, the resulting mechanism comprises many repeated reactions (highlighted in blue and purple (Figure 5-2.b) which have been grouped, and their kinetic parameter corresponds to the sum of all the repeated reactions, as described in (Figure 5-2.b).

It is important to notice, that the reactions which yield the same “class” have no chemical sense, and therefore are eliminated from the mechanism.

This procedure has been applied to the whole molecular mechanism (representing the pyrolysis of the 11 n-alkanes studied) and a further reduced mechanism has been obtained, comprising 296 reactions and 26 molecular compounds.

Additional trimming of the number of classes was done in order to further reduce the mechanism, whilst still reflecting the reactants, and classes of interest for this study.

a)

					Arrhenius Parameters A	*Ea*
C5H12	=>	C2H4	+	C3H8	1.79E+17	70500
C5H12	=>	C3H6	+	C2H6	1.79E+17	70500
C5H12	=>	C4H8	+	CH4	1.79E+17	70500
C4H10	=>	C2H4	+	C2H6	1.55E+17	70500
C4H10	=>	C3H6	+	CH4	1.55E+17	70500
C3H8	=>	C2H4	+	CH4	2.53E+17	70500

b)

					Arrhenius Parameters *A*	*E*
C3-C5	=>	C2H4	+	C3-C5	1.79E+17	70500
C3-C5	=>	C3-C5	+	C2H6	1.79E+17	70500
C3-C5	=>	C3-C5	+	CH4	1.79E+17	70500
C3-C5	=>	C2H4	+	C2H6	1.55E+17	70500
C3-C5	=>	C3-C5	+	CH4	1.55E+17	70500
C3-C5	=>	C2H4	+	CH4	2.53E+17	70500
C3-C5	=>	Alkene	+	C2H6	3.34E+17	70500
C3-C5	=>	Alkene	+	CH4	5.87E+17	70500

Figure 5-2. Stoichiometric reduction of nC_5H_{12} (a) and reduction by class of "C3-C5"(b).

Therefore, a new class has been introduced: "C_{15} plus" which will represents the lumping of $nC_{15}H_{32}$ with the classes: C_{17}-C_{19}, C_{21}-C_{24}, C_{26}-C_{29}, C_{31}-C_{34}, C_{36}-C_{39}, C_{41}-C_{49}, C_{51}-C_{59}, C_{61}-C_{69} and C_{71}-C_{79}.

Thus, the final reduced molecular mechanism, accounts for the 11 original n-alkanes (reactants) and the 6 following classes: alkene, CH_4, C_2H_6, C_3-C_5, C_6-C_{13} and C_{15} plus. In this case, three rearrangements are applied:

a) Lumping of molecules belonging to the global class "C_{15} plus" which are produced by an n-alkane reactant.
b) Lumping of n-alkane reactants which produced n-alkane reactants or lighter class.
c) Lumping of global class C_{15} as reactant.

In case (a), all of the reactions which will yield the class "C_{15} plus" will be added. For example, in the case of $C_{25}H_{52}$, the products: C_{21}-C_{24}, C_{17}-C_{19}, and $C_{15}H_{32}$, belong to the

global class "C_{15} plus", and therefore the three reactions will be added to represent a single reaction, as shown in the Figure 5-3.

				Arrhenius Parameters *A*	*E*	Kinetic
C25H52	=>	Alkene	+ C21-C24	2.92E+17	70500	K_1
C25H52	=>	Alkene	+ C17-C19	2.19E+17	70500	K_2
C25H52	=>	Alkene	+ C15H32	7.30E+16	70500	K_3
C25H52	=>	Alkene	+ C15plus	5.84E+17	70500	Ks

Figure 5-3 Reduction of the Mechanism by "class" for the $C_{25}H_{52}$ yielding class "C15plus"

The kinetic parameters will be calculated with Equation 5-2:

$$K_{Alkane \rightarrow C15plus} * [Alkane] = \sum K_{Alkane \rightarrow classes\ >C15}\,[Alkane]$$

Equation 5-2

Then in the case of Figure 5-3, $Rs = Ks \cdot [C_{25}H_{52}] = K_1 \cdot [C_{25}H_{52}] + K_2 \cdot [C_{25}H_{52}] + K_3 \cdot [C_{25}H_{52}]$. Therefore, the pre-exponential parameter will be the sum of the corresponding values for the reactions yielding the classes which belong to the global class ""C_{15} plus" ", and the remaining reactions are highlighted in blue in Figure 5-3.

In the case (b), since there is no lumping, the reactions remain the same, either for the n-alkanes lighter than the reactant as well as for the lighter classes C_6-C_{13}, C_3-C_5, C_2H_6, and CH_4.

In the case (c), it is necessary to rewrite the equations for every class heavier than $nC_{15}H_{32}$ (shown in Figure 5-4) and to calculate the percentage of the classes heavier than $nC_{15}H_{32}$, which yields the 11 n-alkanes and the classes lighter than $nC_{15}H_{32}$, using Equation 5-3.

$$\%flux\ toward\ reactant = \frac{kinetic\ parameter\ of\ the\ reaction\ yielding\ the\ reactant}{sum\ of\ all\ the\ kinetic\ parameters}$$

Equation 5-3

Thus, it is necessary to know the total kinetic flux that the given classes heavier than $nC_{15}H_{32}$ will produce, which in turn, is the sum of all the kinetic flux producing either heavier or lighter classes than $nC_{15}H_{32}$ and pure alkanes.

The equivalent kinetic data are then calculated using Equation 5-4:

$$K_{\mathrm{C15plus\rightarrow produit}} = (\%flux_{\ \mathrm{class>}C15\rightarrow produit}) \cdot K_{\mathrm{class>}C15\rightarrow produit}$$

Equation 5-4

As (Figure 5-4) illustrates, the reactions highlighted in green will disappear, since they do not have chemical sense (C_{15} plus => C_{15} plus + alkene). But for the remainder of the reactions, it is necessary to calculate the equivalent flux that generates them, using Equation 5-3 and Equation 5-4.

For example, the kinetic parameter for the reaction: "C_{15} plus" → alkene+ $C_{70}H_{142}$, comes from the reaction C_{71}-C_{79} → alkene+ $C_{70}H_{142}$. Therefore, the flux of these reactions will be using Equation 5-3 and according to Figure 5-4:

$$\%flux_{\ \mathrm{class>}C15\rightarrow produit} = \frac{3.72 \cdot 10^{17}}{(\sum K) = 2.61 \cdot 10^{19}} = 1.43 \cdot 10^{-2}$$

and the equivalent kinetic will be using Equation 5-4 and according to Figure 5-4:

$$K_{\mathrm{C15plus\rightarrow produit}} = (\ 1.43 \cdot 10^{-2}) \cdot (\ 3.72 \cdot 10^{17} e^{-\frac{70500}{RT}}) = 5.31 \cdot 10^{15}\ e^{-\frac{70500}{RT}}$$

					Arrhenius Parameters A	Ea
C71-C79	=>	Alkene	+	C70H142	3.72E+17	70500
C71-C79	=>	Alkene	+	C61-C69	3.35E+18	70500
C71-C79	=>	Alkene	+	C60H122	3.72E+17	70500
C71-C79	=>	Alkene	+	C51-C59	3.35E+18	70500
C71-C79	=>	Alkene	+	C50H102	3.72E+17	70500
C71-C79	=>	Alkene	+	C41-C49	3.35E+18	70500
C71-C79	=>	Alkene	+	C40H82	3.72E+17	70500
C71-C79	=>	Alkene	+	C36-C39	1.49E+18	70500
C71-C79	=>	Alkene	+	C35H72	3.72E+17	70500
C71-C79	=>	Alkene	+	C31-C34	1.49E+18	70500
C71-C79	=>	Alkene	+	C30H62	3.72E+17	70500
C71-C79	=>	Alkene	+	C26-C29	1.49E+18	70500
C71-C79	=>	Alkene	+	C25H52	3.72E+17	70500
C71-C79	=>	Alkene	+	C21-C24	1.49E+18	70500
C71-C79	=>	Alkene	+	C20H42	3.72E+17	70500
C71-C79	=>	Alkene	+	C17-C19	1.12E+18	70500
C71-C79	=>	Alkene	+	C16H34	3.72E+17	70500
C71-C79	=>	Alkene	+	C15H32	3.72E+17	70500
C71-C79	=>	Alkene	+	C14H30	3.72E+17	70500
C71-C79	=>	Alkene	+	C6-C13	2.98E+18	70500
C71-C79	=>	Alkene	+	C3-C5	1.12E+18	70500
C71-C79	=>	Alkene	+	C2H6	3.72E+17	70500
C71-C79	=>	Alkene	+	CH4	3.72E+17	70500
				Σ total	2.61E+19	

C15plus	=>	Alkene	+	C70H142	5.31E+15	70500
C15plus	=>	Alkene	+	C60H122	5.31E+15	70500
C15plus	=>	Alkene	+	C50H102	5.31E+15	70500
C15plus	=>	Alkene	+	C40H82	5.31E+15	70500
C15plus	=>	Alkene	+	C35H72	5.31E+15	70500
C15plus	=>	Alkene	+	C30H62	5.31E+15	70500
C15plus	=>	Alkene	+	C25H52	5.31E+15	70500
C15plus	=>	Alkene	+	C20H42	5.31E+15	70500
C15plus	=>	Alkene	+	C16H34	5.31E+15	70500
C15plus	=>	Alkene	+	C14H30	5.31E+15	70500
C15plus	=>	Alkene	+	C6-C13	3.41E+17	70500
C15plus	=>	Alkene	+	C3-C5	4.81E+16	70500
C15plus	=>	Alkene	+	C2H6	5.31E+15	70500
C15plus	=>	Alkene	+	CH4	5.31E+15	70500

Figure 5-4. Reduction of the Mechanism by "class" for the class C_{71}-C_{79} which become class "C_{15} plus"

After applying this process to the whole mechanism, the kinetic data for all of the repeated reactions is the sum of the individual kinetic data using Equation 5-2.

Finally, a "class" molecular mechanism composed of 127 molecular reactions and 17 molecular compounds has been obtained.

5.2.2. Validation of the final class model

After comparing the conversion of the 11 n-alkanes, either pure or in mixture at several temperatures, it was found that the biggest deviation between the original reduced radical model, and the molecular reduced model occurred at higher conversions for the decomposition products. This is to be expected since the developed mechanism accounts only for a primary mechanism capable of describing complete conversion of reactants, but not accurately for the formation of products.

Furthermore, the simplification of the reaction yielding "C_{15} plus" from "C_{15} plus", at the end of the class reductions (no chemical sense for this reaction), may have a chemical effect in the whole decomposition mechanism of this component, which would be interesting to analysis in a future work.

The comparison of the original pyrolysis mechanism and the "class" molecular mechanism for all of the 11 n-alkane reactants (nC_{14}, nC_{16}, nC_{20}, nC_{25}, nC_{30}, nC_{35}, nC_{40}, nC_{50}, nC_{60}, nC_{70}, nC_{80}), is depicted in Figure 5-5.

After reducing the mechanism from 7055 reactions to 127 reactions, and from 336 species to 17 species (Table 5-1), good accuracy was obtained at different temperatures.

In addition, all the kinetic parameters used have a real chemical meaning since no mathematical optimization has been applied for building the "class" reduced mechanism introduced above.

The good agreement achieved between the original model (reduced radical mechanism validated up to $nC_{25}H_{52}$ [3]) and the reduced "class" molecular model, demonstrates the validity of the reduced molecular model for heavy n-alkane mixtures. The deviation at low conversion is the lowest, as expected, since the primary mechanism is capable of accurately predicting the initial production at temperatures below 450°C.

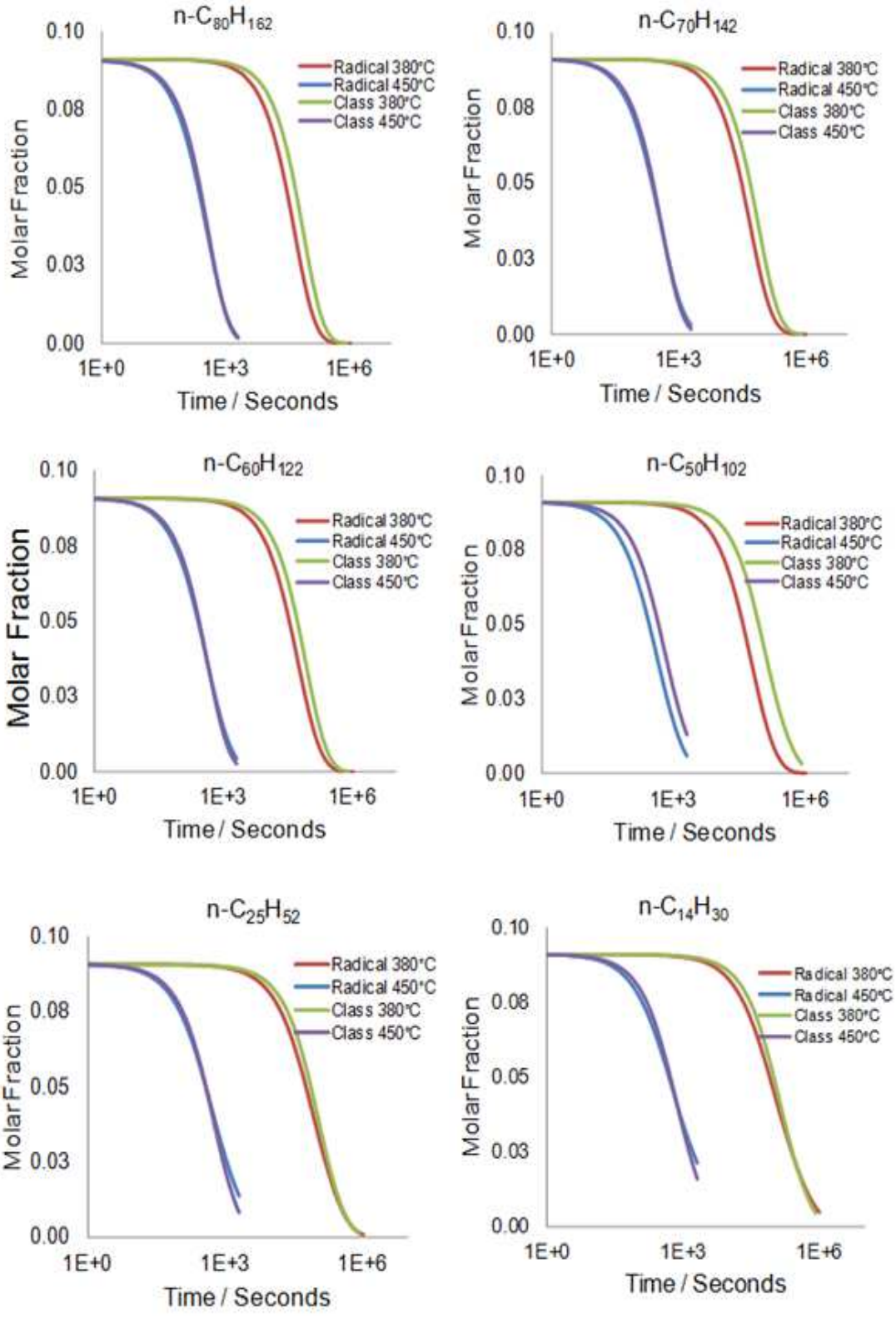

Figure 5-5. Comparison of free radical model and "class" molecular model for heavy n-alkanes mixtures. (simulation of a closed reactor at 1MPa)

For the scope of this work, these results are very satisfactory, due to the shorter residence time of reactants at high temperatures.

5.3. Gas Chromatography model

In CHAPTER 3 –[9] a GC model in MATLAB has been developed for the prediction of retention times of each solute, using a discretization approach introduced by Snijders. [10]. Another GC model in (COMSOL-MATLAB) was then developed to calculate the distribution profile of each component at every time step, and hence its concentration profile.

But as in the case for the large pyrolysis model, the computing time of the latter model represents a constraint when it is coupled to the reduced molecular pyrolysis model. Therefore, the discretization method introduced by Snijders [10] has been used also for the prediction of the peak width of the solute zone, corresponding to the space occupied by a solute migrating in a column [11]). This approach showed superior performance in computing time and has been coupled successfully to the reduced molecular pyrolysis model introduced in Section 5.2.

Snijders [10] proposed to discretize the simulation in equal time segments in order to enable isothermal properties to be applied for every time-step. Also, if the time step chosen is sufficiently small a uniform pressure can be assumed in the space segments travelled.

Thus, at every time step the local plate height (H) is calculated based on the Golay [12] equation for open tubular columns (Equation 5-5).

$$H(x,t) = 2 \cdot \frac{D_M(x,t)}{v_M(x,t)} + v_M(x,t) \left\{ \left[\frac{1 + 6 \cdot k\big(T(t)\big) + 11 \cdot k(T(t))^2}{24 \cdot [1 + k\big(T(t)\big)]^2} \cdot \frac{{r_o}^2}{D_M(x,t)} \right] + \left[\frac{2 \cdot k\big(T(t)\big)}{3 \cdot [1 + k\big(T(t)\big)]^2} \cdot \frac{w^2}{D_s(x,t)} \right] \right\}$$

Equation 5-5

Here, *k* corresponds to the retention factor, which is the ratio (K/ *β; K* corresponds to the distribution factor; and ***β*** is the phase ratio of the column. $\mathbf{r_0}$ and ***w*** correspond respectively to the inner radius of the column and the film thickness of the stationary phase. D_s, and D_m correspond to the diffusion constant respectively in the stationary and mobile phase, and v_m corresponds to the velocity of migration of the carrier gas.

At a given position, *x* the local zone variance (σ_x^2, length unit) of a solute from the zone centroid, represent the solute's spreading and can be calculated with Equation 5-6.

$$\sigma_x{}^2(\Delta x_n) = H(x_n, t_n) \cdot \Delta x_n$$

Equation 5-6

Also, the increment in the zone variance (length unit), is represented by the summation of all the local contributions of zone variances, as described in Equation 5-7. , where at every time step, the correction is applied for the expansion of the solute zone due to the reduction in pressure (P) along the column, as introduced by Giddings [13].

$$\sigma_x{}^2(x_n) = \left[\sum_{i=1}^{n-1} \sigma_x{}^2(\Delta x_i)\right] \cdot \left\{\frac{P(x_{n-1})}{P(x_n)}\right\} + \sigma_x{}^2(\Delta x_n)$$

Equation 5-7

This approach, has been programmed in MATLAB, and has been compared with the solution yielded by the COMSOL-MATLAB model developed in CHAPTER 3 – [9], which solves the diffusive-convective equation by finite elements.

SGE HT5 Column		
Lengh	12	m
diameter	0.53	mm
film thickness	0.15	µm

Table 5-2. Column Dimensions of in-house HTGC

To (°C)	10
Hold at To (min)	0
ramp of T (°C/min)	15
Tmax (°C)	425
Hold at Tmax (min)	12

Table 5-3. Temperature Programming

A comparison of the two methods is depicted in Figure 5-6, for $nC_{12}H_{26}$ migrating in a 12m HT5 column, for which column dimensions and temperature programming details are shown in Table 5-2 and Table 5-3). Excellent agreement was obtained in predictions of the zone's centroid, with an average relative error of 1.1%, and in the case of the zone's standard deviations, an average relative error of 3% was found, with the largest error occurring when the solute approaches the column outlet

However, the lengthy computing time of the method in solving the diffusive-convective equations prohibits its use for a large number of components, especially if coupled with the chemical reactions model.

Thus, in this study, the analytical method introduced by Snijders [10] has been implemented in MATLAB and coupled to the reduced molecular pyrolysis model (described previously in Section 2), by calling CHEMKIN at every time step iteration, and using feedback between the two models until each component elutes from the GC column.

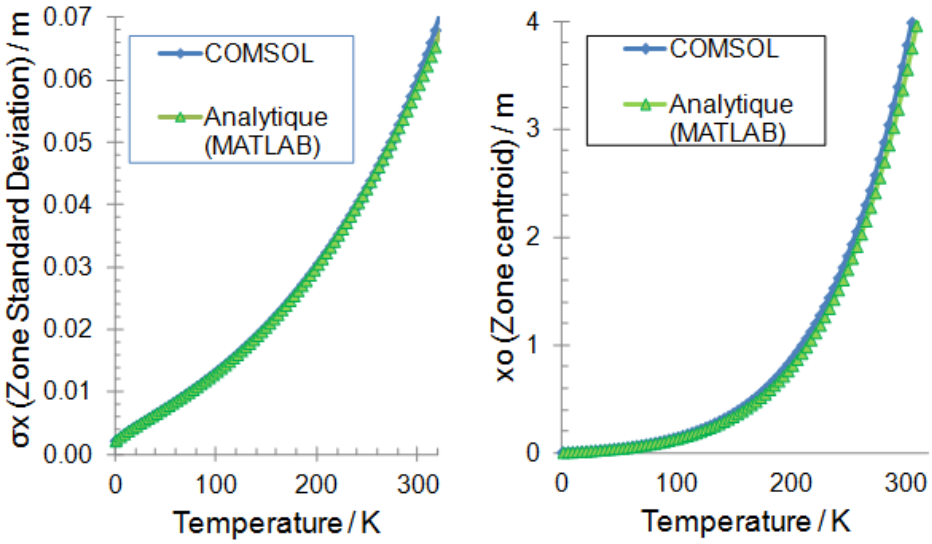

Figure 5-6. Comparison of Zone standard deviation and zone centroid of $nC_{12}H_{26}$, predicted using an iterative analytic approach [10] using MATLAB and solving the diffusive-convection equation by finite element using COMSOL. (Column dimensions Table 5-2 and temperature programming Table 5-3)

Based on Equation 5-7, for predicting the zone's width, and Equation 5-8, for predicting the retention times, a synthetic chromatograms has been assessed for 12m GC column.

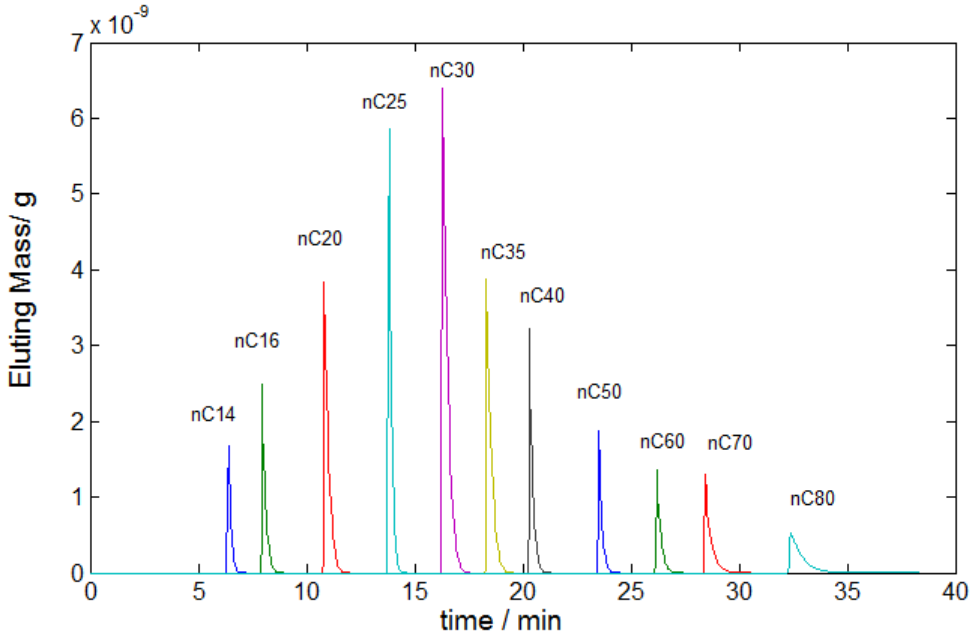

Figure 5-7. Synthetic Chromatogram, obtained using the aone standard deviation and zone centroid, predicted using an iterative analytic approach [10] using MATLAB (Column dimensions Table 5-2 and temperature programming Table 5-3)

5.4. Pyrolysis-Gas Chromatography model (Coupled Model)

Both the reduced molecular pyrolysis model (see Section 5.2.1) and the analytic iterative GC model (introduced previously in Section 5.3) are indivdually efficient, in terms of time computing, for coupling as a single, efficient physic-chemical model.

The latter is capable of predicting at every time-step, the zone's centroid, standard deviation and pyrolysis decomposition (if it occurs at the given temperature and delta time step), of every solute studied, either as a mixture or as a single component.

In order to maintain a constant temperature at every time-step, a constant time-step has been implemented, permitting an increment of 1°C every 4 seconds (due to the ramp of 15°C/min, used in the temperature programming Table 5-3).

Initially, for every component studied, the position of the zone's centroid in the next time step (x_{i+1}), is calculated, using Snijders[10] approach (Equation 5-8) (see CHAPTER 3 –[9]), the distribution factor (K), and the phase ratio (β).

$$x_{i+1} = x_i + \frac{\upsilon_M(x_i, t_i)}{1 + \frac{K_i\left(T(t_i)\right)}{\beta}} \cdot \Delta t$$

Equation 5-8

Figure 5-8, shows the algorithm explaining the global calculation carried out by the coupled model, using the above models as explained previously.

The properties (K, η, vm, Ds, Dm,) of each component are then calculated at the temperature of the next time step T(t(j+1)), and the local pressure at the zone's centroid position (P(x(j+1)).

Then, the local plate height at the next time-step, H(j+1) is calculated using Equation 5-5, with the zone's variance, σ_x^2(j+1) derived using Equation 5-7.

At this point, the degree of elution at the time-step t(j) is calculated in order to determine the fraction of the zone's distribution which traverses the column outlet, enabling calculation of the number of moles which elute and the quantity which remain inside the GC column. The summation of these partial elutions, represents the degree of elution at every time step (see CHAPTER 3 –[9]).

For the scope of this study, the pyrolysis risk is calculated only for the gas phase (further extension of the pyrolysis model to liquid phase will be treated in subsequent studies). Therefore, only the moles in gas phase are taken into account as input for the pyrolysis model.

The zone's distribution of every component serves at this point to calculate their dispersion, and therefore to determine whether the component is dispersed only in the carrier gas (in our case in He), or dispersed also in other components.

For this purpose, the space occupied by every component in the gas phase, has been assumed to be $3*\sigma_x$ on both sides of the zone's centroid (σ_x= standard deviation), covering 99.7% of the total moles in gas phase. The components inside a reactor are then determined, by calculating if the space occupied by one component is intersected by the space occupied by another component, and so on and so forth, i.e. by determining if their dispersions intersect.

By way of example, analysis of a 4-component mixture after injection can be considered, at a given time–step, t(j) when the lightest component is located almost at the column outlet, and an intermediate component is located at the mid-point.

After every partial elution the equilibrium is unbalanced, and therefore a re-equilibrium is required at the temperature of the time-step "j" T(t(j)) in order to calculate the amount of moles, which will remain in the stationary phase and in the gas phase, before pyrolysis calculations.

However, the two heaviest components are still near the column inlet and not yet totally separated, since each has a dispersed mole fraction occupying the same space, i.e. their zones are intersected. Therefore, at time–step t(j), three reactors are calculated: one reactor containing the lightest component, and a second reactor containing the intermediate component, both of which are dispersed only in carrier gas; and a third reactor containing the two heaviest components which are not yet totally separated or resolved.

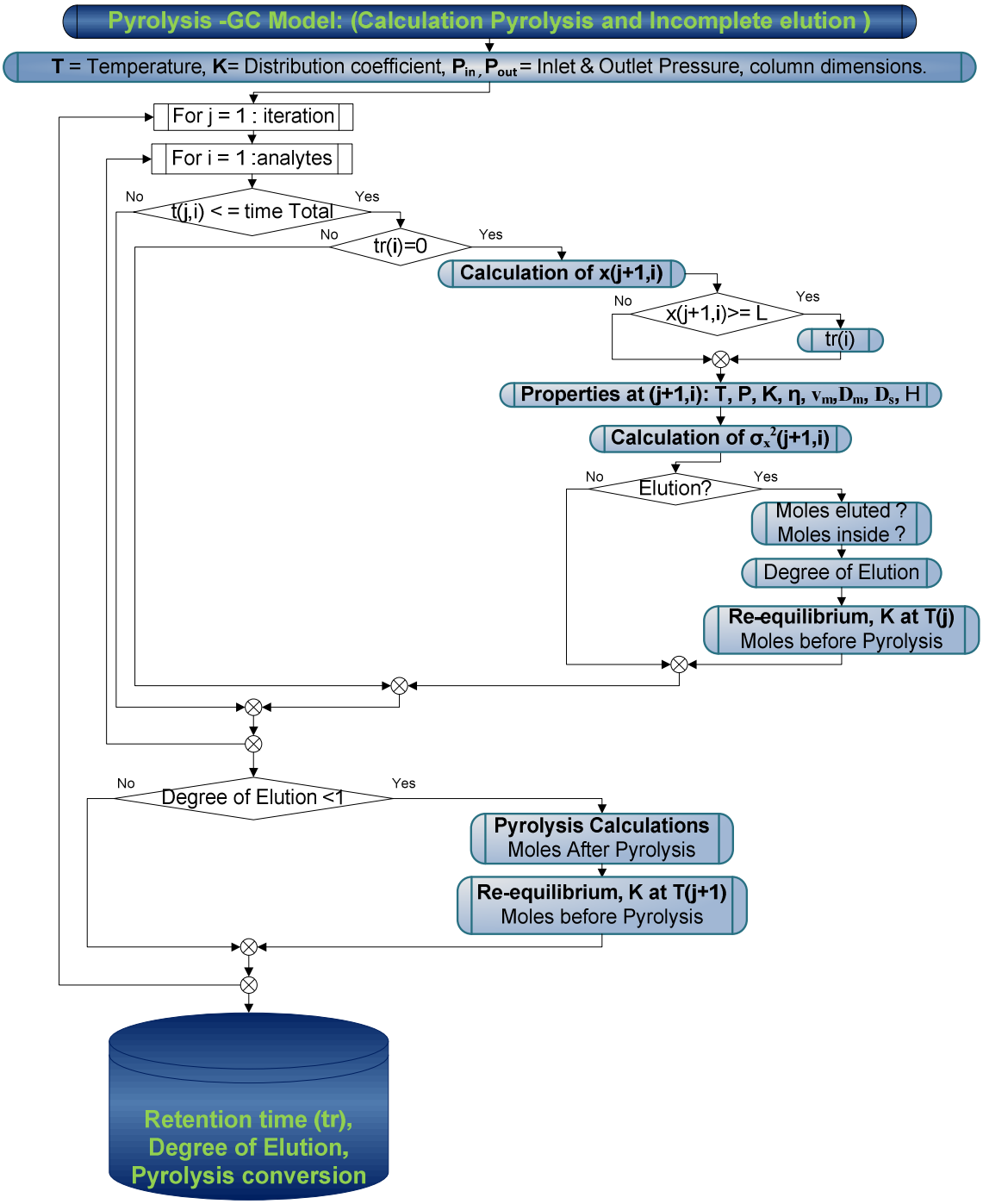

Figure 5-8. Algorithm of the Pyrolysis-GC coupled model.

At each time-step, the pyrolysis risk is calculated for every reactor, and the amount of moles of each component in the reactor is calculated after pyrolysis at the temperature T(t(j)), and pressure P(x(j)) with a residence time equal to the delta time-step (in our case 4 seconds, for isothermal conditions).

In the same way as for elution, after pyrolysis take place, the equilibrium is unbalanced, and a re-equilibrium is required, this time at the temperature of the next time-step T(t(j+1).

Finally, the loop continues until each component has totally eluted (Degree of elution=1), or until the total time of the temperature programme is reached. Thus, the degree of elution of every component is calculated, and incomplete elution can be determined. In the same way, the amount of moles decomposed by pyrolysis of every component is calculated, and the percentage of mass lost due to thermal cracking is determined.

5.5. Modelling of the pyrolysis and degree of elution of heavy n-alkanes at GC (P&T) conditions

The coupled model has been applied to one of the most common temperature programme (Table 5-3) used for HTGC analysis of heavy-oil hydrocarbons.

Compound	a0=ΔS/R	a1=(-)ΔH/R	R^2
nC14	-11.7	7501.6	1.0
nC16	-13.1	8522.5	1.0
nC20	-13.8	9751.5	1.0
nC25	-14.5	11051.7	1.0
nC30	-15.3	12299.2	1.0
nC36	-16.7	13761.2	1.0
nC40	-17.6	15059.3	1.0
nC50	-18.5	16814.7	1.0
nC60	-19.1	18323.7	1.0
nC70	-20.6	20234.2	1.0
nC80	-22.5	22400.5	1.0

Table 5-4. Thermodynamic properties of n-alkanes (nC_{14}-nC_{80}) [14]

This model accounts for 11 n-alkanes (nC_{14}, nC_{16}, nC_{20}, nC_{25}, nC_{30}, nC_{35}, nC_{40}, nC_{50}, nC_{60}, nC_{70}, nC_{80}) travelling throughout the GC column, and 17 species taken into account by the pyrolysis model (11 n-alkanes, and 6 “class” pyrolysis products: Alkene, CH_4, C_2-C_6, C_3-C_5, C_6-C_{13}, “C15 plus”).

Compound	Moles injected
nC14	4.36E-11
nC16	5.08E-11
nC20	6.11E-11
nC25	8.50E-11
nC30	6.82E-11
nC36	3.41E-11
nC40	2.56E-11
nC50	1.23E-11
nC60	6.84E-12
nC70	6.84E-12
nC80	6.84E-12

Table 5-5. Injected moles of n-alkanes in 0.3µL (Mixture of ASTM 54179 and Polywax, assumed values for calculation purposes only), for Pyrolysis-GC calculations.

The distribution factors for the 11 n-alkanes have been obtained from the CHAPTER 4 –[14] and are summarize in (Table 5-4). The injected moles of each of the 11 n-alkanes, are summarized in (Table 5-5), where values are for calculation purpose only, since the real mixture injected is composed of n-alkanes $nC_{14}H_{30}$-$nC_{60}H_{122}$ and Polywaxes, whose individual concentrations are unknown (i.e. for the Polywax constituents). (see CHAPTER 4 –[14])

5.5.1. Determination of components in each reactor (mixture of n-alkanes or single component)

As explained in section 5.4, a reactor is considered to be the space where one or more components are dispersed.

The space occupied by 99.7% of every component in the gas phase, has been assumed to be within three standard deviations ($3*\sigma_x$) of either side of the zone's centroid. Hence, if the spaces occupied by two or more components intersect, they belong to the same reactor.

Figure 5-9 depicts the cumulative mass lost due to thermal cracking for the 11 n-alkanes studied. The colours red(1^{st}), orange ochre(2^{nd}), orange(3^{rd}), yellow ochre(4^{th})

and yellow fluorescent(5^{th}) represent the reactors respectively, at the temperature of every time-step T(t(j)).

Therefore, at the beginning of the GC analysis, the temperature is 10°C, and all the components are present in a single reactor, represented in red; at 29°C, nC_{14} is separated from the rest of the components, and two reactors are found, with one containing nC_{14} and the second containing the 10 n-alkanes remaining. At 38°C, three reactors appear: one containing $nC_{14}H_{30}$, the second one containing $nC_{16}H_{34}$, and the third one, containing the remaining 9 n-alkanes.

At 83°C, four reactors appear, each containing separately $nC_{14}H_{30}$, $nC_{16}H_{34}$ $nC_{20}H_{42}$ and ($nC_{25}H_{52}$-$nC_{80}H_{162}$); and similarly, five reactors appear at 120°C, after separation of nC_{25}, from the mixture containing ($nC_{25}H_{52}$-$nC_{80}H_{162}$) in the previous time-step. But at 122°C, $nC_{14}H_{304}$ elutes from the GC column and therefore one reactor disappears, and four reactors remain in the next time-step.

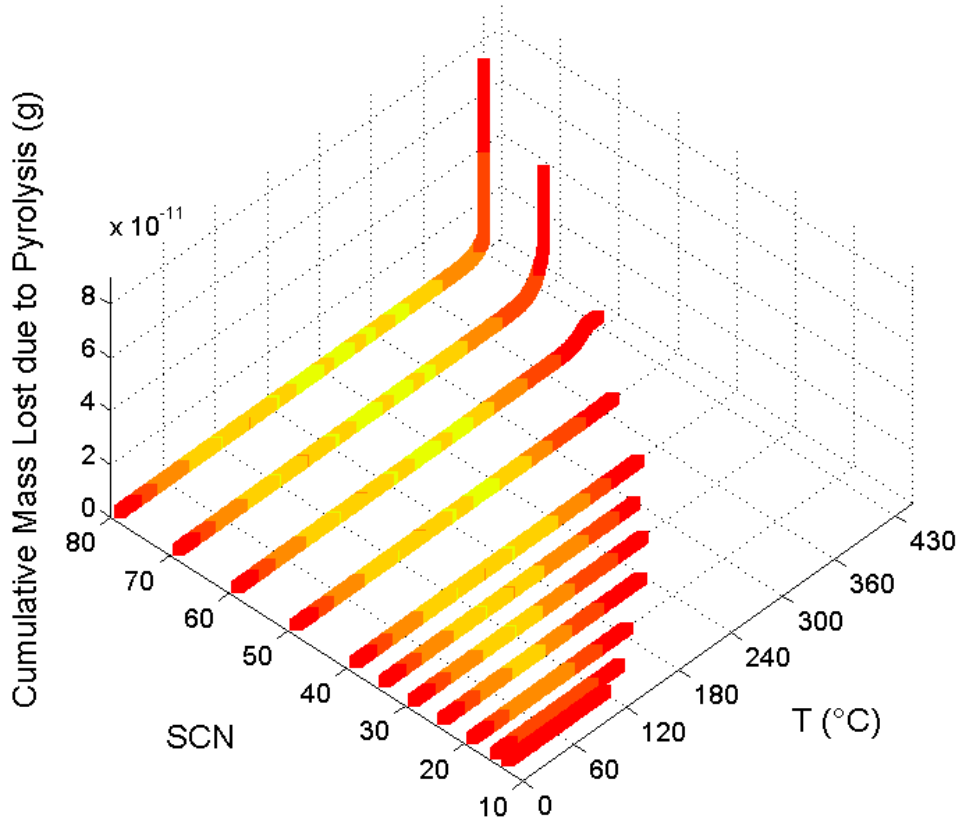

Figure 5-9. Accumulative mass lost due to thermal cracking for n-alkanes (nC_{14}, nC_{16}, nC_{20}, nC_{25}, nC_{30}, nC_{35}, nC_{40}, nC_{50}, nC_{60}, nC_{70}, nC_{80}) at a common HTGC temperature programming (Table 3-2) in a HT5 column with dimension summarized in (Table 5-2).

In the same way, as one component separates from the mixture, one new reactor appears; and as one component elutes another reactor disappears, until every component is totally separated.

At 424°C, $nC_{60}H_{122}$ elutes completely from the column, and only two reactors remain, containing separately $nC_{70}H_{142}$ and $nC_{80}H_{162}$. Thus, after 28.87 minutes, about 52 seconds into the isothermal "final hold" period of the temperature programme at 430°C, $nC_{70}H_{142}$ starts to elute (i.e. is located at the column outlet), while $nC_{80}H_{162}$ is located at 3.5m from the GC inlet. Therefore, there are 2 well separated reactors at these conditions.

Finally, after 3.46 minutes at 430°C, $nC_{70}H_{142}$ elutes completely from the column, while $nC_{80}H_{162}$ is located 7.83 m away from the column inlet, and therefore all the following calculations relate to one reactor, containing only $nC_{80}H_{162}$.

Then, $nC_{80}H_{162}$ starts to elute at 33.9 minutes (after ~5.9 minutes at 430°C), and 99.99 % of the injected moles elute at 40.9 minutes (or after 12.9 minutes in the final isothermal hold period). $nC_{80}H_{162}$ takes about 7 minutes to elute which is as expected, since its elution takes place entirely in isothermal conditions where the distribution factors remain constant.

Conversely, in the case of components eluting during the ramp of temperature, there is an acceleration of elution due to the increase of temperature, which reduces distribution factors by increasing the proportion of each component in the gas phase with respect to the stationary phase. Further conclusions on incomplete elution will be treated in section 5.6.

5.5.2. Determination of pyrolysis risk during HTGC analysis of heavy n-alkanes

The cumulative conversion due to pyrolysis of the 11 n-alkanes studied in this chapter is depicted in Figure 5-10, in order to analyse their pyrolysis risk. The figure for each component is calculated as the ratio of the cumulative mass lost due to thermal cracking, compared to the mass injected.

As Figure 5-10 depicts, absolutely no pyrolysis reaction takes place in the case of $nC_{14}H_{30}$ and $nC_{16}H_{34}$ during the temperature programming (Table 5-3) of the HTGC analysis, hence their absence in the figure). In the case of $nC_{20}H_{42}$ to $nC_{40}H_{82}$, insignificant conversion occurs and in the case of $nC_{50}H_{102}$ the maximum conversion achieved before elution is 0.003% of mass thermally decomposed/mass injected.

For the heaviest n-alkanes studied in this chapter: $nC_{60}H_{122,}$ $nC_{70}H_{142}$ and $nC_{80}H_{162,}$ a low but detectable mass loss occurs. The heavy alkane, nC_{60} starts to accumulate a mass loss due to pyrolysis of $5.83 \cdot 10^{-14}$g related to the $5.77 \cdot 10^{-9}$g injected, equivalent to a 0.001% cumulative mass conversion at 373.5°C. It is important to notice that from the total amount of mass of $nC_{60}H_{1220}$ injected only $2.43 \cdot 10^{-12}$g is released in the gas phase, whereas the rest is trapped in the stationary phase.

Therefore, the combination of the physical separation phenomena (partitioning) and the chemical reaction (pyrolysis) which is only simulated in the gas phase, limits the thermal cracking to the amount of component present in the gas phase, which is the scope of this thesis. However, it would be very interesting to investigate the pyrolysis reactions occurring in the stationary phase, as a future work.

In the case of $nC_{70}H_{142,}$ a cumulative conversion of 0.001% is reached at 385.4 °C, where $2.32 \cdot 10^{-10}$g of $nC_{70}H_{142}$ is present in the gas phase, whereas the rest of the mass injected is trapped in the stationary phase.

It is important to note that the temperature for attaining a cumulative conversion of 0.001% is higher for $nC_{70}H_{142}$ (385.4°C) than that required for $nC_{60}H_{122}$ (373.5 °C), due to the fact that nC_{70} is trapped in the stationary phase longer than $nC_{60}H_{1220}$. Hence the mass available for thermal cracking in the gas phase at a given temperature is lower in the case of $nC_{70}H_{142}$ than $nC_{60}H_{122}$.

$nC_{70}H_{142}$ reaches a maximum cumulative conversion of 0.66 % of the cumulative mass lost due to thermal cracking/mass injected, at 430°C. Thus, $4.45 \cdot 10^{-11}$g of $nC_{70}H_{142}$ has thermally decomposed, relative to the $6.73 \cdot 10^{-9}$g injected.

Finally, in the case of $nC_{80}H_{162}$, a cumulative pyrolysis conversion of 0.001% is triggered at 395.4°C, where only $1.15 \cdot 10^{-10}$g is present in the gas phase, and a cumulative mass loss of $7.86 \cdot 10^{-14}$g is achieved relative to $7.69 \cdot 10^{-9}$g injected.

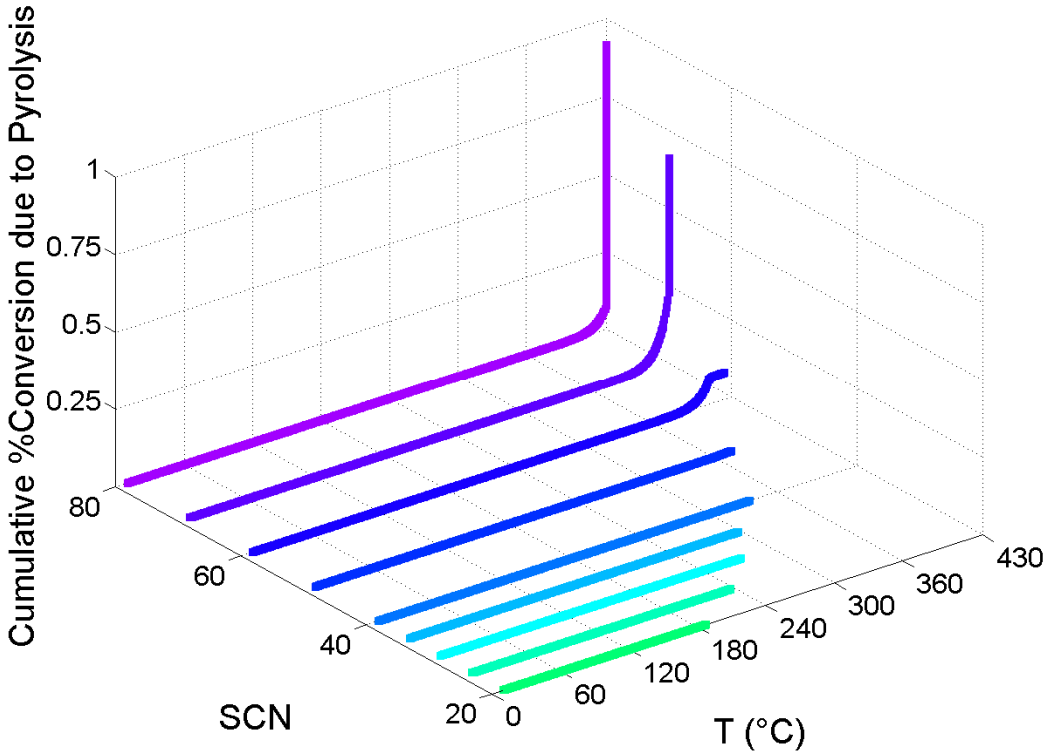

Figure 5-10. Accumulative conversion due to thermal cracking for n-alkanes (nC_{14}, nC_{16}, nC_{20}, nC_{25}, nC_{30}, nC_{35}, nC_{40}, nC_{50}, nC_{60}, nC_{70}, nC_{80}) at a common HTGC temperature programming (Table 3-2) in a HT5 column with dimension summarized in (Table 5-2)

The maximum cumulative pyrolysis conversion reached by $nC_{80}H_{162}$ is 0.92% of the cumulative mass lost due to pyrolysis/mass injected, at 430 °C, i.e. $7.04 \cdot 10^{-11}$g of $nC_{80}H_{162}$ is thermally decomposed during the temperature programme of (Table 5-3), before elution, when $7.69 \cdot 10^{-9}$g has been initially injected.

HTGC analysis of heavy n-alkanes is carried out using an FID detector for which the limit of detection is in the order of $1 \cdot 10^{-12}$g, i.e. the order of magnitude of the mass lost due to thermal cracking presented above, is theoretically detectable.

When, $nC_{60}H_{122}$ starts to decompose, the degree of elution of $nC_{50}H_{102}$ is of 99.9 %, therefore, the pyrolysis products formed by the thermal cracking of $nC_{60}H_{122}$, will have insufficient time to reach and deteriorate the peak of $nC_{50}H_{102}$.

Therefore the pyrolysis products which arise from the thermal cracking of $nC_{60}H_{122}$, should be released step by step until $nC_{60}H_{122}$ elute, probably increasing the baseline signal.

$nC_{70}H_{142}$ starts to decompose when located 1.02m away from the GC inlet, and 0.68 minutes after $nC_{60}H_{122}$ has reached a degree of elution of 99.99%. Therefore, the pyrolysis products formed by the thermal cracking of $nC_{70}H_{142,}$ could not deteriorate the peak and resolution of $nC_{60}H_{122}$.

Finally, when $nC_{80}H_{162}$ starts to decompose it is located at 0.41m from the column inlet, whereas $nC_{70}H_{142}$ is located 1.64m from the inlet. Further, when $nC_{70}H_{142}$ reaches a degree of elution of 99.99%, it is located at 7.83m from the column inlet, and its cumulative conversion is 0.52 % of the cumulative mass lost due to pyrolysis/mass injected.

It is therefore possible to conclude that $3.97.10^{-11}$g of nC_{80} is converted into pyrolysis products and co-elutes with $nC_{70}H_{142}$. That is to say that the peak of $nC_{70}H_{142}$ represents not only the mass injected of $nC_{70}H_{142}$, but also 0.52% of the amount of mass injected of $nC_{80}H_{162}$, converted into pyrolysis products, and therefore the analysis of $nC_{70}H_{142}$ is no longer reliable.

5.6. Determination of non/incomplete elution during HTGC analysis of heavy n-alkanes.

For the determination of non/incomplete elution of heavy n-alkanes, the data set of distribution factors of the n-alkanes spanning the range from $nC_{12}H_{26}$ to $nC_{98}H_{198}$, (as obtained in this thesis -- see CHAPTER 4 – has been used as main input for the calculation of the degree of elution of each of the n-alkanes studied.

Using the values of injected moles summarized in Table 5-5, the degree of elution has been calculated for the 11 n-alkanes studied in this chapter: $nC_{14}H_{30}$, $nC_{16}H_{32}$,

$nC_{20}H_{42}$, $nC_{25}H_{52}$, $nC_{30}H_{62}$, $nC_{35}H_{72}$, $nC_{40}H_{82}$, $nC_{50}H_{102}$, $nC_{60}H_{122}$, $nC_{70}H_{142}$, and $nC_{80}H_{162}$, and is depicted in Figure 5-11

The *degree of elution* has been introduced in order to determine the non/incomplete elution of heavy n-alkanes (as explained in, CHAPTER 3 –, section 3.8).

It should be noted that alkanes heavier than nC_{60} elute during the isothermal plateau of the temperature programme (i.e. 430°C). Thus, the re-establishment of equilibrium after each elution is carried out at the same temperature, and therefore using the same values of distribution factors, i.e. the ratio of moles in the stationary phase to moles in the gas phase.

Isothermal partitioning in GC analysis leads to an increase in the peak broadening. Conversely, using a ramp of temperature the peak broadening is reduced. This occurs due to the acceleration of elution with the increase in temperature, and therefore the increase in the number of solute moles released into the gas phase, i.e the decrease in distribution factors.

Figure 5-11 shows the expected elution time trend with increase in carbon number. $nC_{70}H_{142}$ starts to elute at 29 minutes, and attains a degree of elution of 99.99% at 31.3 minutes, and 100% at 31.5 minutes. That is to say, that $nC_{70}H_{142}$ takes 2.5 minutes eluting, and its peak broadening increase.

$nC_{80}H_{162}$ starts to elute at 33.8 minutes, reaching a degree of elution of 99.99 % at 40.9 minutes and 100 % after 42.3 minutes. Therefore, $nC_{80}H_{162}$ takes 7.1 minutes to elute, increasing the peak broadening, and decreasing its resolution.

Finally, it is possible to conclude that the peaks eluting during the isothermal plateau, at the maximum temperature of the temperature programming (Table 5-3), will have a decrease in resolution, due to the increase in peak broadening at isothermal conditions.

In the case studied in this chapter, from $nC_{70}H_{142}$ the components will elute much more slowly than the lightest components, and therefore an analysis of the resolution of the peak in the chromatogram would be required, when deciding to take into account the peak area of the n-alkanes heavier than $nC_{70}H_{142}$.

It is interesting to note that 99.99% of $nC_{80}H_{162}$ elute 12.9 minutes in the isothermal conditions at the maximum temperature (430°C) of the analysis.. Therefore, this component is not normally taken into account in the GC calculations, due to the shorter period of time that a HTGC column is normally left at high temperature (430 °C), in order to avoid stationary phase bleeding.

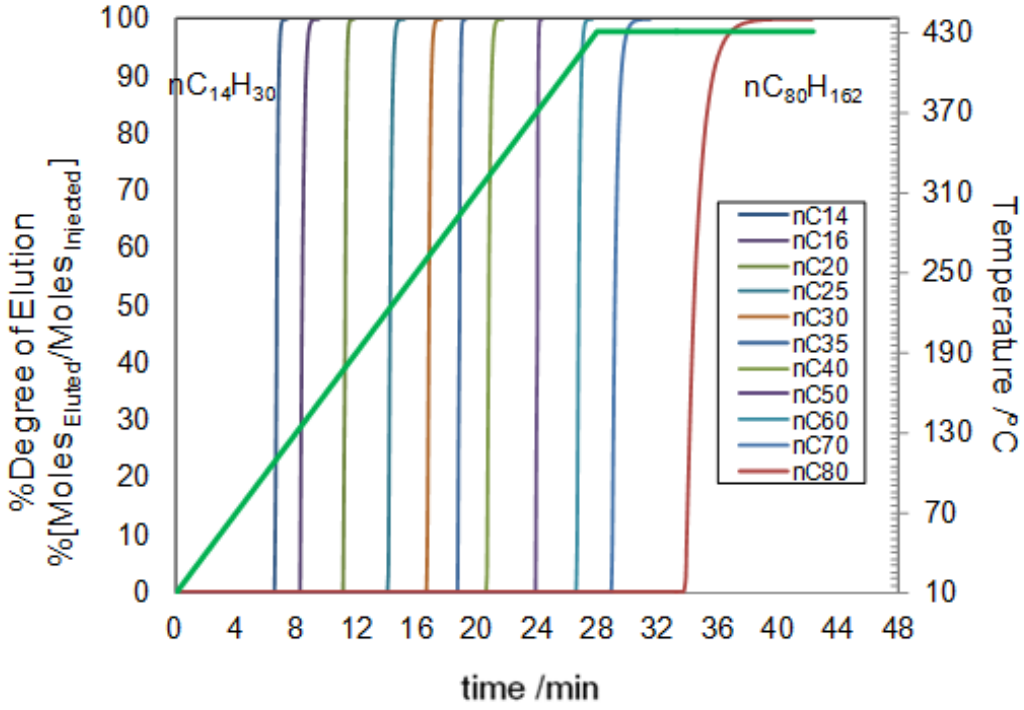

Figure 5-11. Degree of Elution vs time of each component "i" :n-alkanes in the range of $C_{14}H30$ to $nC_{80}H_{162}$. Degree of Elution= Moles of "i" inside the GC column at time (t) /Moles injected of "i".

5.7. Conclusions

This chapter provides an in-depth analysis of the two main HTGC limitations for the analysis of heavy oil hydrocarbons: first, the pyrolysis risk inside the GC column, and secondly, the non/incomplete elution of heavy n-alkanes spanning the range from $nC_{14}H_{30}$ to $nC_{80}H_{162}$.

The large amount of species of the reduced free-radical pyrolysis model developed in CHAPTER 2 – has imposed a need to develop a reduced molecular pyrolysis model, comprising 11 n-alkanes ($nC_{14}H_{30}$, $nC_{16}H_{32}$, $nC_{20}H_{42}$, $nC_{25}H_{52}$, $nC_{30}H_{62}$, $nC_{35}H_{72}$, $nC_{40}H_{82}$, $nC_{50}H_{102}$, $nC_{60}H_{122}$, $nC_{70}H_{142}$, and $nC_{80}H_{162}$). The number of reactions has

been reduced from 7055 to 127, and the number of species from 336 to 17, whilst still yielding very good accuracy.

For similar reason, the excessive computing time of the GC model developed in COMSOL-MATLAB as explained in CHAPTER 3,has imposed a need to develop an analytical and more efficient GC model. The comparison between predictions of zones' centroids and variances has been found to be less than 1.1% and 3% of average relative error.

Thus, using these two models, a Pyrolysis-GC coupled model has been developed in MATLAB, running at constant time-step, enabling isothermal conditions to be assumed at every time-step calculation. In this model, a series of physic-chemical phenomena occurs in a loop, at every time-step until each component has totally eluted: partition, degree of elution calculation, re-equilibrium if partial elution takes place, pyrolysis calculations, and finally re-equilibrium if pyrolysis occurs.

Finally, two conclusions have been made from the results obtained using the Pyrolysis-GC model. First, the cumulative pyrolysis conversion of the 11 n-alkanes studied in the chapter, suggests that 0.52% of the mass injected of $nC_{80}H_{162}$, thermally decomposed before $nC_{70}H_{142}$ has eluted. Therefore, co-elution of $nC_{70}H_{142}$ and the pyrolysis product of nC_{80} (comprising 0.52% of its injected mass injected) is possible, making the GC analysis of $nC_{70}H_{142}$ and heavier n-alkanes no longer reliable.

Secondly, the degree of elution of the 11 n-alkanes studied in the chapter has been calculated, confirming that alkanes heavier than $nC_{70}H_{142}$ take progressively longer to elute completely from the column, i.e. $nC_{70}H_{142}$ takes 2.3 minutes and $nC_{80}H_{162}$ takes 7.1 minutes using the stated column configuration and temperature programme. The resolution of the peaks is therefore compromised as a result.

Moreover, $nC_{80}H_{162}$ takes 12.9 minutes to completely elute during the isothermal plateau, implying that no distinct peak will be observable. Rather, the eluting component will be masked by the FID plateau signal, in combination with column bleed products, but too diffuse to be distinguishable. The $nC_{80}H_{162}$ peak will therefore be overlooked under these HTGC conditions.

5.8. References

[1] Tomlin, A.S., T. Turănyi, and M.J. Pilling, *Mathematical tools for the construction, investigation and reduction of combustion mechanisms*, (Ed): M.J. Pilling and G. Hancock, Elsevier, , 293-437 (1997)

[2] Kovács, T., et al., *Kinetic analysis of mechanism of complex pyrolytic reactions*, Journal of Analytical and Applied Pyrolysis, **79**(1-2), 252-258 (2007)

[3] Hernandez-Baez, D.M., et al., *Establishing the Maximum Carbon Number for Reliable Quantitative Gas Chromatographic Analysis of Heavy Ends Hydrocarbons. Part 1: Low-Conversion Thermal Cracking Modeling*, Energy & Fuels (2011)

[4] Bounaceur, R., *Modélisation cinétique de l'évolution thermique des pétroles dans les gisements, « Kinetic modeling of the thermal evolution of crude oil in sedimentary basins* PhD thesis, l'Institut National Polytechnique de Lorraine, ENSIC: Nancy, France., (2001)

[5] Niclause, M., Review Institut Francais du Petroleo, 327-419 (1954)

[6] Baronnet, F. and M. Niclause, *Industrial-problems and basic research in pyrolysis and oxidation reactions*, Industrial & Engineering Chemistry Fundamentals, **25**(1), 9-19 (1986)

[7] Goldfinger, P., M. Letort, and M. Niclause, *Volume commémoratif Victor Henri: Contribution a l'étude de la structure moléculaire*, Desoer. Liege, **283**, (1947-1948)

[8] Bounaceur, R., et al., *Modelling of hydrocarbons pyrolysis at low temperature. Automatic generation of free radicals mechanism*, Journal of Analytical and Applied Pyrolysis, **64**, 103-122 (2002)

[9] Hernandez-Baez, D.M., et al., *Establishing the Maximum Carbon Number for Reliable Quantitative Gas Chromatographic Analysis of Heavy Ends Hydrocarbons. Part 2. (Migration & Separation Gas Chromatography Modelling)*, Energy & Fuels, (2013)

[10] Snijders, H., H.G. Janssen, and C. Cramers, *Optimization of temperature-programmed gas chromatographic separations .1. Prediction of retention times and peak widths from retention indices*, Journal of Chromatography A, **718**(2), 339-355 (1995)

[11] Blumberg, L.M., *Book Title: Temperature-Programmed Gas Chromatography*: WILEY-VCH Verlag GmbH & Co. KGaA, Weinheim, (2010)

[12] Golay, M.J.E., *Theory of chromatography in open and coated tubular columns with round and rectangular cross-sections*, 36–53, (1958)

[13] Giddings, J.C., et al., *Plate Height in gas chromatography*, Analytical chemistry, **32**(8), 867-870 (1960)

[14] Hernandez-Baez, D.M., et al., *Establishing the Maximum Carbon Number for Reliable Quantitative Gas Chromatographic Analysis of Heavy Ends Hydrocarbons. Part 3. (Determination of Distribution Factors (nC12-nC98) in an HT5 GC column),* in *Unpublished manuscript*,(2013)

CHAPTER 6 – CONCLUSIONS & FUTURE WORK

High Temperature Gas chromatography (HTGC) is the industry standard separation technique for compositional characterization of heavy oil hydrocarbons, capable of separating, detecting and quantifying a wide range of n-alkanes distribution, with Single Carbon Number (SCN) up to $nC_{100}H_{202}$.

However, the reliability of HTGC analyses is questioned and limited by two main factors: the possible incomplete elution of some heavy n-alkanes; and the high temperatures required (up to 430°C), which may induce thermal decomposition and thereby cause possible over-estimation of light and intermediate fractions in the analysed composition of the oil.

Therefore, this thesis was carried out as shown in Figure 6-1, in order to address the two main GC limitations: the pyrolysis risk inside the GC column, and the non/incomplete elution of heavy n-alkanes, by developing a pyrolysis model and a GC model spanning respectively the range of n-alkanes of ($nC_{14}H_{30}$- $nC_{80}H_{162}$) and ($nC_{12}H_{26}$- $nC_{98}H_{198}$) . Finally, these two models were coupled in order to calculate the pyrolysis risk and the non/incomplete elution of heavy n-alkanes.

Therefore, in the first step, this thesis provides a first insight into the limitations in the practice of high temperature gas chromatography (HTGC), regarding the residence time and maximal temperature conditions for a given sample, based on a developed reduced mechanistic free-radical kinetic thermal cracking model, covering the range of n-alkane hydrocarbons: $nC_{14}H_{30}$, $nC_{16}H_{34}$, $nC_{20}H_{42}$, $nC_{25}H_{52}$, $nC_{30}H_{62}$, $nC_{35}H_{72}$, $nC_{40}H_{82}$, $nC_{45}H_{92}$, $nC_{50}H_{102}$, $nC_{55}H_{112}$, $nC_{60}H_{122}$, $nC_{65}H_{132}$, $nC_{70}H_{142}$, $nC_{75}H_{152}$, $nC_{80}H_{162}$.

This model has been validated with very good agreement, for $nC_{14}H_{30}$, $nC_{16}H_{34}$ and $nC_{25}H_{52}$ yielding respectively an average relative error of 5.4%, 17.4 % and 7% when compared with literature data. This model preserves the physical meaning of thermal cracking in a wide range of temperatures, without any previous optimization or adjustments made.

It would be interesting to undertake validation of longer chain hydrocarbons, such as $nC_{40}H_{82}$ and $nC_{60}H_{122}$, for which a lumped mechanistic kinetic model has been developed in this thesis. This subject may therefore be examined in a future work.

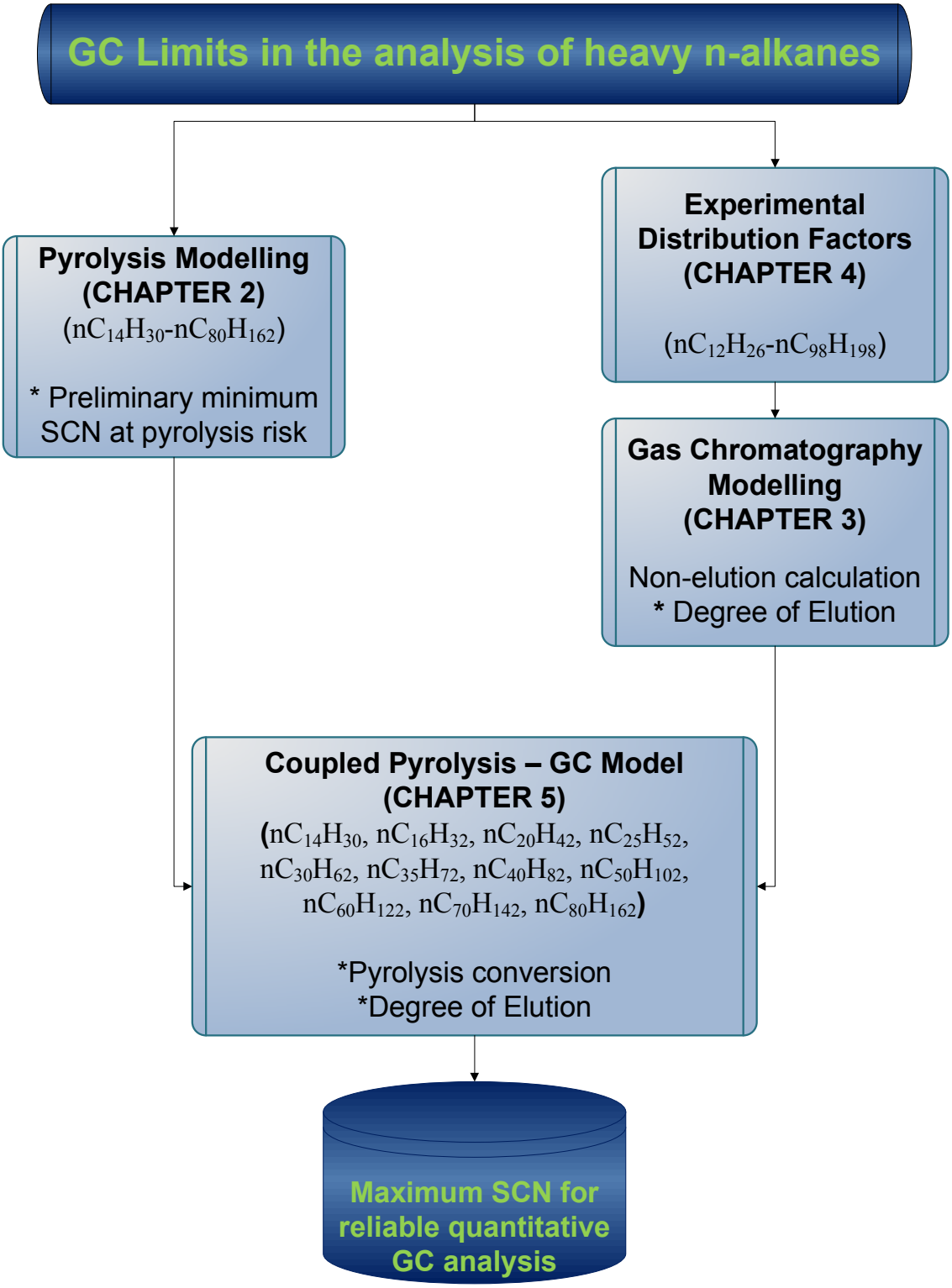

Figure 6-1. Flow diagram of the objectives reached during the PhD thesis

A new approach was introduced in the first stage of this thesis for determining the minimum SCN which undergoes pyrolysis inside the GC column, based on the intercept of the thermal cracking and residence time curves. The new approach demonstrated that for the cases studied in a mixture containing up to $C_{80}H_{162}$, heavy hydrocarbons greater than $nC_{50}H_{102}$-$nC_{52}H_{106}$ will crack before eluting from an HT5 column, at 0.1% of conversion, and from $nC_{55}H_{112}$-$nC_{57}H_{116}$ at 1% of conversion.

However, these preliminary results were obtained without taking into account the partitioning process that each component undertakes during its migration throughout the GC column. The GC separation process accounts for continuous migration and re-equilibrium in the stationary and gas phases. Thus, the number of moles in the gas phase migrating changes continuously during the HTGC analysis and therefore the effects of the pyrolysis risk would require to take into account theses variations.

Therefore, in the second step of this thesis, a Gas Chromatography migration and separation model in MATLAB has been developed in order to predict the retention times of each solute, based on a discretization approach. Also a GC model in COMSOL-MATLAB has been developed to calculate the distribution profile of each component at every time step, and thereby determining its concentration profile.

The predicted retention times using the in-house GC model were validated with literature data: first, for a DB-1 column where relative average deviations were obtained of 1.9% for n-alkanes, and 2.0% for PAH's; and secondly, for a DB-5 column, where relative average deviations of 2.2% for n-alkanes and 2.6% for PAH's were found.

Also, validation of predicted retention times was carried out for in-house measured values obtained on an HT5 column, yielding respectively average relative errors of 1.3%, 1.1% and 2.2% for analyses involving temperature ramps of 10°C/min,15°C/min and 20°C/min.

At this stage, this thesis proposed a new approach for determining the non/incomplete elution of every component by introducing the term *degree of elution*, defined as the amount of component which has been eluted in relation to the amount injected.

The degree of elution of the n-alkane hydrocarbons in the range, $nC_{12}H_{28}$ to $nC_{62}H_{126}$ has been calculated based on the continuous equilibrium re-established during the interval of elution for every component, using their corresponding retention factors, and assuming no cracking inside the GC column.

The thesis introduced a preliminary method of calculating, at each moment during a temperature-programmed analysis, the molar fraction of the components in the gas phase, in accordance with the standard deviations of their Gaussian distribution at the point where 95% of the molecules are travelling through the column.

A deeper understanding of the separation of components in a gas chromatographic column is provided in this thesis, along with a basis for analysis of non/incomplete elution of heavy n-alkanes.

The main input used in the GC modelling is the database of distribution factors (*K*), derived from isothermal GC analyses, and as HT5 capillary columns are widely used for HTGC analysis of heavy oil hydrocarbons, such a column was selected for determining the limits of the technique.

For this purpose, in the third step, this thesis provided an extension of the data set of distribution factors for n-alkanes up to $nC_{98}H_{198}$ over the temperature range 10°C-430°C, based on isothermal gas chromatography measurements carried out at both constant inlet pressure and constant flow rate.

Two conventional HTGC configurations were applied: for efficient resolution with a long column operated at low flow rate; and true SimDist HTGC with a short column operated at high flow rate for inefficient resolution.

Using the common, high-efficiency HTGC configuration of a long column with low flow rate, a data set of distribution factors was generated for the n-alkane range spanning $nC_{12}H_{26}$-$nC_{64}H_{130}$. But, as the purpose of this thesis is to determine the GC limits for heavy n-alkanes, and since the extrapolation of the above distribution factors yielded poor predictions, this thesis proposed the extension of the data set of *K* values

(distribution factors), covering the $nC_{12}H_{26}$-$nC_{98}H_{198}$ range, by use of a true SimDist configuration with a short HTGC column operated at high flow rate.

When the distribution factors used in the modelling have been obtained at the same conditions as the experimental data with which they were being compared, an average relative error of 1.5% was found for constant inlet pressure mode; and of 4.4% for constant flow rate mode.

Nevertheless, when the distribution factors used were obtained at different conditions, an average relative error of 4.8% was found (e.g. when distribution factors at constant flow mode were applied to measurements to be validated at constant inlet pressure). The average relative error increased to 9.2% when distribution factors obtained at constant inlet pressure were applied to experiments conducted at constant flow.

A model running at constant inlet pressure, utilizing the average value applied through the temperature programming was used in order to improve the predictions when the experiments were carried out at constant flow rate, giving an average relative error of 2.35%.

Finally, this thesis provides an in-depth analysis of the two main limitations in HTGC analysis of heavy oil hydrocarbons: first, the pyrolysis risk inside the GC column; and secondly, the non/incomplete elution of heavy n-alkanes spanning the range from $nC_{14}H_{30}$ to $nC_{80}H_{162}$.

In the four steps of this thesis, the large number of species of the reduced free-radical pyrolysis model initially developed for heavy n-alkane mixtures up to $nC_{80}H_{162}$ has imposed development of a reduced molecular pyrolysis model, comprising 11 n-alkanes ($nC_{14}H_{30}$, $nC_{16}H_{32}$, $nC_{20}H_{42}$, $nC_{25}H_{52}$, $nC_{30}H_{62}$, $nC_{35}H_{72}$, $nC_{40}H_{82}$, $nC_{50}H_{102}$, $nC_{60}H_{122}$, $nC_{70}H_{142}$, $nC_{80}H_{162}$). As a result, the number of reactions has been reduced from 7055 to 127, and the number of species from 336 to 17, whilst still yielding very good accuracy.

In the same way, the excessive computing time of the GC model initially developed in COMSOL-MATLAB for predicting the zones' variances while every component is

migrating and partitioning between the stationary and the gas phase, has imposed development of an analytical and more efficient GC model. The comparison between predictions of each zone's centroid and variance has been found to be lower than 1.1% and 3% of average relative error, respectively.

Thus, using these two efficient models, a Pyrolysis-GC coupled model has been developed in MATLAB in the four stages of this thesis. In this model, a series of processes is evaluated in a loop, at every time-step until each component has totally eluted: partitioning, degree of elution calculation, re-equilibrium if partial elution takes place, pyrolysis calculations, and finally re-equilibrium if pyrolysis occurs.

Finally, two conclusions have been deduced from the results obtained using the Pyrolysis-GC model in a 12m*0.53mm*0.15µm HT5 column, at the most common temperature programming (10 °C, 15 °C/min, 430 °C, 10 min hold).

First, the cumulative pyrolysis conversion of the 11 n-alkanes ($nC_{14}H_{30}$, $nC_{16}H_{32}$, $nC_{20}H_{42}$, $nC_{25}H_{52}$, $nC_{30}H_{62}$, $nC_{35}H_{72}$, $nC_{40}H_{82}$, $nC_{50}H_{102}$, $nC_{60}H_{122}$, $nC_{70}H_{142}$, $nC_{80}H_{162}$), suggests that 0.5% of the mass injected of $nC_{80}H_{162}$, thermally decomposed before $nC_{70}H_{142}$ eluted. Therefore, some co-elution of $nC_{70}H_{142}$ and the pyrolysis products of $nC_{80}H_{162}$ (comprising 0.5% of its injected mass) is suggested, making the GC analysis of $nC_{70}H_{142}$ and heavier n-alkanes no longer reliable.

Secondly, the degree of elution of the 11 n-alkanes ($nC_{14}H_{30}$, $nC_{16}H_{32}$, $nC_{20}H_{42}$, $nC_{25}H_{52}$, $nC_{30}H_{62}$, $nC_{35}H_{72}$, $nC_{40}H_{82}$, $nC_{50}H_{102}$, $nC_{60}H_{122}$, $nC_{70}H_{142}$, $nC_{80}H_{162}$) has been calculated, suggesting that the n-alkanes heavier than $nC_{70}H_{142}$ will require extended intervals for complete elution from the GC column: e.g. $nC_{70}H_{142}$ takes 2.5 minutes and $nC_{80}H_{162}$ takes 7.1 minutes. Therefore the resolution of the peaks is compromised due to the excessive peak (or band) widths corresponding to these long elution times.

Moreover, $nC_{80}H_{162}$ takes 12.9 minutes to completely elute during the isothermal plateau at the maximum temperature of 430°C, which means that $nC_{80}H_{162}$ is not normally seen in the HTGC analysis at the conditions studied, where the "hold" time at the maximum temperature is minimized in order to avoid stationary phase bleeding.

As suggested guidelines for future work on the optimization of the HTGC practice in the analysis of heavy oils, it would be very interesting to explore the required compromise between GC column length and carrier gas velocity, since based on the modelling obtained in CHAPTER 3 –, the use of high velocities and short length GC columns, permit the elution of heavy components up to $nC_{98}H_{198}$, with the inconvenient of low peak resolutions, whereas, the use of low velocities and long length GC columns, permit the elution of heavy component only up to $nC_{60}H_{122}$, with very good resolutions. Therefore, a compromise between GC column length and carrier gas velocity would be very interesting in order to obtain an extended elution of heavy components with good peak resolution, and avoiding reaching the maximum temperature of 430° C, at which the components are prompt to pyrolysis risk.

The use of a series of ramps and isothermal programming temperature may improve the residence times at which a given component will elute, permitting to elute before 430°C, therefore an optimization on the programming temperature would be also a very interesting approach to undertake.